FIELD OBSERVATIONS OF GAS-CONDENSATE WELL TESTING

A REPORT SUBMITTED TO THE DEPARTMENT OF ENERGY RESOURCES ENGINEERING

OF STANFORD UNIVERSITY

IN PARTIAL FULFILLMENT OF THE REQUIREMENTS FOR THE DEGREE OF MASTER OF SCIENCE

By
Maytham I. Al Ismail
August 2010

I certify that I have read this report and that in my opinion it is fully adequate, in scope and in quality, as partial fulfillment of the degree of Master of Science in Petroleum Engineering.

Prof. Roland N. Horne
(Principal Advisor)

Abstract

The deliverability of rich gas wells producing below the dew-point pressure is impacted severely due to condensate banking around the wellbore. Condensate banking also complicates the pressure transient test analysis due to multiphase flow and mixture composition change. The three-zone method to compute the two-phase pseudopressure gives more accurate estimates of reservoir properties than the single-phase pseudopressure method, because it accounts for the composition change in the reservoir. The three flow regions are: inner region 1 where gas and condensate flow simultaneously, middle region 2 where gas and condensate are present but only gas is mobile and outer region 3 where only gas is present.

In this work, three pressure build-up tests for a Middle Eastern gas-condensate well were matched to responses calculated with a compositional simulator. First, the PVT test results of the reservoir fluid were simulated using the Peng-Robinson equation of state. Then, the generated fluid model was included in a radial compositional model that considered the three flow regions. The compositional model was used to match the pressure build-up tests by modifying the reservoir properties. Then, the generated pressure buildup tests were analyzed using three pseudopressure techniques for comparison: the single-phase pseudopressure, the two-phase steady-state pseudopressure and the two-phase three-zone pseudopressure.

Results indicated that all three pseudopressure techniques were capable of estimating permeability accurately. However, variations in estimates of skin factor were observed. The three-zone pseudopressure approach was able to consistently estimate skin factor accurately because it always represented the pressure-saturation relationship around the wellbore correctly. On the other hand, both the single-phase pseudopressure and the two-phase steady-state pseudopressure were unable to estimate skin factor accurately. The skin effect due to liquid dropout caused the skin factor estimations by the single-phase pseudopressure approach to be high. Additionally, the steady-state method overestimated the pressure-saturation relationship which ultimately caused the skin estimates to be low for the steady-state pseudopressure approach.

Acknowledgments

I would like to express my sincere gratitude to my advisor Prof. Roland Horne for his guidance and support throughout the project. Without his insightful comments, completion of this work would not have been possible.

I would like to also thank my colleagues at the Well Testing research group (SUPRI-D) for sharing their constructive comments about the progress of my research during our weekly meetings. Special thanks go to Denis Voskov for his great help with the General Purpose Research Simulator (GPRS). Special thanks go also to my friends at Stanford community for all the fun we had during the past two years.

I am grateful to Saudi Aramco for sponsoring my graduate studies at Stanford University and for providing the necessary data for the project. Special thanks go to my superiors at Gas Reservoir Management Division, Mr. Adnan Al Kanaan, Mr. Mohammed Al Nasser and Dr. Ismail Buhidma for their continuous support.

My appreciation goes to my great parents for all the care and advice I have received and continue to receive from them. They have sowed into me the eagerness to learn and I am now reaping the benefits. My appreciation goes also to my brothers and sisters for their valuable support.

My special appreciation goes to my love, Fatemah, for believing in me and to my lovely daughter, Samar, the best thing that happened to me. To them, this work is dedicated.

Contents

Abstract v

Acknowledgments vii

Contents ix

List of Tables xi

List of Figures xiii

1. Introduction 17
   - 1.1. Single-Phase Pseudopressure 17
   - 1.2. Two-Phase Pseudopressure 17
     - 1.2.1. Steady-State Model 17
     - 1.2.2. Three-Zone Model 18
   - 1.3. Research Background 18
   - 1.4. Research Objective 19

2. Gas-condensate Flow Behavior 21
   - 2.1. Gas-condensate Systems 21
   - 2.2. Flow Behavior 23
   - 2.3. PVT Measurement 23
     - 2.3.1. Fluid Components 24
     - 2.3.2. Constant Volume Depletion (CVD) Experiment 24
     - 2.3.3. Constant Composition Expansion (CCE) Experiment 25
   - 2.4. PVT Simulation 26

3. Compositional Simulation 31
   - 3.1. Radial Model 31
     - 3.1.1. Reservoir Fluid Model 31
     - 3.1.2. Rock-Fluid Petrophysical Model 31
     - 3.1.3. Well Model 32
     - 3.1.4. Grid Model 33
   - 3.2. Model Applicability 35
   - 3.3. Simulation Runs 36
     - 3.3.1. second Pressure Buildup Test (Poststimulation) 36
     - 3.3.2. first Pressure Buildup Test (Prestimulation) 37
     - 3.3.3. Third Pressure Buildup Test 38

4. Well Test Analysis 39
   - 4.1. Introduction 39
     - 4.1.1. Pseudopressure and Pseudotime 39
     - 4.1.2. Dimensionless Variables 40
     - 4.1.3. Horner Plot Analysis 41
   - 4.2. Single-Phase Pseudopressure 44

4.3. Two-Phase Steady-State Pseudopressure 46
4.4. Two-Phase Three-Zone Pseudopressure 49

5. Well Test Results 55
5.1. First Pressure Buildup Test (Prestimulation) 55
5.1.1. Single-Phase Pseudopressure 55
5.1.2. Steady-State Pseudopressure 56
5.1.3. Three-Zone Pseudopressure 57
5.1.4. Discussions on First Pressure Buildup Test 59
5.2. Second Pressure Buildup Test (Poststimulation) 60
5.2.1. Discussions on Second Pressure Buildup Test 61
5.3. Third Pressure Buildup Test 62
5.3.1. Discussions on third Pressure Buildup Test 63
5.4. Conclusions 64

6. Further Investigations 67
6.1. GOR Behavior During Depletion 67
6.2. Condensate Saturation Behavior During Buildup 69
6.2.1. Eclipse-300 vs. GPRS 70

7. Conclusions 75

References 77

Nomenclature 81

A. PVT Experiments 83
A.1 Constant Volume Depletion CVD 83
A.2 Constant Composition Expansion CCE 84

B. Radial Model 85
B.1 Eclipse-300 Code 85

C. Plots for Second Pressure Buildup Test Analysis 91
C.1 Pressure-Saturation Relationship 91
C.2 Horner Plots 93

D. Plots for Third Pressure Buildup Test Analysis 96
D.1 Pressure Saturation Relationship 96
D.2 Horner Plots 98

E. Cartesian Model 100
E.1 Well Index Calculation 100
E.2 GPRS Code 101

List of Tables

Table 2-1: Typical composition of three fluid types from Wall (1982). 22

Table 2-2: Hydrocarbon analysis of separator products and well stream......................... 24

Table 3-1: Simulation parameters for the well radial model. 32

Table 3-2: Cell sizes in radial direction. 33

Table 4-1: Calculation of the Real Gas Pseudopressure 45

Table 5-1: Summary of Horner analysis results for first pressure buildup test 59

Table 5-2: Summary of Horner analysis results for second pressure buildup test 61

Table 5-3: Summary of Horner analysis results for third pressure buildup test 63

Table 6-1: Simulation Parameters for Eclipse-300 and GPRS. 71

List of Figures

Figure 1-1: Gas-condensate three flow regions (from Roussennac 2001)........................ 18

Figure 2-1: Ternary visualization of hydrocarbon classification (from Whitson and Brule 2000). 21

Figure 2-2: Phase diagram of a gas-condensate system from Fan et. al. (2005). 22

Figure 2-3: Condensate saturation as a function of pressure from CVD experiment....... 25

Figure 2-4: Total relative volume as a function of pressure from CCE experiment. 26

Figure 2-5: Observed vs. calculated condensate saturation during CVD experiment...... 27

Figure 2-6: Observed vs. calculated total relative volume during CCE experiment........ 28

Figure 2-7: Measured vs. calculated gas phase composition at separator conditions. 28

Figure 2-8: Measured vs. calculated liquid phase composition at separator conditions. . 29

Figure 2-9: Critical temperatures and pressures for well stream components................. 29

Figure 3-1: Relative permeability curves used on Well-A radial model. 32

Figure 3-2: Radial grid size distribution with nonsmooth changes (from Roussennac 2001). 34

Figure 3-3: Radial grid size distribution with smooth changes (from Roussennac 2001).34

Figure 3-4: Producing GOR behavior during the second well test.................................. 35

Figure 3-5: Pressure buildup test to examine model applicability. 35

Figure 3-6: History plot of the second well test... 36

Figure 3-7: Radial distribution of condensate saturation at the end of the second test drawdown.. 37

Figure 3-8: Radial distribution of condensate saturation at the end of the first test drawdown.. 37

Figure 3-9: History plot of first well test. 38

Figure 3-10: Radial distribution of condensate saturation at the end of the third test drawdown.. 38

Figure 4-1: Semilog analysis using pseudopressure (from Roussennac 2001). 42

Figure 4-2: Semilog Horner plot for a pressure buildup test (from Horne 1995)............. 43

Figure 4-3: Real gas pseudopressure *m(p)* as a function of pressure............................... 46

Figure 4-4: Pressure-saturation relationship estimated by the steady-state model for original gas-condensate system. 48

Figure 4-5: Two-phase steady-state pseudopressure *m(p)* as a function of pressure........ 49

Figure 4-6: *p** estimation for Region 1 pressure boundaries... 51

Figure 4-7: Pressure-saturation relationship estimated by the three-zone model at the end of the drawdown for first test.. 53

Figure 4-8: Two-phase three-zone pseudopressure as a function of pressure for first test. 53

Figure 5-1: Horner plot for first pressure buildup test (single-phase pseudopressure). ... 55

Figure 5-2: Pressure-saturation relationship by the steady-state model for the first test. 56

Figure 5-3: Radial distribution of condensate saturation by the steady-state model for the first test. 56

Figure 5-4: Horner plot for first pressure buildup test (steady-state pseudopressure). 57

Figure 5-5: Pressure-saturation relationship by the three-zone model for the first test.... 58

Figure 5-6: Radial distribution of condensate saturation by the three-zone model for the first test. 58

Figure 5-7: Horner plot for first pressure buildup test (three-zone pseudopressure). 59

Figure 5-8: Semilog plot of dimensionless pressure as a function of dimensionless time for first pressure buildup test. 60

Figure 5-9: Semilog plot of dimensionless pressure as a function of dimensionless time for second pressure buildup test... 62

Figure 5-10: Radial distribution of condensate saturation by the steady-state model and the three-zone model for the third well test. 63

Figure 5-11: Semilog plot of dimensionless pressure as a function of dimensionless time for third pressure buildup test. 64

Figure 6-1: Producing GOR behavior during the first well test. 67

Figure 6-2: Producing GOR behavior for a zero-skin case (from Roussennac 2001)...... 68

Figure 6-3: Gas rate (blue), condensate rate (black) and GOR (red) as a function of time during first well test. 68

Figure 6-4: Radial distribution of condensate saturation at GOR = 12 Mscf/STB. 69

Figure 6-5: Radial distribution of condensate saturation at GOR = 11.3 Mscf/STB. 69

Figure 6-6: Condensate saturation at the end of drawdown vs. buildup for second well test.. 70

Figure 6-7: The Cartesian model used in *Eclipse-300* and *GPRS*. 71

Figure 6-8: Estimated bottom hole pressure (BHP) behavior by *Eclipse-300* and *GPRS*.72

Figure 6-9: Grid block pressures at the end of drawdown estimated by *Eclipse-300* (left) and *GPRS* (right).. 72

Figure 6-10: Condensate saturation distribution at the end of drawdown estimated by *Eclipse-300* and *GPRS.* 73

Figure 6-11: Condensate saturation distribution at the end of buildup estimated by *Eclipse-300* and *GPRS.* 73

Figure A-1: Schematic of constant volume depletion experiment. 83

Figure A-2: Schematic of constant composition expansion experiment. 84

Figure C-1: Pressure-saturation relationship by the steady-state model for the second test. 91

Figure C-2: Radial distribution of cond. saturation by the steady-state model for the second test. 92

Figure C-3: Pressure-saturation relationship by the three-zone model for the second test. 92

Figure C-4: Radial distribution of cond. saturation by the three-zone model for the second test. 93

Figure C-5: Horner plot for second pressure buildup test (single-phase pseudopressure). 93

Figure C-6: Horner plot for second pressure buildup test (syteady-state pseudopressure). 94

Figure C-7: Two-phase three-zone pseudopressure as a function of pressure for the second test. 94

Figure C-8: Horner plot for second pressure buildup test (three-zone pseudopressure). . 95

Figure D-1: Pressure-saturation relationship by the steady-state model for the third test. 96

Figure D-2: Radial distribution of cond. saturation by the steady-state model for the third test. 97

Figure D-3: Pressure-saturation relationship by the three-zone model for the third test.. 97

Figure D-4: Radial distribution of cond. saturation by the three-zone model for the third test. 98

Figure D-5: Horner plot for third pressure buildup test (single-phase pseudopressure). . 98

Figure D-6: Horner plot for third pressure buildup test (steady-state pseudopressure). .. 99

Figure D-7: Horner plot for third pressure buildup test (three-zone pseudopressure). 99

Figure E-1: Determining the pressure of the block containing the well (drawn from Aziz et al., 2006) 101

Chapter 1

1. Introduction

The optimization of gas-condensate reservoirs requires an adequate understanding of the phase behavior of gas-condensate systems under isothermal depletion and also requires accurate estimates of reservoir properties of zones bearing gas-condensate systems.

At the time of discovery, gas-condensate reservoirs are often above the dew-point pressure and single-phase gas is only present in the reservoir. However, as the reservoir is being depleted, the pressure drops below the dew point and a condensate bank develops around the wellbore. The condensate bank is richer in the heavier components of the original fluid and it impairs the deliverability of the wells due to the lower permeability to gas in the presence of condensate liquid.

Condensate banking also complicates the pressure transient test analysis due to multiphase flow and change in composition of the flowing mixture. Compared to the single-phase pseudopressure technique which assumes dry gas around the wellbore, the two-phase pseudopressure technique is expected to give more accurate estimates of reservoir properties because it considers the decrease in permeability to gas in the presence of condensate.

1.1. Single-Phase Pseudopressure

The single-phase pseudopressure technique was first proposed by Al Hussainy and Ramey (1966) and Al Hussainy et al. (1966) in order to linearize the real gas flow equation. The single-phase method works best for dry gas; therefore it can be applied on gas-condensate wells producing above the dew-point pressure. Once the pressure falls below the dew-point pressure, a condensate bank forms around the wellbore and the single-phase method deviates from the liquid-flow solution.

1.2. Two-Phase Pseudopressure

The two-phase pseudopressure can be estimated using two different models: the steady-state flow model and the three-zone flow model.

1.2.1. Steady-State Model

The steady-state model was first proposed by O’Dell and Miller (1967) and was later examined by Fussel (1973). The steady-state saturation-pressure relationship predicted by O’Dell and Miller (1967) and Fussel (1973) was later reproduced by Chopra and Carter

(1985) and Jones and Raghavan (1988). The steady-state model can be used to approximate the actual reservoir pressure-saturation relationship by assuming a hypothetical steady-state flow. The model assumes two flow regions around the wellbore with no transition zone: a near-wellbore region below the dew-point pressure where both gas and condensate are present and mobile, and an outer region above the dew-point pressure containing single-phase gas only. The pseudopressure computed by the steady-state model is referred to as the steady-state pseudopressure.

1.2.2. Three-Zone Model

The three-zone flow model was first introduced by Fevang (1995). Unlike the steady-state model, the three-zone flow model considered the existence of a transition zone (Region 2) where both gas and condensate are present, but only gas is mobile. The three flow regions around the wellbore assumed by the model are: a near-wellbore region where condensate and gas are present and mobile, a condensate build-up region where the condensate phase is immobile and only gas is flowing, and an outer region where only gas is present as shown on Figure 1-1. A pressure-saturation relationship was developed separately in each of the three regions. The pseudopressure computed by the three-zone model is referred to as the three-zone pseudopressure.

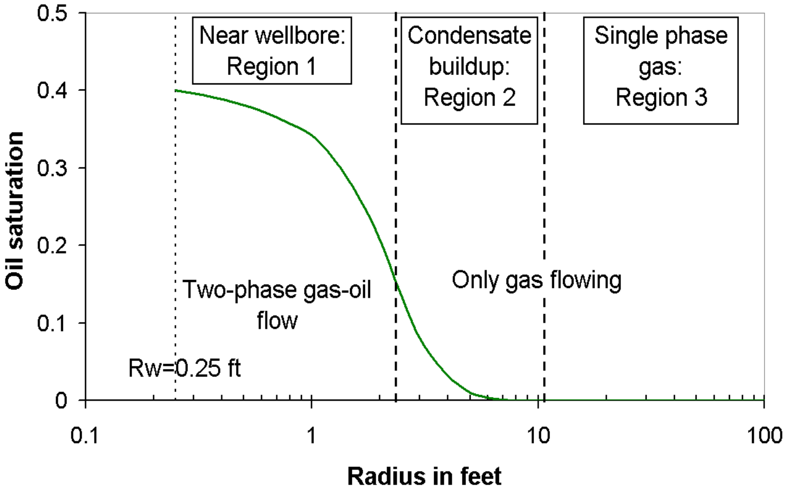

Figure 1-1: Gas-condensate three flow regions (from Roussennac 2001)

1.3. Research Background

Several published papers have compared the accuracy of each pseudopressure technique in estimating permeability and skin of well tests producing below the dew-point pressure. Jones et al. (1989) indicated that the single-phase method and the steady-state method estimated the formation flow capacity accurately. However, estimates of the skin factor would be high if the single-phase analog were used and would be low if the steady-state analog were used.

Using synthetic pressure drawdown data for a simple three-component gas mixture, Roussennac (2001) compared the accuracy between the steady-state method and the three-zone method in analyzing the data. Conclusions indicated that unlike the steady-state method which estimated permeability accurately but underestimated mechanical skin, the three-zone method estimated both accurately, permeability as well as mechanical skin.

1.4. Research Objective

The objective of the research was to investigate and quantify the deviations from the liquid-flow solutions that result from applying different pseudopressure estimations on actual fluid properties and actual pressure transient tests. The effect of condensate dropout around the wellbore on the well test analyses was also investigated. The pseudopressure estimations tested were: the single-phase pseudopressure, the steady-state pseudopressure and the three-zone pseudopressure. The results were compared to the conclusions of Roussennac (2001) in which the different pseudopressure techniques were applied on a self-generated synthetic data set representing a test of a gas-condensate well.

Chapter 2

2. Gas-condensate Flow Behavior

2.1. Gas-condensate Systems

At the original reservoir conditions, a gas-condensate is a single-phase fluid. Uusually, the fluid consists predominantly of methane (C_1) and other short-chain hydrocarbons. The fluid also contains small amounts of long-chain hydrocarbons (heavy ends). The methane content in gas-condensate systems ranges from 65 to 90 mol%, whereas in crude oil systems, methane content ranges from 40 to 55 mol%. On the other hand, lower heptanes-and-heavier (C_{7+}) content is reported for gas-condensate systems than for crude oil systems. Figure 2-1 compares the composition of gas-condensate systems with other categories of hydrocarbon systems. Typical compositions for the various hydrocarbon categories are compared on Table 2-1.

Most known gas-condensate reservoirs are discovered in formation pressures and temperatures in the ranges of 3,000 to 8,000 psi and 200 to 400^{o}F, respectively (Moses and Donohoe, 1962). These wide ranges of pressures and temperatures, along with the wide composition ranges, provide a large variety of conditions for gas-condensate phase behaviors. This increases the challenge for reservoir engineers when studying the gas-condensate systems to achieve the optimum development and operation plan.

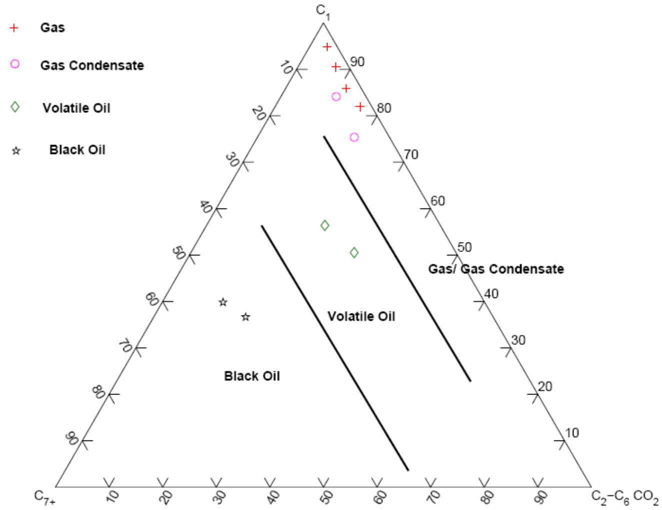

Figure 2-1: Ternary visualization of hydrocarbon classification (from Whitson and Brule 2000).

At pressures below the dew-point pressure and at certain conditions of temperature, retrograde condensation will occur in the single-phase fluid and the fluid system will separate into two phases: a gas phase and liquid phase. The liquid phase is richer in heavy ends and the gas phase is depleted of heavy ends. As the pressure continues to decrease, more liquid phase is dropped out of solution up to a maximum volume. Then, liquid volume starts to decrease as illustrated in the pressure-temperature (*p*-*T*) diagram (Figure 2-2). Typically, a gas-condensate system yields from about 30 bbl of condensate per MMscf of gas for lean gas-condensate to 300 bbl of condensate per MMscf of gas for rich gas-condensate (Kamath, 2007).

Table 2-1: Typical composition of three fluid types from Wall (1982).

Component	Black Oil	Volatile Oil	Condensate	Gas
Methane	48.83	64.36	87.07	95.85
Ethane	2.75	7.52	4.39	2.67
Propane	1.93	4.74	2.29	0.34
Butane	1.6	4.12	1.74	0.52
Pentane	1.15	2.97	0.83	0.08
Hexane	1.59	1.38	0.6	0.12
C7+	42.15	14.91	3.8	0.42

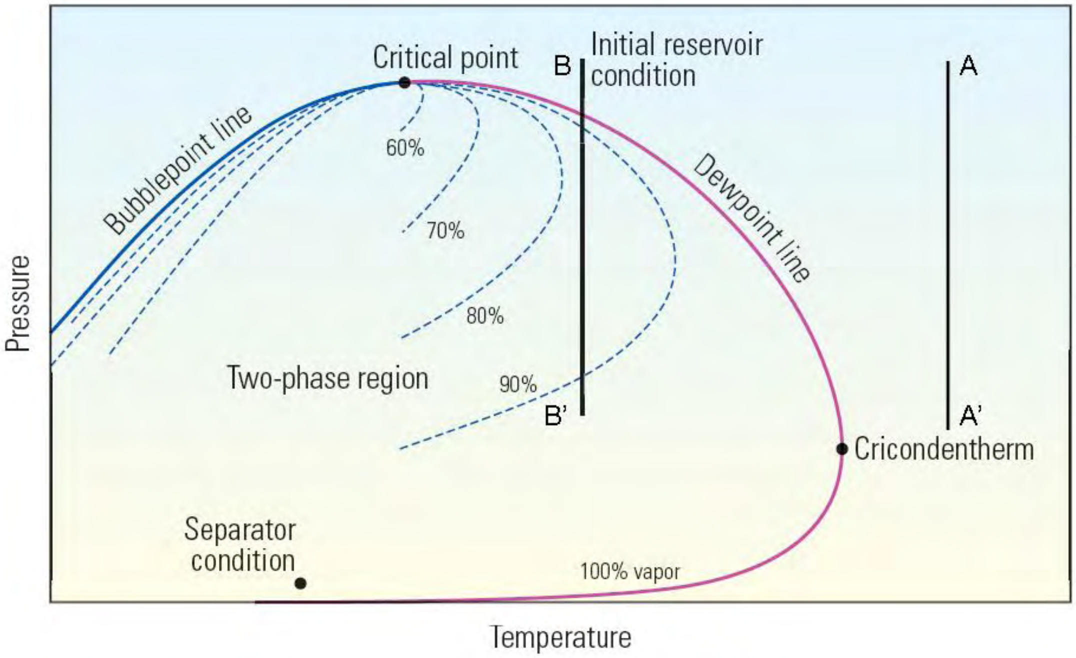
Critical point
B
Initial reservoir condition
A
Bubblepoint line
60%
70%
80%
90%
Dewpoint line
Pressure
Two-phase region
B'
A'
Cricondentherm
Separator condition
100% vapor
Temperature

Figure 2-2: Phase diagram of a gas-condensate system from Fan et. al. (2005).

2.2. Flow Behavior

The flow behavior of a gas-condensate reservoir depends on the phase envelope of the fluid system and the reservoir conditions. The phase envelope consists of the bubble-point line and the dew-point line meeting at the critical point. During isothermal expansion, the first bubble of gas vaporizes from the liquid at the bubble-point line. In contrast, the first droplet of liquid condenses from vapor at the dew-point line. At the critical point, the vapor and liquid phases cannot be distinguished because the composition and all other intensive properties of the two phases become identical.

Gas and gas-condensate reservoirs are determined by the phase envelope in the initial reservoir conditions. If the reservoir temperature is above the cricondentherm temperature, the reservoir will follow the A-A’ path during isothermal expansion and the two-phase region will not be entered. Therefore, the reservoir fluid will remain as gas and the fluid composition will remain constant during depletion.

On the other hand, if the reservoir temperature is between the critical temperature and the cricondentherm temperature, the reservoir will follow the B-B’ path during isothermal expansion. Retrograde condensation will start to occur at the reservoir when the B-B’ path crosses the dew-point line. Below the critical condensate saturation, the condensate mobility is zero and only gas will flow. Consequently, the flowing fluid composition will change. This phenomenon is captured by the three-zone assumption as will be explained later in Chapter 4. As the pressure decreases in the reservoir, more condensate will drop out until the condensate saturation reaches the critical saturation. At this event, condensate will start to mobilize in the reservoir. If the pressure is further depleted, some of the condensate will start to revaporize and the condensate volume will decrease.

The properties of the separated phases in the gas-condensate systems can vary considerably. The C_1 contents of the gas phase remain high and can vary from 70 to 90 mol%. In addition, the C_{7+} fractions remain very low at less than one mol%. In contrast, for the liquid phase (condensate), the C_1 contents can vary from 10 to nearly 30 mol% and the C_{7+} contents vary from 40 to 70 mol% (Moses and Donohoe, 1962). The properties of the separated phases will be highlighted next when the behavior of the gas-condensate system under study is further investigated.

2.3. PVT Measurement

An important prerequisite for using an EOS-based compositional model is achieving satisfactory agreement between equation of state (EOS) results and laboratory fluid property measurements (PVT). Here, a commercial simulator was used to perform phase-equilibrium and property calculations based on the Peng-Robinson (PR) EOS in order to match a variety of laboratory PVT results. The commercial simulator is capable of using nonlinear regression calculation that performs automatic adjustments of EOS parameters to match the PVT measurements. The PVT measurements for the gas-condensate system included fluid compositional analysis at separator conditions, constant volume depletion (CVD) and constant composition expansion (CCE).

2.3.1. Fluid Components

The first step in the PVT simulation was to define the components that comprise the fluid system. The 12-component system contained 11 well-defined components: N_2, CO_2, H_2S, C_1, C_2, C_3, i-C_4, n-C_4, i-C_5, n-C_5 and n-C_6, and one pseudocomponent (C_{7+}) into which the heavy components were lumped. Table 2-2 lists the separation data for the gas and condensate samples collected in the field and the well stream composition at the dew-point pressure obtained from the CVD experiment.

Table 2-2: Hydrocarbon analysis of separator products and well stream

Component	Separator Liquid Mol%	Separator Gas Mol%	Well Stream Mol%
N_2	0.52	10.95	10.07
CO_2	0.65	2.14	2.01
H_2S	2.24	2.69	2.65
C_1	12.29	71.92	66.89
C_2	4.30	7.08	6.85
C_3	4.43	2.92	3.05
iC_4	1.50	0.51	0.59
nC_4	4.04	0.99	1.25
iC_5	2.40	0.28	0.46
nC_5	2.97	0.27	0.50
C_6	6.07	0.18	0.68
C_{7+}	58.59	0.07	5.00
Total	100	100	100

Coats and Smart (1986) argued that extensive splitting of the C_{7+} fraction to match laboratory data was generally unnecessary. In compositional simulation, lumping has been a common industry practice in order to significantly speed up the simulation process.

2.3.2. Constant Volume Depletion (CVD) Experiment

The CVD experiment is designed to provide the well stream composition at different reservoir pressures, to determine the dew-point pressure for the fluid system and to estimate the condensate saturation in the reservoir during pressure depletion. The procedures to conduct the CVD experiment are presented in Appendix A.

At 275^{o}F reservoir temperature, the dew-point pressure for the gas-condensate system was determined to be approximately 5,718 psi. During the experiment, the maximum liquid dropout was estimated to be around 9.5% at 2,200 psi. Figure 2-3 plots the condensate saturation at different cell pressures obtained from the CVD experiment. This plot was matched by the PVT simulator as will be discussed later in this chapter.

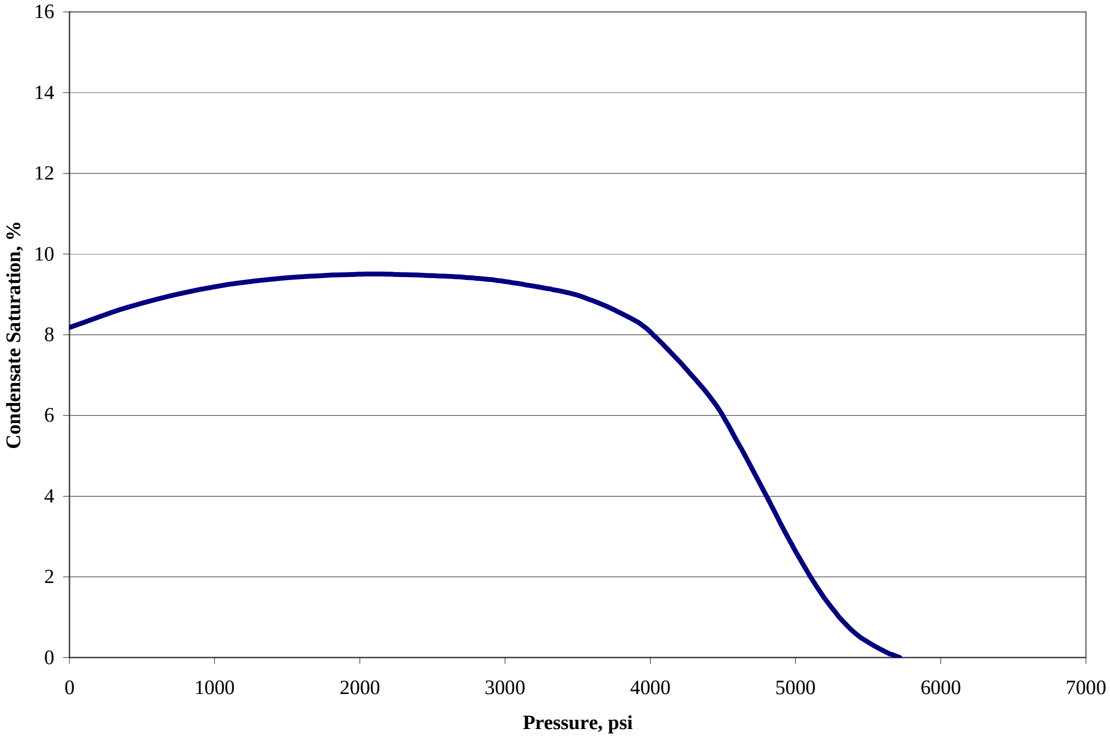

Figure 2-3: Condensate saturation as a function of pressure from CVD experiment.

2.3.3. *Constant Composition Expansion (CCE) Experiment*

The CCE experiment for gas-condensate samples is usually conducted to estimate the total relative volume, V_{rt}. V_{rt} is defined as the volume of gas or gas and condensate mixture divided by the volume at the dew-point pressure (Whitson and Brule, 2000). Figure 2-4 plots the total relative volume as a function of pressure obtained from the CCE experiment. This plot was also matched by the PVT simulator. More information about the CCE experiment is presented in Appendix A.

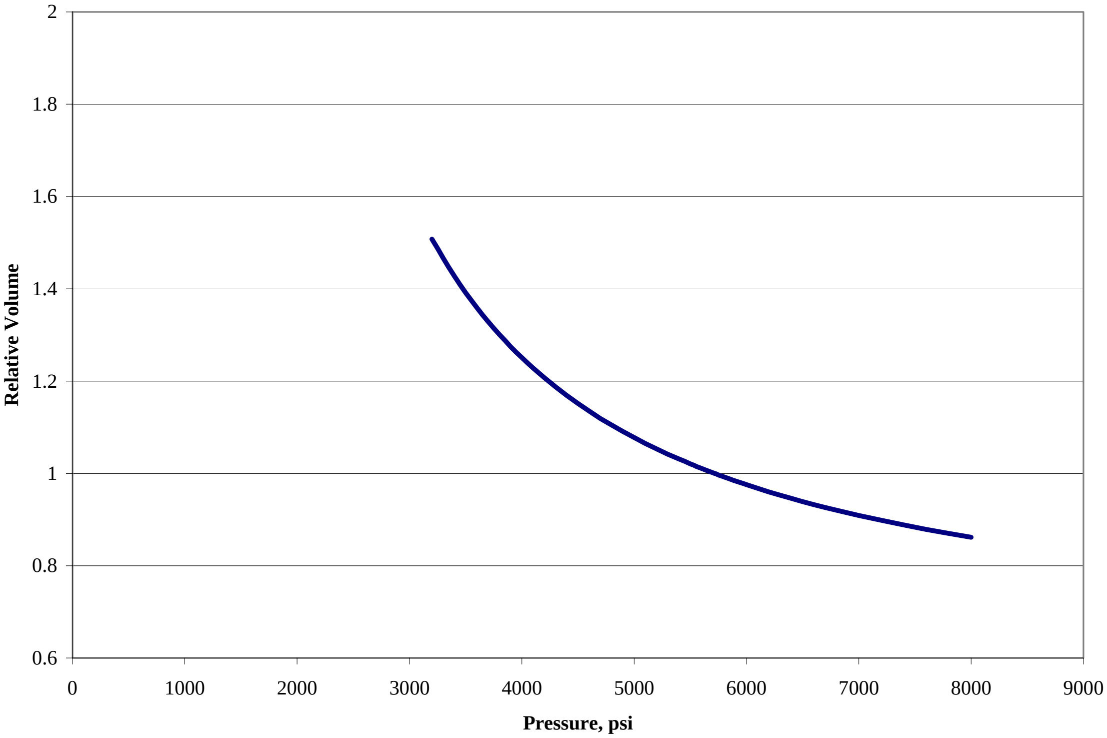

Figure 2-4: Total relative volume as a function of pressure from CCE experiment.

2.4. PVT Simulation

The first step of simulating the PVT measurements was defining the components that comprised the well stream. The reservoir conditions were also input into the program. The binary interaction coefficients between C_1 and C_2 through C_6 were assumed to be zero as recommended by Katz and Firoozabadi (1978). The Peng-Robinson EOS was assumed. Then, nonlinear regression was applied in order to match the actual PVT measurements.

As outlined by Coats and Smart (1986), nonlinear regression was applied on Ω_a and Ω_b of the C_{7+} fraction. The adjustment of Ω_a and Ω_b should be interpreted as an adjustment to the critical properties because they are related by cubic EOS parameters, a and b as shown in Eq. (2-1) and Eq. (2-2):

$$a = \Omega_a \frac{R^2 T_c^2}{p_c} \qquad \textbf{(2-1)}$$

$$b = \Omega_b \frac{R T_c}{p_c} \qquad \textbf{(2-2)}$$

Ω_a and Ω_b of C_1 were also included in the nonlinear regression as recommended by Coats and Smart (1986). Using sensitivity analysis, it was determined that the fluid model is very sensitive to the binary interaction coefficients between methane and the plus fractions. Binary interaction coefficients are introduced in order to compensate for the nonsphericity of the heavy hydrocarbons (Pederson et al., 1989). Therefore, methane-plus fraction binary interaction coefficients were included in the nonlinear regression.

Figure 2-5 shows the liquid saturation match for the CVD experiment and Figure 2-6 shows the relative volume match for the CCE experiment. The observed dew-point pressure was 5,718 psia and the model estimated the dew-point pressure to be 5,720 psia which indicated a very good match.

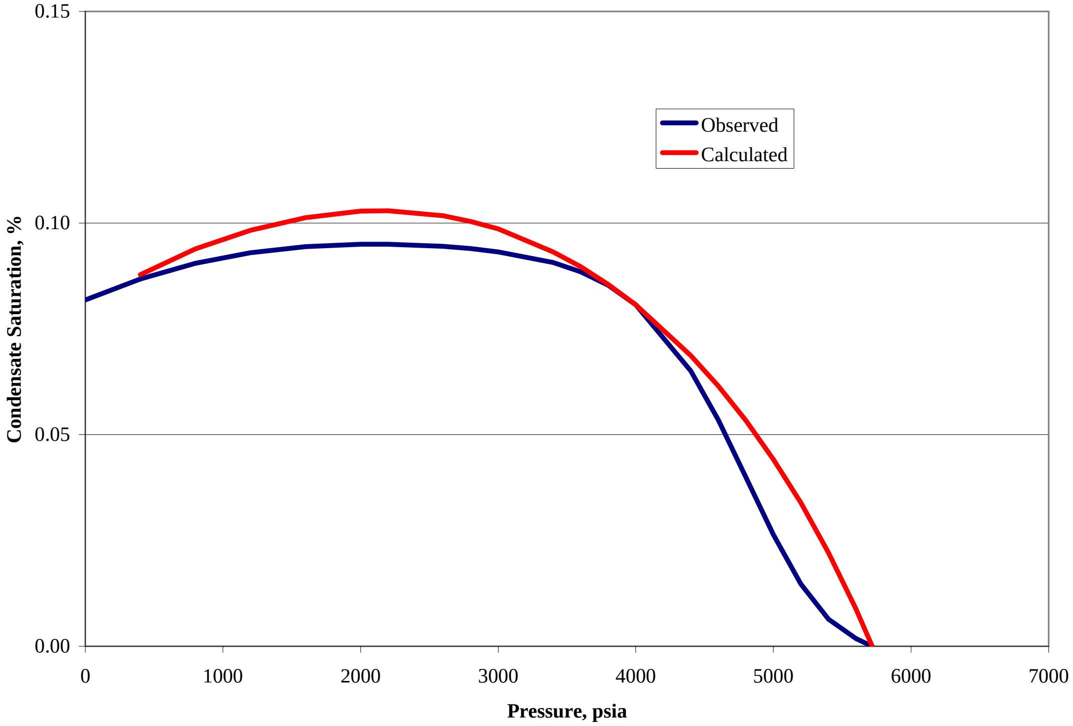

Figure 2-5: Observed vs. calculated condensate saturation during CVD experiment.

Compositional data of the separator fluid samples were used to confirm the accuracy of the EOS model. When the fluid model was flashed to separator conditions of 675 psia pressure and 152°F temperature, a good agreement between the measured and calculated compositions for vapor and liquid phases was observed as illustrated on Figure 2-7 and Figure 2-8, respectively.

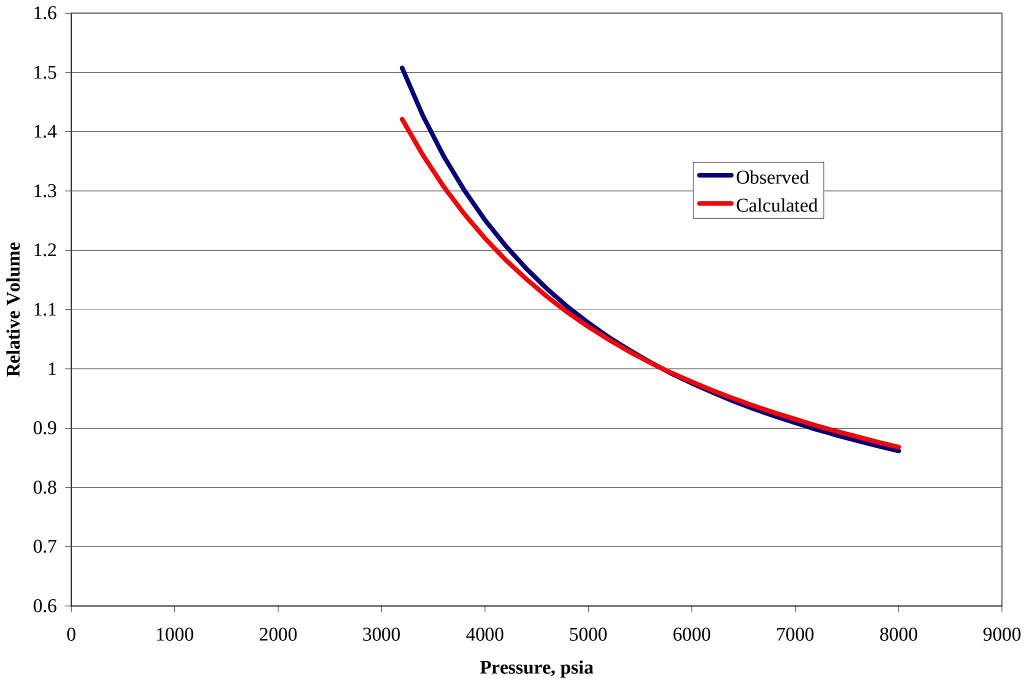

Figure 2-6: Observed vs. calculated total relative volume during CCE experiment.

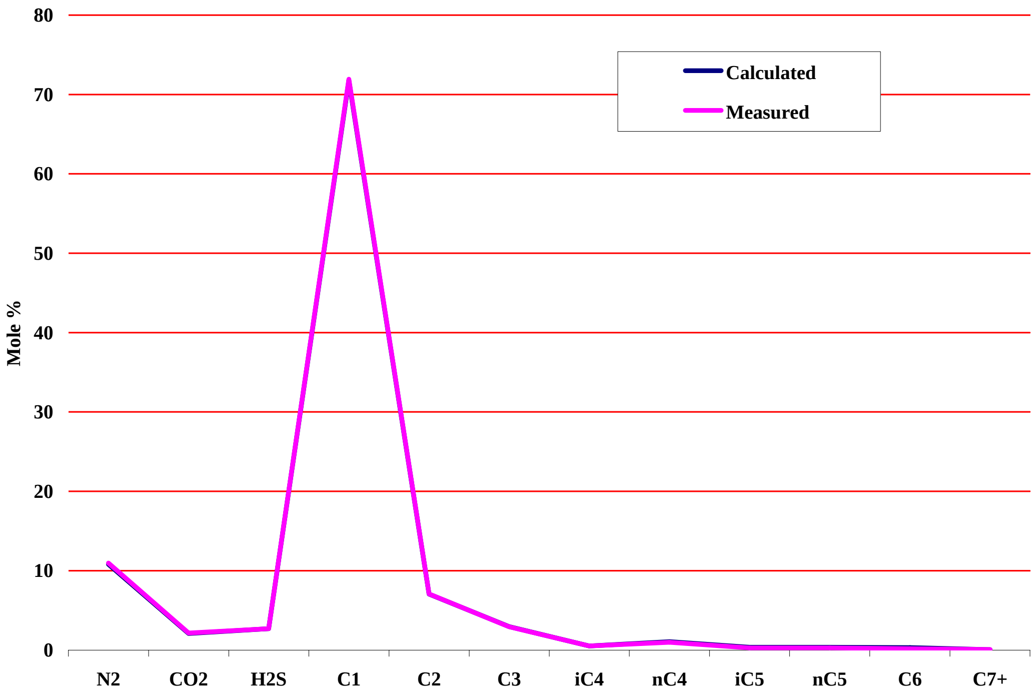

Figure 2-7: Measured vs. calculated gas phase composition at separator conditions.

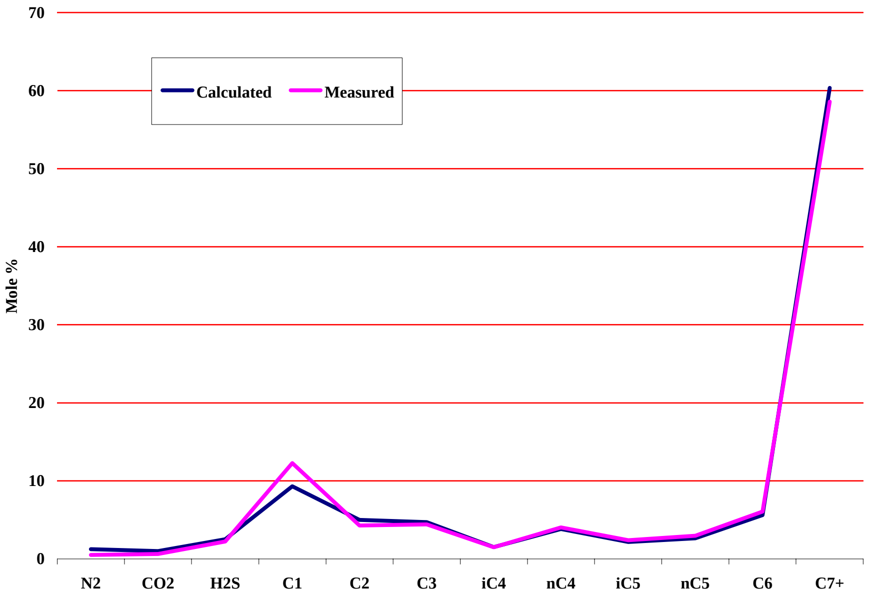

Figure 2-8: Measured vs. calculated liquid phase composition at separator conditions.

Figure 2-9 shows a plot of the critical pressure and critical temperature for all hydrocarbon elements in the mixture. The plot indicates that the calculated critical pressure and critical temperature for the C_{7+} fraction follows the overall trend observed for the well-defined components. The critical pressure decreases as the molecular weight of the hydrocarbon increases. On the other hand, the critical temperature increases as the molecular weight of the hydrocarbon increases. Therefore, the calculated critical properties were considered acceptable.

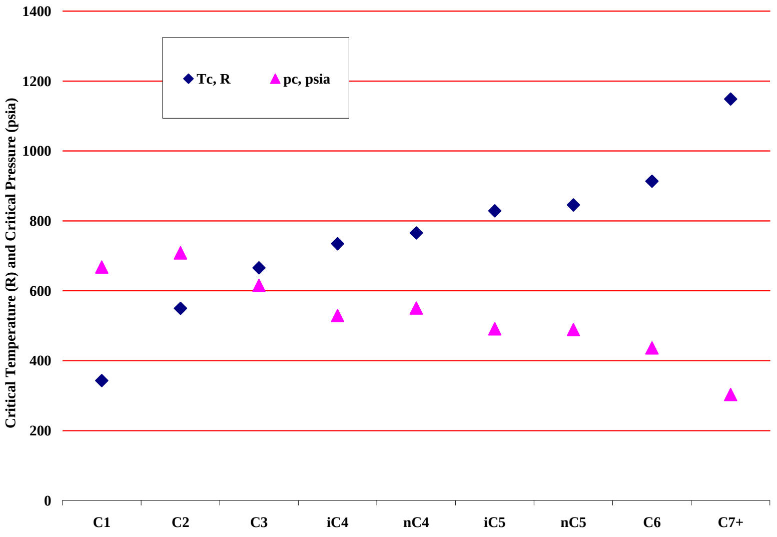

Figure 2-9: Critical temperatures and pressures for well stream components.

Chapter 3

3. Compositional Simulation

3.1. Radial Model

A commercial compositional simulator equipped with Peng-Robinson (PR) equation of state was used to model the behavior of a gas-condensate well and to regenerate pressure transient test data. The final radial model consisted of a reservoir fluid model, a fluid-rock petrophysical model, a well model and a grid-block model. The fluid and reservoir properties of these models were obtained from a gas-condensate well (Well-A) drilled in a Middle Eastern field.

The compositional simulator was then used to regenerate three actual pressure buildup tests conducted on Well-A. The first test was conducted after Well-A was drilled and before an acid stimulation job was pumped. After the acid stimulation job was completed and before the well was put on production, a second pressure buildup test was conducted. Finally, a third pressure buildup test was conducted after the well had been on production for around a year.

3.1.1. Reservoir Fluid Model

The reservoir fluid model was obtained from the simulation of the actual PVT measurements as presented in Chapter 2.

3.1.2. Rock-Fluid Petrophysical Model

There are two different sets of laboratory experiments required to describe the petrophysical model. One set is under single-phase flow conditions and is conducted to estimate porosity and absolute permeability. The other set is conducted under multiphase flow conditions to construct the relative permeability curves.

At laboratory conditions, the porosity and permeability measured using a representative core sample acquired from the field were approximately 17% and 11 md, respectively. However, permeability values measured from cores at laboratory conditions are considered uncertain (Penuela and Civan, 2000). The actual permeability value for Well-A was expected to be lower due to overburden pressure. Therefore, the permeability variable was chosen as a parameter to be adjusted in the history matching process.

A set of multiphase experiments were also carried out to determine the relative permeability curves. Both steady-state and unsteady-state oil-gas relative permeability experiments were performed on a core sample taken from the reservoir. Steady-state experiments were carried out to define the oil-gas relative permeability curve, while unsteady-state experiments were used to define the end points. Figure 3-1 plots the relative permeability curves that were included in the radial model.

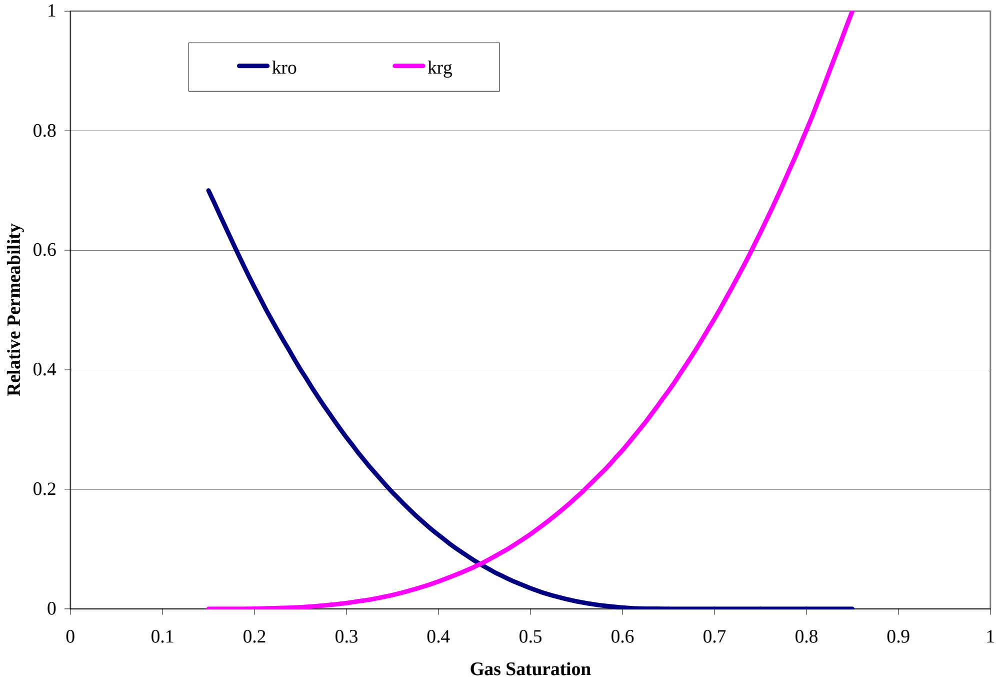

Figure 3-1: Relative permeability curves used on Well-A radial model.

3.1.3. Well Model

The well model used engineering data from the drilling and completion history of the well, such as the wellbore radius and the net pay interval. The stimulation job was captured as a negative mechanical skin factor in the well model. Additional data contained in the well model were information about the reservoir properties as summarized in Table 3-1.

Table 3-1: Simulation parameters for the well radial model.

Parameter	Value
Initial reservoir pressure, psi	7000
Average porosity	0.17
Formation thickness, ft	75
Reservoir top level, ft	10,500
Roc compressibility, psi^{-1}	5.00E-06
Wellbore radius, ft	0.25

3.1.4. Grid Model

The use of fine grids near the wellbore is required for compositional simulation due to several physical effects of gas-condensate wells, such as:

- flowing pressure profile,
- phase distribution,
- relative permeability.

In gas-condensate wells where the bottom hole pressure is below the dew-point pressure, the gas becomes saturated in the near-wellbore region and condensate is dropped out of solution. Depending on the condensate relative permeability, the volume of liquid that is actually deposited in the reservoir is significantly higher than the liquid volume estimated by the CVD experiment. Therefore, fine near-well gridding is required to accurately predict the pressure profile that the gas experiences on its way to the wellbore. Away from the wellbore, pressure drops are lower and wider-spaced gridding is considered acceptable (Bertram et. al. 1997).

A single-layer radial model consisting of 30 cells whose sizes were increased logarithmically away from the wellbore was used in the compositional simulation. The sizes of the grid blocks are shown on Table 3-2.

Table 3-2: Cell sizes in radial direction.

Cell size, ft:	0.4429	0.5300	0.6539	0.9655	1.4255	2.1046
	3.1072	4.5867	6.7732	10	10	10
	10	35	40	47	68	100
	150	200	200	300	500	500
	500	500	500	500	500	500

In his radial model study, Roussennac (2001) pointed out that producing gas-oil ratio (GOR) and block condensate saturation could be used to indicate the numerical stability of the grid model when simulating two-phase flow cases. Large oscillations in the producing GOR and in the condensate saturation resulted in reservoir pseudopressure that did not match the liquid solution indicating instability in numerical simulation as shown on Figure 3-2. After tuning the grid size, the oscillations were minimized and a match between the reservoir pseudopressure and the liquid solution was achieved as shown on Figure 3-3. The grid size distribution was then optimized.

Figure 3-4 plots the producing GOR behavior during the second well test simulated for the study. The minimum oscillation in the GOR behavior indicated a stable numerical simulation. The gradual increase in the producing GOR and then the sudden drop will be further investigated in Chapter 6.

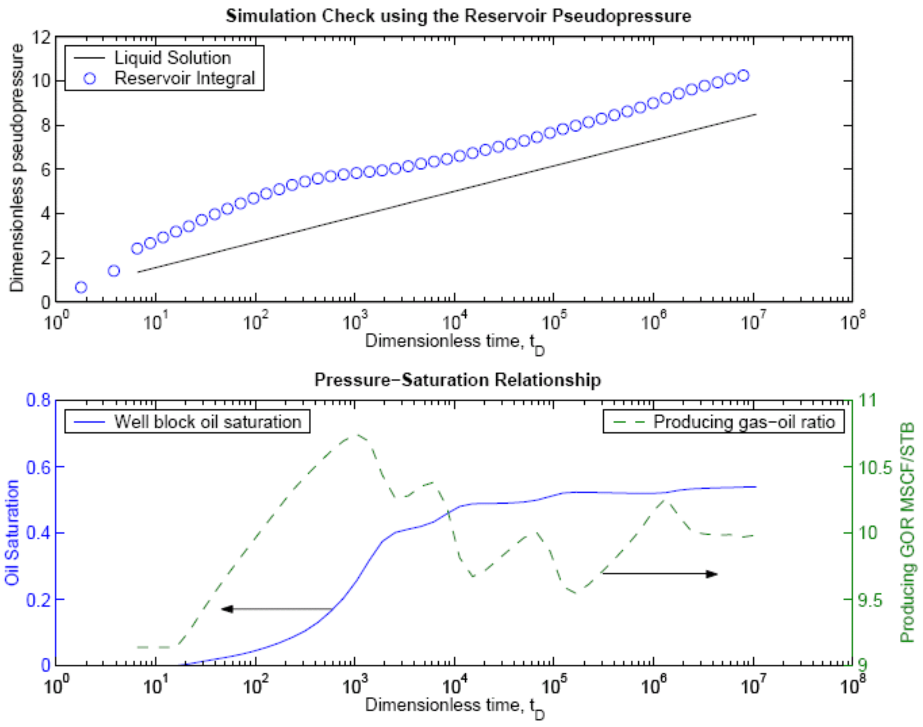

Figure 3-2: Radial grid size distribution with nonsmooth changes (from Roussennac 2001).

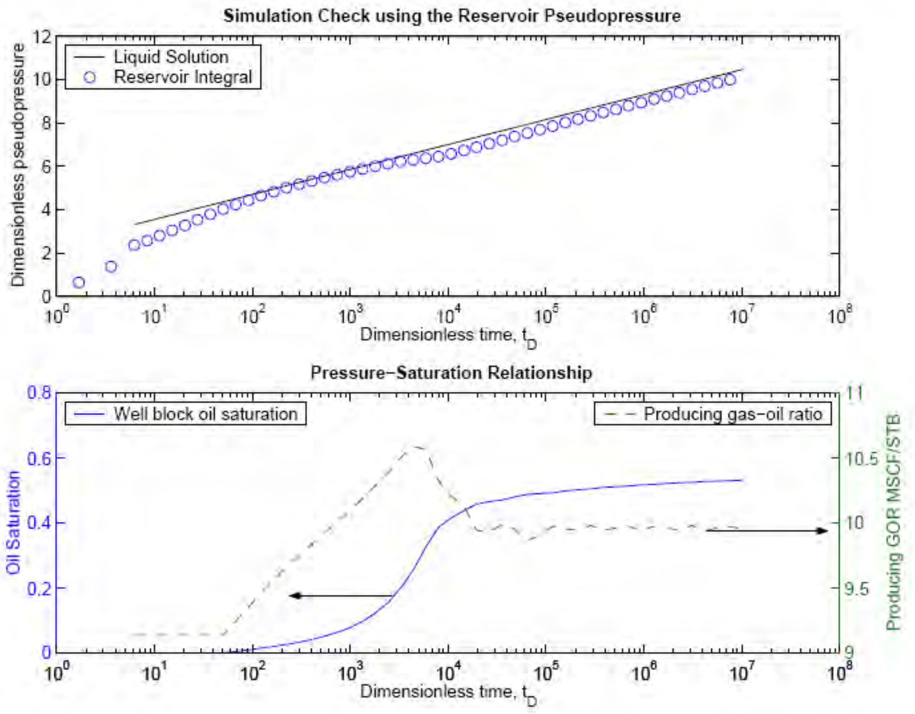

Figure 3-3: Radial grid size distribution with smooth changes (from Roussennac 2001).

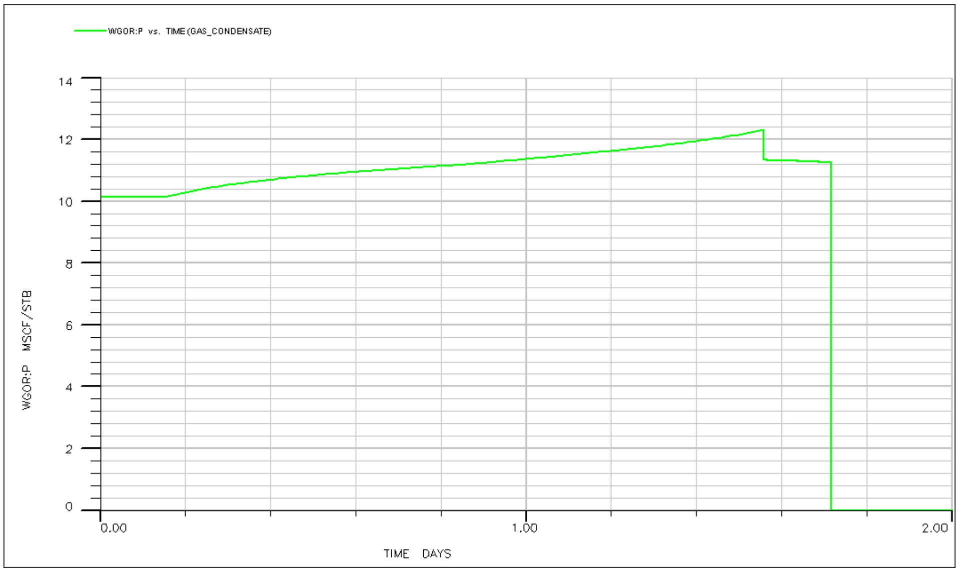

Figure 3-4: Producing GOR behavior during the second well test.

3.2. Model Applicability

In order to test the applicability of the model, a short drawdown in which the bottom hole pressure was above the dew-point pressure, followed by a pressure buildup was simulated as shown on Figure 3-5. The model input permeability and skin were 3 md and -3.6, respectively. The buildup test was then analyzed using a commercial well test analysis software. Permeability and skin estimated by the single-phase pseudopressure analysis on the generated pressure data were 2.7 md and -3.5, respectively, which are very close to the model input parameters. Therefore, a good agreement between the model input parameters and the pressure buildup analysis results was observed.

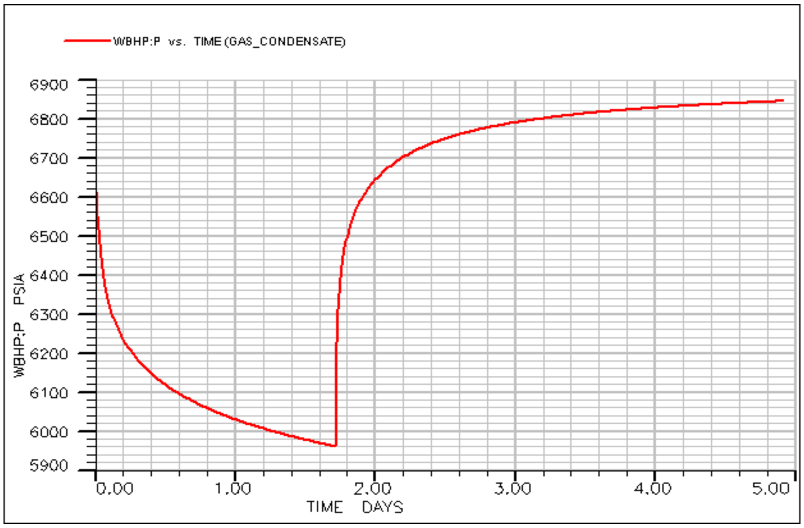

Figure 3-5: Pressure buildup test to examine model applicability.

3.3. Simulation Runs

The final radial model was employed by *Eclipse-300* to regenerate and history match the actual pressure tests conducted on Well-A by modifying the model permeability and mechanical skin. The model was also used to predict the condensate behavior around the wellbore during the tests. Appendix B shows a sample of *Eclipse-300* input file that was used during the study.

The second pressure buildup test was regenerated first because, unlike the first test, an onsite separator was employed during the second test. Therefore, the production rates measured by the separator for the second test were more reliable compared to the production rates estimated during the first test which only used a venturi meter on the wellhead. Venturi meters are considered less accurate than the onsite separators. The permeability value that was input to history match the second test was assumed again for the first test; however, the assumed skin value for the first test was higher (prestimulation).

3.3.1. second Pressure Buildup Test (Poststimulation)

During the second test, the well was allowed to flow at 50 MMscfd for 41.2 hrs and then the well was shut for a buildup period of 76.6 hrs. A permeability of 5.5 md and a skin of -4.0 were used to generate the pressure data using the compositional simulator. Figure 3-6 shows a fairly good match for the downhole pressure gauge data during the second test which was conducted after the acid stimulation job. The compositional simulator also predicted the condensate bank radius (two-phase region) at the end of the drawdown to be around 30 ft as shown on Figure 3-7.

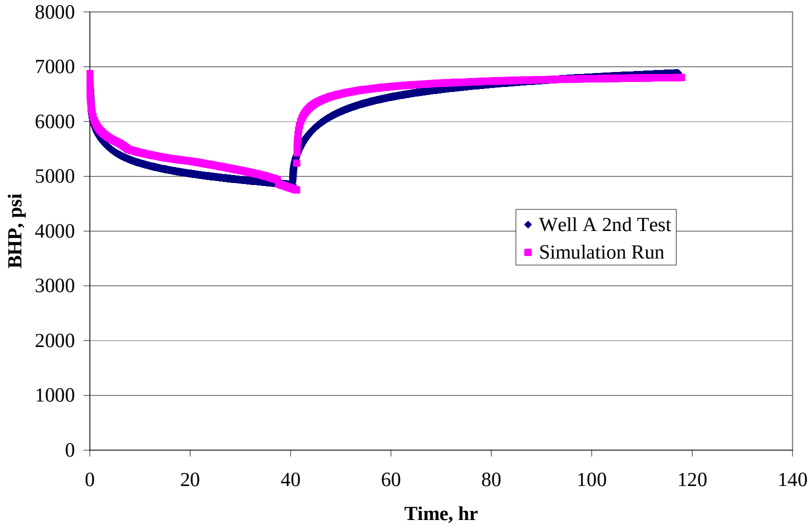

Figure 3-6: History plot of the second well test.

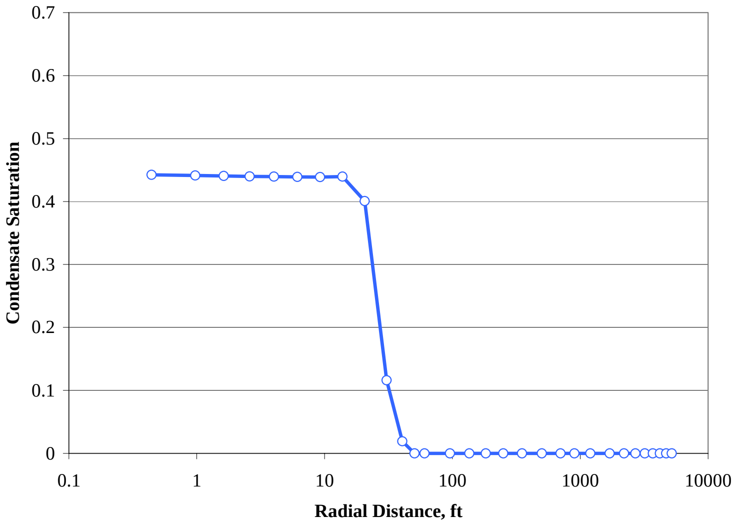

Figure 3-7: Radial distribution of condensate saturation at the end of the second test drawdown.

3.3.2. first Pressure Buildup Test (Prestimulation)

During the prestimulation test or first test, the well was allowed to flow at 52 MMscfd for 24.9 hrs and then the well was shut for a buildup period of 48.8 hrs. The test was history matched assuming the same permeability (5.5 md). However, the mechanical skin was higher (-3.3). The negative skin prior to the stimulation job could have been caused by the perforation job that was conducted across the pay zone. Figure 3-8 shows the condensate saturation around the wellbore at the end of the drawdown. 30 ft of condensate bank around the wellbore was also predicted. Figure 3-9 compares the downhole pressure gauge data measured during the actual test and the pressure data predicted by the compositional simulator. Due to inaccuracy of rate measurement during the drawdown, this part of the test could not be matched properly.

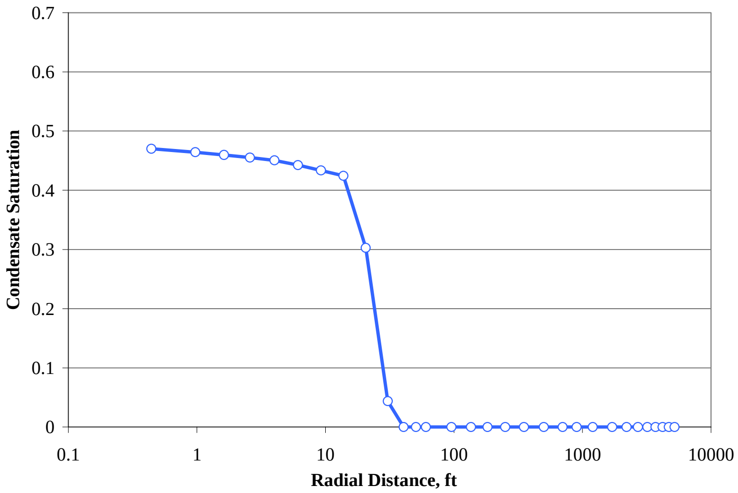

Figure 3-8: Radial distribution of condensate saturation at the end of the first test drawdown.

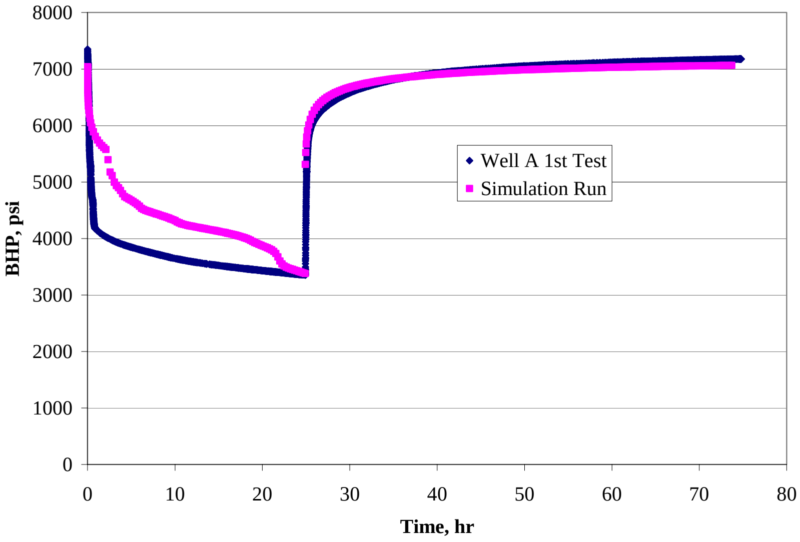

Figure 3-9: History plot of first well test.

3.3.3. Third Pressure Buildup Test

The third test that was conducted after one year of gas production was history matched using similar permeability and mechanical skin used in the second test because the well completion was not modified and the well was not intervened any time between the two tests. During the test, the well was allowed to flow for 57.6 hrs and then the well was shut for a buildup period of 153.6 hrs. Simulation results indicated that the one year of production at pressures below the dew point caused the condensate bank radius to increase to around 180 ft as shown on Figure 3-10. The effect of the increase in the condensate bank radius or the two phases on the pseudopressure analyses will be discussed in Chapter 5.

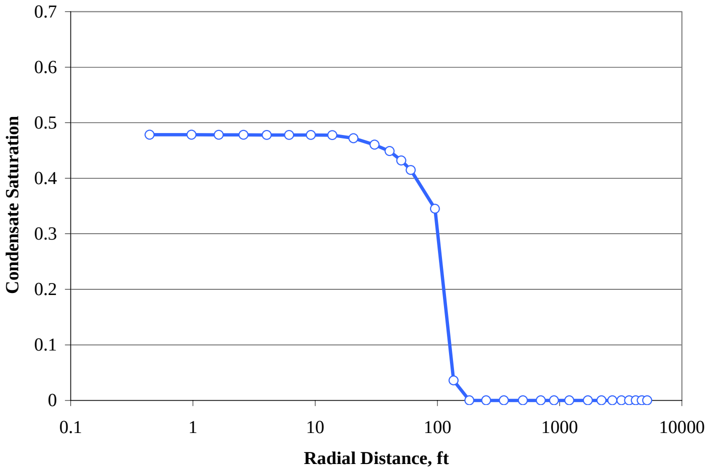

Figure 3-10: Radial distribution of condensate saturation at the end of the third test drawdown.

Chapter 4

4. Well Test Analysis

4.1. Introduction

The linear diffusion equation governing the pressure transient of a well test is given by:

$$\nabla^2 p - \frac{1}{K}\frac{\partial p}{\partial t} = 0 \tag{4-1}$$

$K = \frac{k}{\phi \mu c_t}$ is called the hydraulic diffusivity of the porous medium.

The following assumptions listed in Horne (1995) are inherent in Eq. (4-1):

a. Darcy’s law applies,

b. Flow is single phase,

c. Porosity, permeability, viscosity and compressibility are constant,

d. Fluid compressibility is small,

e. Gravity and thermal effects are negligible,

f. Pressure gradients in the reservoir are small.

4.1.1. Pseudopressure and Pseudotime

Eq. (4-1) was established for a single-phase slightly compressible fluid. However, in gas reservoirs, viscosity and compressibility vary with pressure and Darcy’s law may not apply. In addition, for gas-condensate reservoirs producing below the dew-point pressure, gas and condensate are present together and multiphase flow occurs in the reservoir. Consequently, Eq. (4-1) is not valid for such fluids in porous media.

For gas and gas-condensate reservoirs, the equations governing pressure transmission in porous medium are nonlinear. Therefore, a variable $m(p)$ named pseudopressure was introduced by Al Hussainy and Ramey (1966) and Al Hussainy et al. (1966) to linearize the equation governing pressure transmission:

$$\nabla^2 m(p) - \frac{1}{K}\frac{\partial m(p)}{\partial t} = 0 \tag{4-2}$$

Eq. (4-2) is linear with respect to pseudopressure, *m(p)*. However, the hydraulic diffusivity term, *K*, is still a function of pressure and therefore, of pseudopressure. In practice, treating this equation as linear is permissible and it only requires substituting the values of viscosity, μ, and compressibility, c_t, estimated at the initial reservoir pressure (Horne 1995). Nevertheless, the above equation can be further linearized by the introduction of pseudotime developed by Agarwal (1979). Agarwal's pseudotime is defined as:

$$t_{pseudo} = \int_0^t \frac{1}{\mu c_t} dt \tag{4-3}$$

For multiphase well tests, i.e. gas-condensate reservoirs, the relative permeability data at reservoir conditions must be considered for the pseudopressure calculation. Thus, the multiphase pseudopressure becomes more complex.

In this study, three different methods to compute the pseudopressure were applied to the three pressure buildup tests introduced in Chapter 3. The three pseudopressure methods were:

1. single-phase pseudopressure,
2. two-phase steady-state pseudopressure,
3. two-phase three-zone pseudopressure.

The accuracy of each method in estimating permeability and skin will be discussed by comparing the computed dimensionless pseudopressure with the liquid solution and also by applying Horner plot analysis.

4.1.2. Dimensionless Variables

In dimensionless form, Eq. (4-2) can be written as:

$$\nabla^2 p_D - \frac{\partial p_D}{\partial t_D} = 0 \tag{4-4}$$

The dimensionless pseudopressure, as described by Al Hussainy et al. (1966), is given by:

$$p_D(t_D) = \frac{0.00633\pi kh}{q_t TR}[m(p_{ws}) - m(p_{wf,s})] \quad \textbf{(4-5)}$$

where $m(p_{ws})$ is the pseudopressure at the bottom hole shut-in pressure and $m(p_{wf,s})$ is the pseudopressure at the instant the wellbore is shut-in.

The dimensionless shut-in time is defined by:

$$\Delta t_D = \frac{0.0002637k\Delta t}{\phi\left(\mu_g c_g\right)_s r_w^2} \quad \textbf{(4-6)}$$

where $(\mu_g c_g)_s$ is viscosity/compressibility product evaluated at the instant the well is shut in, $p_{wf,s}$.

The liquid solution for a well in an infinite homogeneous reservoir is given by:

$$p_{wD}(t_D) = \frac{1}{2}(\ln t_D + 0.8091) + s \quad \textbf{(4-7)}$$

where s is the skin factor defined by Hawkins (1956) as:

$$s = \left(\frac{k}{k_s} - 1\right)\ln\frac{r_s}{r_w} \quad \textbf{(4-8)}$$

On a semilog plot of dimensionless pressure, p_D, as a function of logarithmic dimensionless time, t_D, the liquid solution, p_{wD}, is represented by a straight line. The slope of the straight line is 1.1513. The pseudopressure should give exactly the same straight line on the semilog plot if the pseudopressure is the right liquid analog. Then, the pseudopressure method should yield the correct permeability and skin. Hence, the semilog plot of p_D vs. t_D was utilized in this work to determine the accuracy of each pseudopressure method in estimating permeability and skin.

Errors in permeability estimation by the pseudopressure method are represented by a deviation in the slope between the pseudopressure and the liquid solution. On the other hand, errors in skin estimation are represented by vertical shifts. The semilog analysis using pseudopressure for a drawdown test is summarized in Figure 4-1.

4.1.3. Horner Plot Analysis

The Horner method to analyze pressure buildup tests was developed by Horner (1951). The Horner method plots pressure as a function of logarithm Horner time *HT* (Eq. 4-9).

During infinite-acting radial flow, Horner straight line shown on Figure 4-2 can be used to estimate permeability and skin.

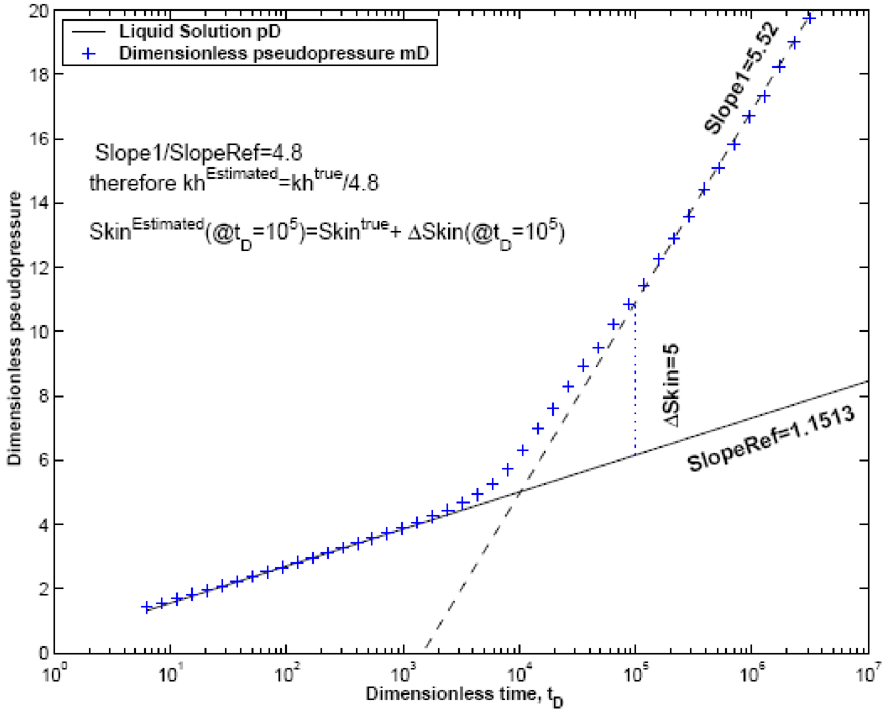

Figure 4-1: Semilog analysis using pseudopressure (from Roussennac 2001).

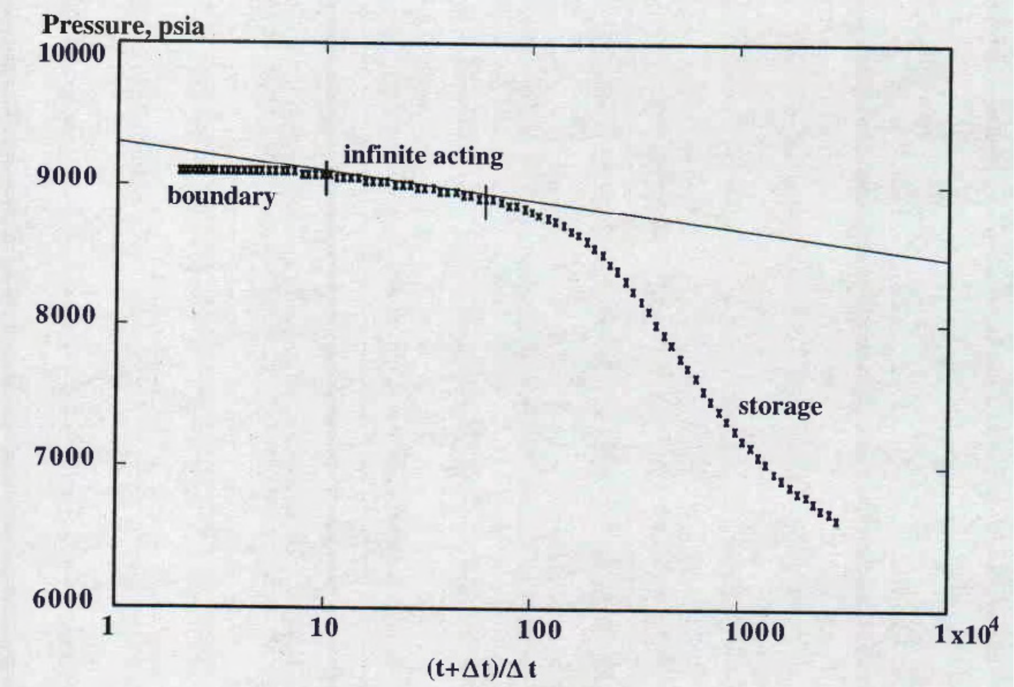

Figure 4-2: Semilog Horner plot for a pressure buildup test (from Horne 1995).

$$HT = \frac{t_p + \Delta t}{\Delta t} \tag{4-9}$$

For gas-condensate pressure buildup tests, the Horner method is employed to plot the pseudopressure as a function logarithm Horner time. However, Horner time is now given by:

$$HT = \frac{t_p + \Delta t}{\left[\dfrac{(\mu_g c_g)_i}{(\mu_g c_g)_s}\Delta t\right]} \tag{4-10}$$

where $(\mu_g c_g)_i$ is computed with the initial composition and $(\mu_g c_g)_s$ is computed using the gas composition at the bottom hole shut-in pressure, p_{ws}. Reynolds et al. (1987) indicated that this Horner time ratio yielded more accurate estimates of permeability and skin.

As mentioned earlier, the infinite-acting radial flow is indicated by a straight line on the semilog Horner plot. The slope of straight line, *m*, can be used to calculate the flow capacity using the following equation (Horne 1995):

$$kh = \frac{5.794 \times 10^4 q_{sc} p_{sc} T}{m T_{sc}} \tag{4-11}$$

where T_{sc} and p_{sc} are the temperature and pressure at standard conditions (520^{o}R and 14.7 psia), q_{sc} is the gas flow rate at standard conditions, measured in MCF/d and T is the reservoir temperature, measured in ^{o}R. Finally, skin factor can be estimated using the following equation:

$$s = 1.151\left[\frac{m(p_{1hr}) - m(p_{wf,s})}{m} - \log\frac{kt_p}{(t_p+1)\phi(\mu c_t)_i r_w^2} + 3.2274\right] \quad \textbf{(4-12)}$$

where $m(p_{1hr})$ is the pseudopressure at Δt = 1 hr, obtained from the straight line or its extrapolation.

The procedure to quantify permeability and skin by the Horner plot provides another tool to test the accuracy of each pseudopressure method. In this work, the Horner plot analysis was applied on the three pressure buildup tests assuming pseudopressures computed by: the single-phase method, the two-phase steady-state method and the two-phase three-zone method.

4.2. Single-Phase Pseudopressure

Al Hussainy and Ramey (1966) and Al Hussainy et al. (1966) showed that the flow equation for real gases in porous media can be linearized using the real gas pseudopressure:

$$m(p) = 2\int_{p_b}^{p} \frac{p}{\mu_g z_g}\,dp \quad \textbf{(4-13)}$$

The following assumptions were made in deriving the flow equations and establishing the solutions:

a. The medium is homogenous,

b. The flowing gas is of constant composition,

c. The flow is laminar and isothermal.

The single-phase pseudopressure method also assumes dry gas around the wellbore, and if condensate is present, it is immobile and the effect of the condensate on the gas relative permeability is negligible (Raghavan et al., 1995).

From gas-condensate system presented in Chapter 2, the gas viscosity and the gas compressibility factor were estimated as a function of pressure. Then, the integral in Eq. (4-13) was evaluated using the trapezoidal rule as follows:

$$m(p) = 2\sum_{i=2}^{n} \frac{1}{2}\left[\left(\frac{p}{\mu z}\right)_{i-1} + \left(\frac{p}{\mu z}\right)_{i}\right](p_i - p_{i-1}) \qquad \textbf{(4-14)}$$

The real gas pseudopressure calculation is tabulated below and the pseudopressure as a function of pressure is plotted in Figure 4-3.

Table 4-1: Calculation of the Real Gas Pseudopressure

P	**Visc. Cp**	**z_g**	**dp**	**p/(mu.z)**	**p/(mu.z) Ave**	**2.dp.Ave**	**m(p)**
14.7	0.0121	1.000		1.210E+03			
500	0.0136	0.965	485.3	3.810E+04	1.965E+04	1.908E+07	1.908E+07
1000	0.0151	0.940	500	7.045E+04	5.428E+04	5.428E+07	7.335E+07
1500	0.0166	0.930	500	9.716E+04	8.381E+04	8.381E+07	1.572E+08
2000	0.0181	0.925	500	1.195E+05	1.083E+05	1.083E+08	2.655E+08
2500	0.0196	0.930	500	1.372E+05	1.283E+05	1.283E+08	3.938E+08
3000	0.0211	0.945	500	1.505E+05	1.438E+05	1.438E+08	5.376E+08
3500	0.0226	0.970	500	1.597E+05	1.551E+05	1.551E+08	6.926E+08
4000	0.0241	0.997	500	1.665E+05	1.631E+05	1.631E+08	8.557E+08
4500	0.0256	1.047	500	1.679E+05	1.672E+05	1.672E+08	1.023E+09
5000	0.0271	1.097	500	1.682E+05	1.681E+05	1.681E+08	1.191E+09
5500	0.0286	1.147	500	1.677E+05	1.680E+05	1.680E+08	1.359E+09
6000	0.0301	1.197	500	1.666E+05	1.671E+05	1.671E+08	1.526E+09
6500	0.0316	1.247	500	1.650E+05	1.658E+05	1.658E+08	1.692E+09
7000	0.0331	1.297	500	1.631E+05	1.640E+05	1.640E+08	1.856E+09
7500	0.0346	1.347	500	1.609E+05	1.620E+05	1.620E+08	2.018E+09

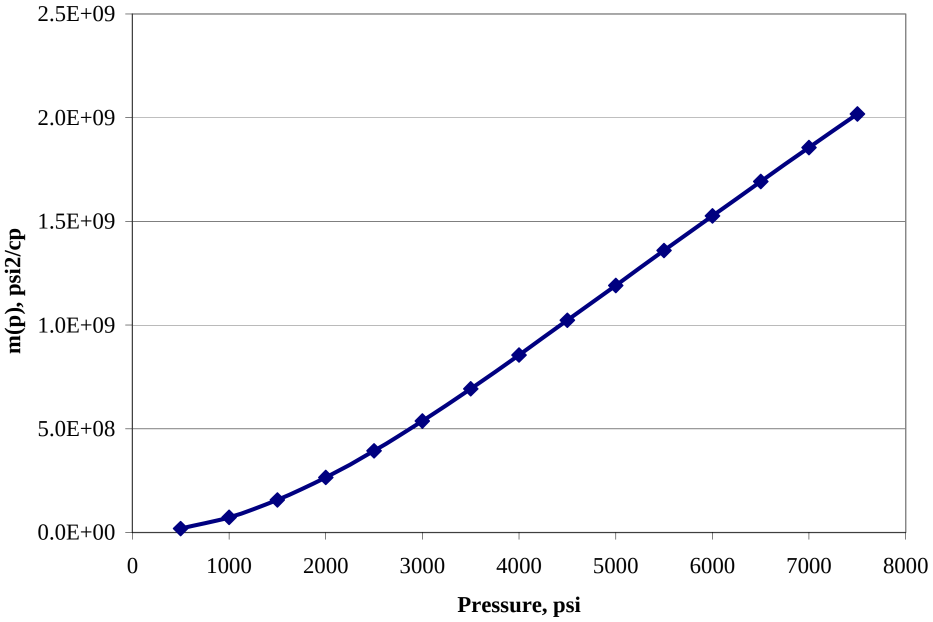

Figure 4-3: Real gas pseudopressure *m(p)* as a function of pressure.

For each pressure build up test, this plot was then used to compute the pseudopressure change [$m(p_{ws}) - m(p_{wf,s})$] at each pressure point generated from the compositional simulator during the buildup as a function of Horner time and the results were plotted on a semilog graph. Finally, permeability and skin were estimated by the semilog analysis of the Horner plot straight line during infinite-acting behavior. The final results will be presented in Chapter 5.

4.3. Two-Phase Steady-State Pseudopressure

The two-phase steady-state theory to predict the performance of single-well gas-condensate systems was first proposed by O'Dell and Miller (1967) and was later examined by Fussel (1973). The steady-state saturation-pressure relationship predicted by O'Dell and Miller (1967) and Fussel (1973) was later reproduced by Chopra and Carter (1985) and Jones and Raghavan (1988). The steady-state model can be used to approximate the actual reservoir pressure-saturation relationship by assuming a hypothetical steady-state flow. The pseudopressure computed by the steady-state model is referred to as the steady-state pseudopressure.

The model assumes two flow regions around the wellbore:

> Region 1: a near-wellbore region below the dew-point pressure where both gas and condensate are present and mobile, and,
>
> Region 2: an outer region above the dew-point pressure containing single-phase gas only.

This model does not allow for a region of immobile condensate at or below the critical condensate saturation. When two phases exist, the steady-state model assumes that both are mobile. Therefore, the steady-state model has the tendency to overestimate the condensate saturation.

The steady-state pseudopressure can only be applied if the relative permeability data are available and it can be computed for pressure buildup tests by the following integral:

$$m(p) = 2\int_{p_b}^{p} \left(\frac{k_{rg}}{\mu_g z_g} + \frac{k_{ro}}{\mu_o z_o}\right) p\,dp$$

(4-15)

Relative permeability data are known as functions of saturation only. Therefore, a relationship between reservoir pressure and saturation is required to compute the integral. In this work, the following step-by-step procedure was applied in order to establish the pressure-saturation relationship and to estimate the steady-state pseudopressure as a function of pressure:

1. The condensate-gas relative permeability ratio as a function of pressure was calculated using the following expression:

   $$\frac{k_{ro}}{k_{rg}} = \frac{L\rho_g\mu_o}{V\rho_o\mu_g}$$

   (4-16)

   where *L* and *V* refer to the molar fraction of liquid and vapor derived from flash calculations. The left hand side of Eq. (4-16) is a function of saturation only and the right hand side is a function of pressure and is approximated by a CCE experiment for the original mixture. This assumption implies that the overall composition of the flowing mixture at any location in the reservoir is the composition of the original reservoir fluid and a region where the composition of the flowing mixture is changing does not exist.

2. Using the relative permeability curves, condensate saturation was estimated from the condensate-gas relative permeability ratio.

   $$\frac{k_{ro}}{k_{rg}} \rightarrow S_c$$ **(4-17)**

   By combining the first two steps, the pressure-saturation relationship by the steady-state method was established as shown on Figure 4-4.

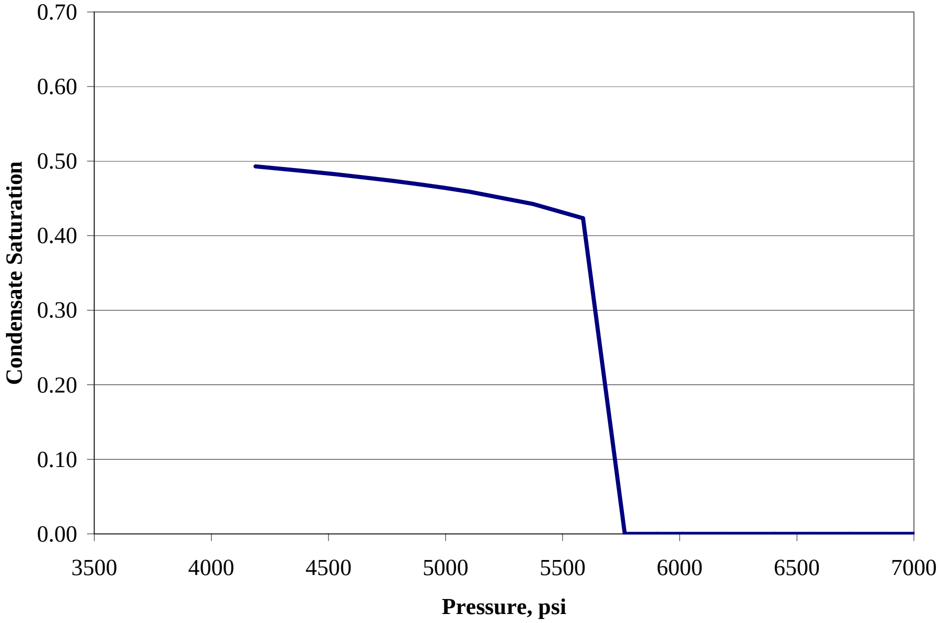

Figure 4-4: Pressure-saturation relationship estimated by the steady-state model for original gas-condensate system.

3. Using the condensate saturation estimated in the previous step, the condensate and gas relative permeabilities were computed. The condensate and gas relative permeabilities as functions of saturation were defined from the relative permeability curves.

$$k_{ro} = f(S_c) \qquad \textbf{(4-18)}$$

$$k_{rg} = f(S_c) \qquad \textbf{(4-19)}$$

4. The gas viscosity and gas compressibility factor were estimated as functions of pressure from the CCE flash calculation.

5. The integral in Eq. (4-15) was evaluated to compute the two-phase steady-state pseudopressure. Below the dew-point pressure, both phases contributed for evaluating the integral. However, above the dew-point pressure, k_{rg} was assumed to be one and k_{ro} was assumed to be zero and the integral was evaluated similar to the single-phase pseudopressure discussed earlier. The two-phase steady-state pseudopressure as a function of pressure is plotted on Figure 4-5.

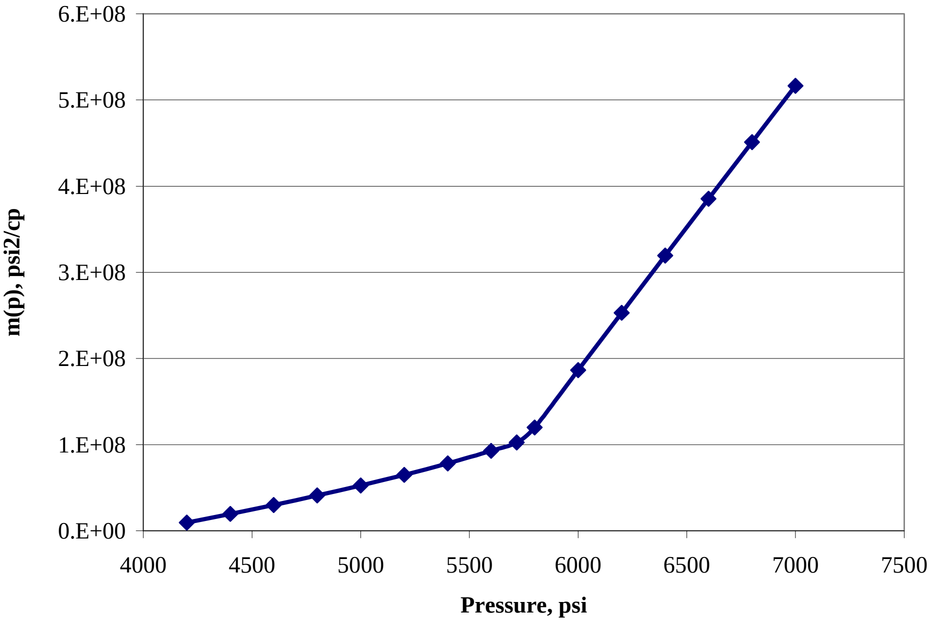

Figure 4-5: Two-phase steady-state pseudopressure *m(p)* as a function of pressure.

Similar to the single-phase pseudopressure analysis, this plot was used to compute the pseudopressure change [$m(p_{ws}) - m(p_{wf,s})$] at each pressure point generated from the compositional simulator during the three pressure buildup tests. Then, Horner plot analyses were applied to estimate permeability and skin for each test. The final results will be presented in Chapter 5.

4.4. Two-Phase Three-Zone Pseudopressure

The three-zone flow model was first introduced by Fevang (1995). Unlike the steady-state model, the three-zone flow model considers the existence of a transition zone where both gas and condensate are present, but only gas is mobile. The three flow regions around the wellbore assumed by the three-zone model are as follows:

> Region 1: a near-wellbore region where gas and condensate are present and mobile. The composition of the flowing mixture in this region is constant. Therefore, the producing GOR stabilizes once this region starts to develop at a pressure p^*. The pressure range that corresponds to this region extends from the wellbore flowing pressure, p_{wf}, to pressure p^*.
>
> Region 2: condensate buildup region where the condensate saturation is below the critical saturation and only gas is flowing. The composition of the flowing mixture in this region changes and the gas becomes leaner. Therefore, once this region starts to develop at the dew-point pressure, p_{dew}, the producing GOR increases. The pressure range that corresponds to this region extends from p^* (inner boundary) to p_{dew} (outer boundary).

Region 3: an outer region above the dew-point pressure, p_{dew}, where only gas is present.

Similar to the steady-state method, the three-zone pseudopressure is only applied if the relative permeability data are available and it can be evaluated using the following integral (Fevang, 1995):

$$m^{3Z}(p) = region1 + region2 + region3$$

$$m^{3Z}(p) = \int_{p_{wf}}^{p^*} \left(\frac{\rho_o k_{ro}}{\mu_o} + \frac{\rho_g k_{rg}}{\mu_g}\right) dp + \int_{p^*}^{p_{dew}} \frac{\rho_g k_{rg}}{\mu_g} dp + k_{rg}(S_{wi}) \int_{p_{dew}}^{p_r} \frac{\rho_g}{\mu_g} dp \tag{4-20}$$

To compute the integral, the pressure limits for each region are required. **Region 1** starts to develop after the well flowing pressure, p_{wf}, drops sufficiently below the dew-point pressure, p_{dew}, and reaches p^*. At p^*, condensate becomes mobile. Roussennac (2001) illustrated the process to estimate p^*:

1. The solution oil gas ratio, r_s, obtained from the PVT characterization was plotted as a function of pressure.

2. The producing GOR, R_p, was determined from the compositional simulation results. For example, the producing GOR during the first well test was 12 Mscf/STB.

3. p^* was determined to be the pressure where $r_s = 1/R_p = 0.083$ STB/Mscf. In this case, p^* was estimated to be approximately 5,400 psi as illustrate on Figure 4-6.

Because only single-phase gas is flowing from Region 2 to Region 1, p^* is considered to be the dew-point pressure of the gas entering Region 1. If $p_{wf} > p^*$, then Region 1 does not exist. On the other hand, if $p^* > p_r$, then only Region 1 exists and Regions 2 and 3 do not exist. Accordingly, the integral in Eq. (4-20) should be evaluated for Region 1 only from p_{wf} to p_r.

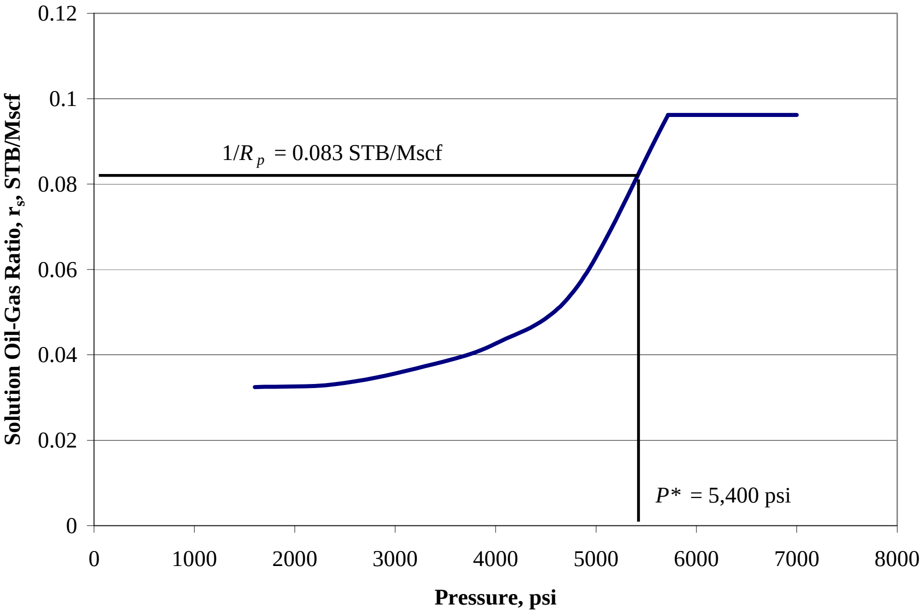

Figure 4-6: p^* estimation for Region 1 pressure boundaries.

Region 2 starts to develop when the well flowing pressure, p_{wf}, drops to the dew-point pressure, p_{dew}, of the initial gas-condensate system and the region extends to the point where the pressure is p^*. At early times, the size of Region 2 is largest. However, the size of Region 2 decreases with time because Region 1 is expanding as indicated by Fevang and Whitson (1996).

The integral for Region 2 is evaluated from p^* (lower limit) to the initial dew-point pressure, p_{dew}, if $p_{dew} < p_r$. If $p_{dew} > p_r$, then the upper limit of the integral becomes the reservoir pressure, p_r.

Region 3 exists only if $p_r > p_{dew}$. Then, the integral for Region 3 is evaluated between the dew-point pressure, p_{dew} (lower limit) and the reservoir pressure, p_r (upper limit).

Similar to the steady-state pseudopressure, the pressure-saturation relationship was established in order to compute the three-zone pseudopressure integral. However, unlike the steady-state model, the pressure-saturation relationship for the three-zone model was estimated for each region separately.

For **Region 1**, the corresponding pressure saturation relationship can be estimated using a modified Evinger and Muskat (1942) approach as proposed by Fevang (1995):

$$\frac{k_{ro}}{k_{rg}}(p) = \left(\frac{R_p - R_s}{1 - r_s R_p}\right)\frac{\mu_g B_{gd}}{\mu_o B_o} \tag{4-21}$$

where PVT properties: R_s, B_o, r_s, B_{gd}, μ_o and μ_g are functions of pressure only. Eq. (4-21) is equivalent to the following formulation:

$$\frac{k_{ro}}{k_{rg}}(p) = \frac{L\rho_g\mu_o}{V\rho_o\mu_g} \qquad \textbf{(4-22)}$$

where L and V are the producing stream liquid and vapor molar fraction as opposed to the original mixture which is normally applied in the steady-state method.

Eq. (4-22) was applied to estimate the condensate-gas relative permeability ratio as a function of pressure for Region 1 first. Then, the condensate saturation was derived from the relative permeability ratio using the relative permeability curves as illustrated previously for the steady-state model (Eq. 4-17).

For **Region 2**, the pressure-saturation relationship was obtained directly from the CVD experiment corrected for initial water saturation using Eq. (4-23). Finally, for **Region 3**, the pressure is above the dew-point pressure, p_{dew}, therefore, the condensate saturation is zero. Figure 4-7 shows the pressure-saturation relationship estimated at the end of the drawdown for the first well test.

$$S_c(p) = (1 - S_{wi})S_{cCVD} \qquad \textbf{(4-23)}$$

Similar to the steady-state model, the condensate saturation as a function of pressure was then coupled with the relative permeability curves in order to define the gas and condensate relative permeabilities as functions of pressure. Ultimately, all the parameters in the three-zone pseudopressure integral (Eq. 4-20) were defined as functions of pressure and the pseudopressure was evaluated across the three regions. The two-phase three-zone pseudopressure as a function of pressure used in the first pressure buildup test analysis is plotted on Figure 4-8. The pseudopressure plots for the second and third pressure buildup test along with the corresponding Horner analysis will be presented in Chapter 5.

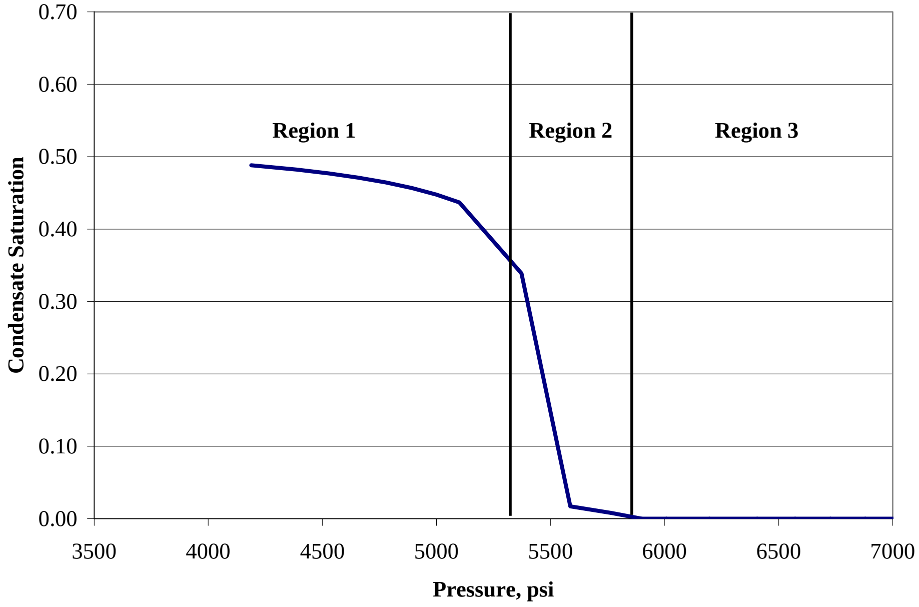

Figure 4-7: Pressure-saturation relationship estimated by the three-zone model at the end of the drawdown for first test.

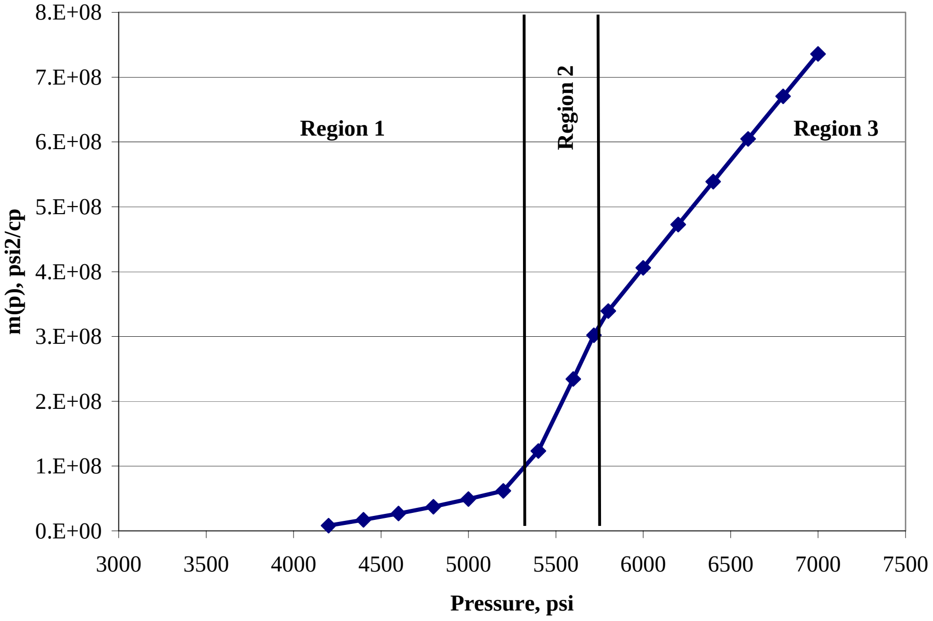

Figure 4-8: Two-phase three-zone pseudopressure as a function of pressure for first test.

Chapter 5

5. Well Test Results

In this chapter, the results of applying the three pseudopressure methods on each pressure buildup test will be presented. The accuracy of each pseudopressure method in reproducing the permeability and skin of the model will also be discussed.

5.1. First Pressure Buildup Test (Prestimulation)

As indicated in Chapter 3, the first pressure buildup test was conducted prior to the acid stimulation job. The downhole pressure data were regenerated using *Eclipse-300* assuming the permeability and skin of the radial model to be 5.5 md and -3.3, respectively. The compositional simulator predicted 30 ft of condensate bank around the wellbore at the end of the drawdown.

5.1.1. Single-Phase Pseudopressure

After evaluation the single-phase pseudopressure integral, the pseudopressure change [$m(p_{ws}) - m(p_{wf,s})$] was plotted on a semilog graph as a function of Horner time as shown in Figure 5-1. The Horner straight line analysis estimated permeability to be around 4.5 md, which was within 18% accuracy. However, the skin factor was significantly overestimated. The Horner straight line analysis indicated the skin factor to be around -1.8, which was 45% higher than the skin factor assumed for the radial model.

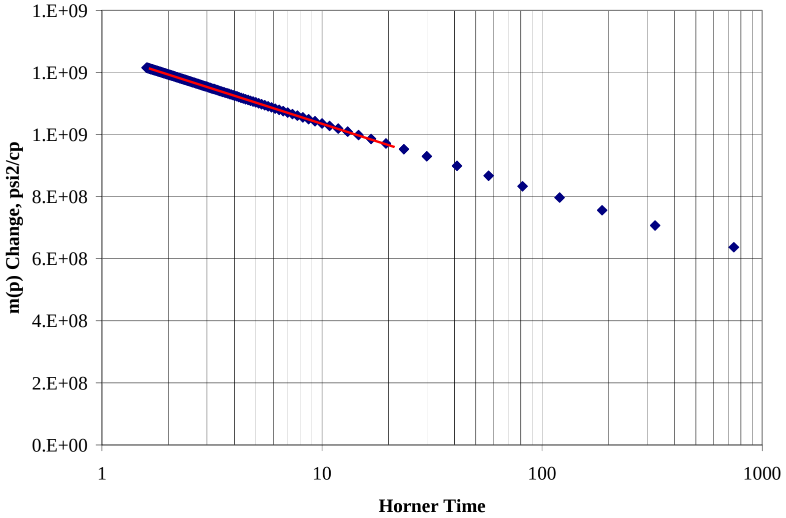

Figure 5-1: Horner plot for first pressure buildup test (single-phase pseudopressure).

5.1.2. Steady-State Pseudopressure

The pressure-saturation relationship determined by the steady-state model for the first test was compared with the simulator output on Figure 5-2. The condensate saturation as a function of radial distance inferred from pressure-saturation relationship is plotted on Figure 5-3. Results indicated that the steady-state model overestimated the condensate saturation around the wellbore. The pseudopressure change for the steady-state pseudopressure was also plotted as a function of Horner time as shown on Figure 5-4.

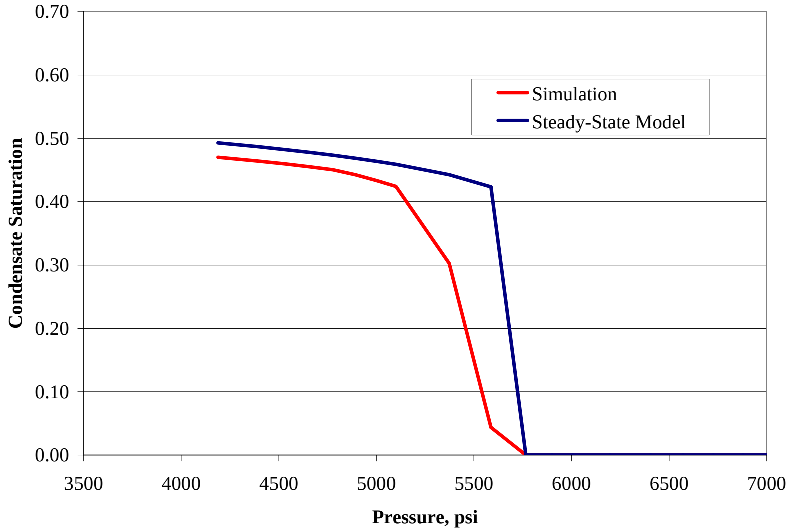

Figure 5-2: Pressure-saturation relationship by the steady-state model for the first test.

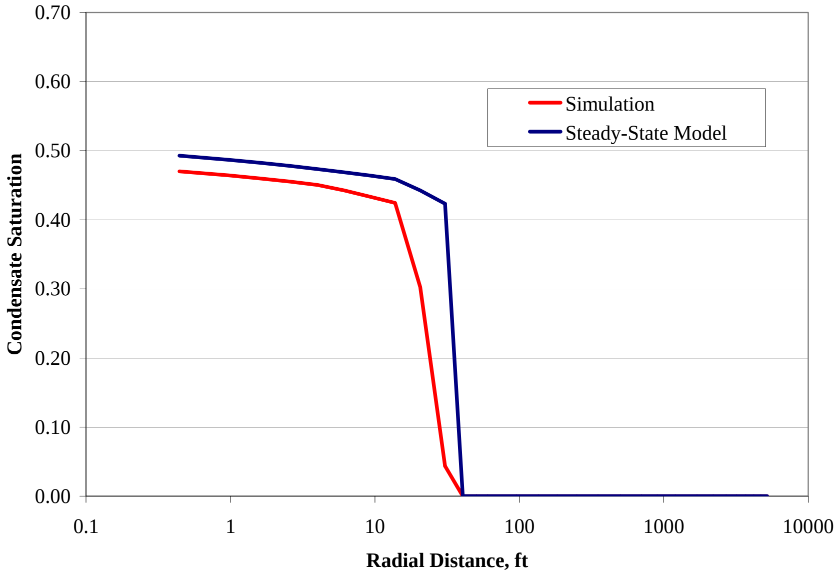

Figure 5-3: Radial distribution of condensate saturation by the steady-state model for the first test.

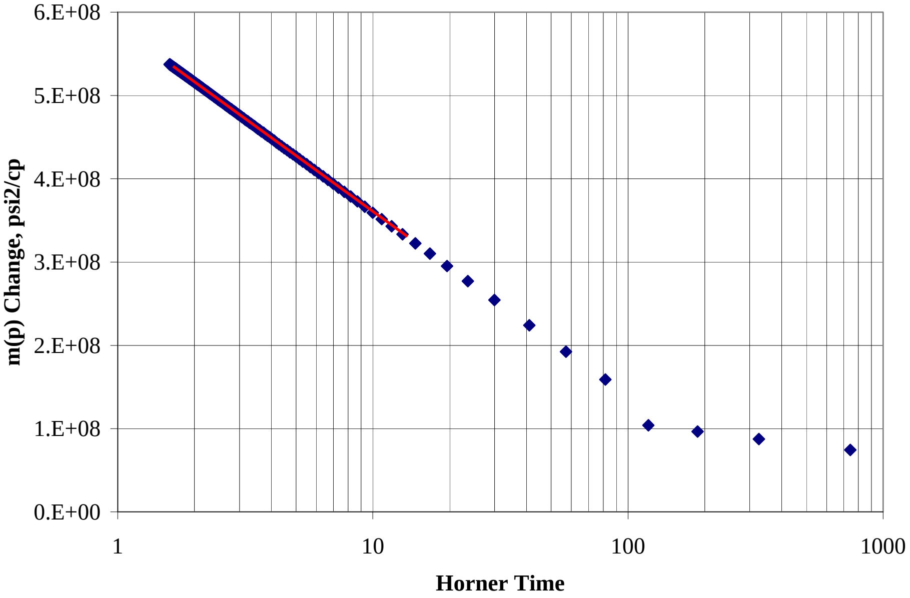

Figure 5-4: Horner plot for first pressure buildup test (steady-state pseudopressure).

Horner straight line analysis indicated that permeability and skin were 4.5 md and -5.3, respectively. Therefore, the permeability was estimated within 18% accuracy. On the other hand, skin was significantly underestimated. The skin factor predicted by the Horner analysis was 60% lower than the skin factor assumed for the radial model.

5.1.3. Three-Zone Pseudopressure

Similar to the steady-state model, the pressure-saturation relationship predicted by the three-zone model was compared with the simulator output as shown on Figure 5-5. The radial distribution of condensate saturation was also plotted on Figure 5-6. Results indicated that the three-zone model predicted the pressure-saturation accurately and therefore the condensate saturation around the wellbore was estimated accurately.

The semilog graph showing the three-zone pseudopressure change as a function of Horner time is plotted in Figure 5-7. Horner analysis estimated permeability to be 4.5 md. Skin was estimated to be -4.0. Therefore, the skin factor predicted by the Horner analysis for the three-zone pseudopressure was only 20% higher than the skin factor assumed for the radial model.

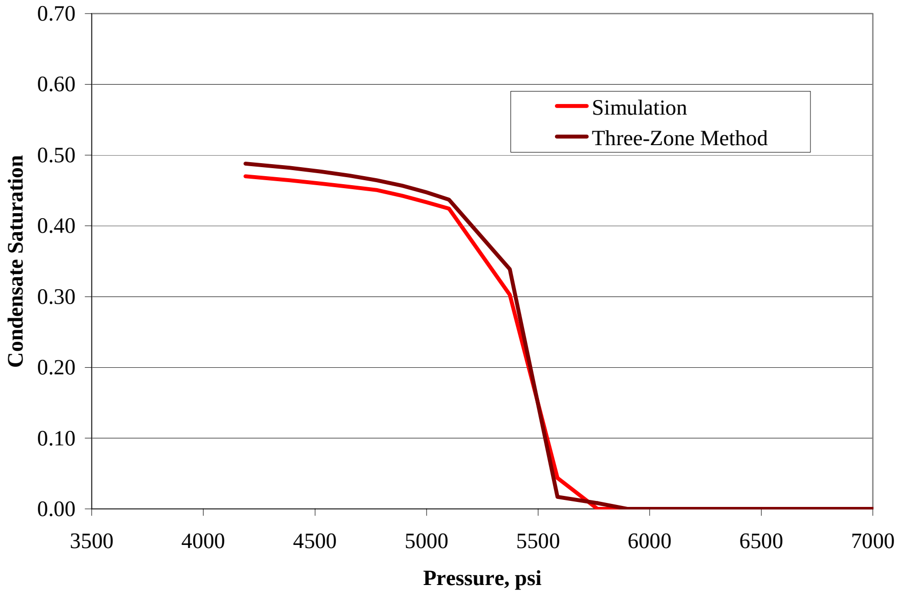

Figure 5-5: Pressure-saturation relationship by the three-zone model for the first test.

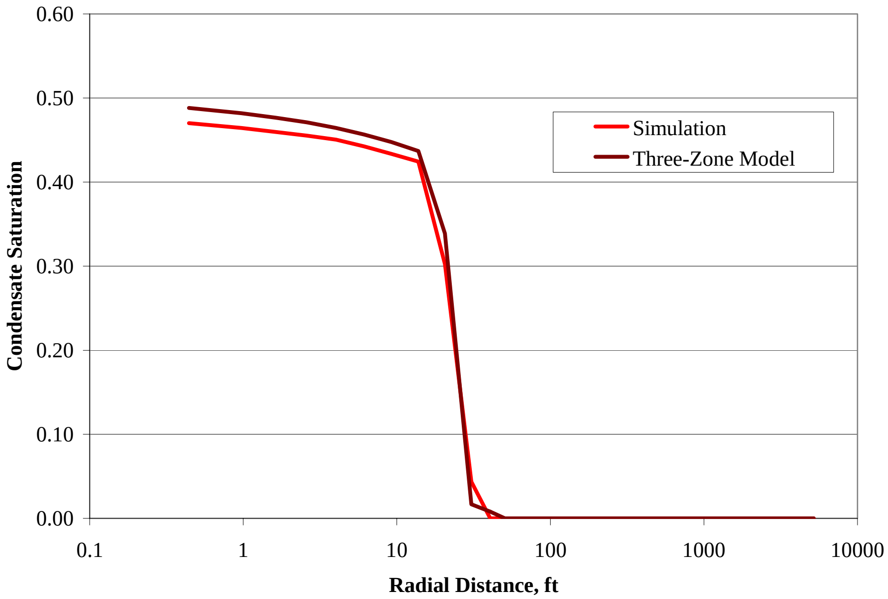

Figure 5-6: Radial distribution of condensate saturation by the three-zone model for the first test.

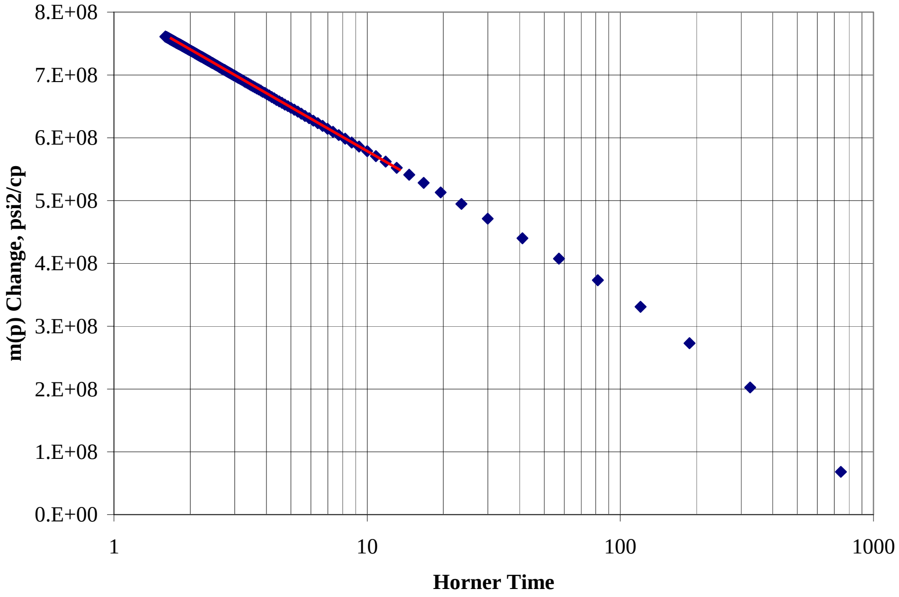

Figure 5-7: Horner plot for first pressure buildup test (three-zone pseudopressure).

5.1.4. Discussions on First Pressure Buildup Test

The overall results of applying the three pseudopressure methods on the first pressure buildup test are tabulated in Table 5-1. The results were compared with the actual model used for the first well test, i.e., 5.5 md permeability and -3.3 skin factor.

Table 5-1: Summary of Horner analysis results for first pressure buildup test

Pseudopressure	**Permeability, md**	**Change**	**Skin**	**Change**
Single-Phase	4.5	-18%	-1.8	+45%
Steady-State	4.5	-18%	-5.3	-60%
Three-Zone	4.5	-18%	-4.0	+20%

Results indicated that all three pseudopressure methods were capable of predicting permeability within 18% of the actual model permeability. On the other hand, variations in skin estimates were observed. The least deviation in skin estimates was predicted by the three-zone pseudopressure method. However, skin estimates by the single-phase and steady-state pseudopressures were significantly different from the actual model skin factor.

The single-phase pseudopressure overestimated skin by 45%. The skin factor estimated by the single-phase pseudopressure contained contributions from mechanical skin as well as the liquid dropout effects. Therefore, skin estimates by the single-phase pseudopressure tend to be overestimated.

The steady-state pseudopressure underestimated skin by 60%. Unlike the three-zone model, the steady-state model was unable to accurately predict the pressure-saturation relationship and the condensate saturation around the wellbore was therefore overestimated as shown on Figure 5-3. Consequently, the skin estimates were low.

Dimensionless analysis on the pseudopressures was also performed to determine the accuracy of the each pseudopressure method in estimating permeability and skin. The dimensionless pseudopressures computed by each method along with the liquid solution were all plotted on a semilog graph as a function of dimensionless time (Figure 5-8). The slopes of the lines are similar. Therefore, each pseudopressure method should yield permeability estimates that are close to the model permeability value. On the other hand, vertical shifts indicate that the single-phase pseudopressure and the steady-state pseudopressure should yield high and low skin estimations, respectively. The least vertical shift (~0.5) is observed for the three-zone pseudopressure. Hence, the three-zone pseudopressure should deliver fairly accurate skin estimation.

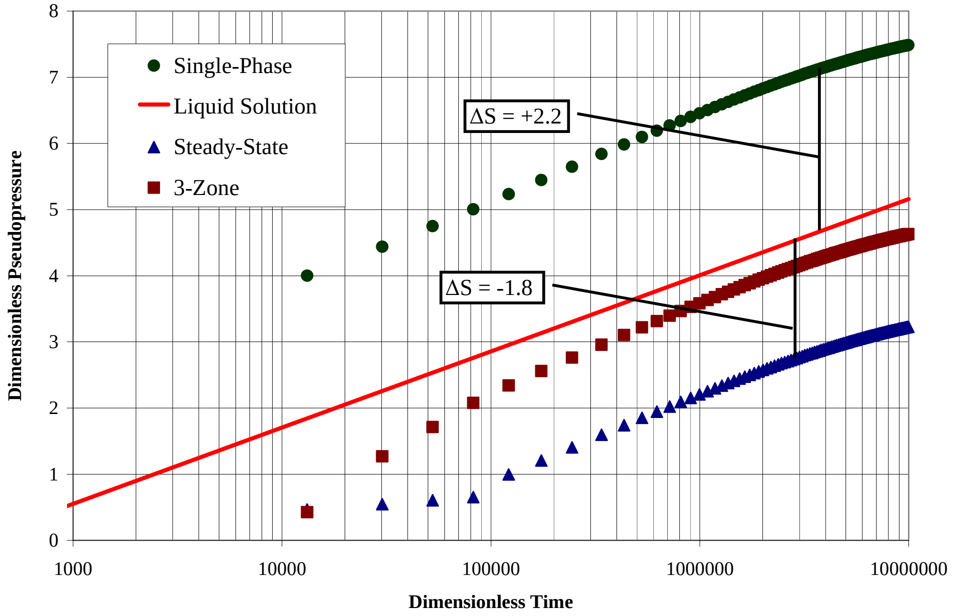

Figure 5-8: Semilog plot of dimensionless pressure as a function of dimensionless time for first pressure buildup test.

5.2. Second Pressure Buildup Test (Poststimulation)

The second pressure buildup test was conducted after the acid stimulation job. The downhole pressure data were regenerated using *Eclipse-300* assuming the permeability and mechanical skin of the radial model to be 5.5 md and -4.0, respectively. The compositional simulator predicted 30 ft of condensate bank around the wellbore at the end of the drawdown.

The plots that were generated for analyzing the second pressure buildup test data are presented in Appendix C. The plots include the pressure-saturation relationship estimated for the steady-state and three-zone models. The plots also include the semilog Horner plots generated for the three pseudopressure methods.

The pseudopressure as a function of pressure plots (Figure 4-3 and Figure 4-5) used in the first well test were employed again to generate the Horner plots for the single-phase pseudopressure and the steady-state pseudopressure in the second well test because both pseudopressures assume initial fluid composition when evaluating the integrals. In contrast, the three-zone pseudopressure considers composition change in the reservoir. Therefore, the three-zone pseudopressure was updated to reflect the accurate fluid composition and a new three-zone pseudopressure as a function of pressure plot was generated for the second well test (Figure C-7).

5.2.1. Discussions on Second Pressure Buildup Test

The overall results of applying the three pseudopressure methods on the second pressure buildup test are tabulated in Table 5-2. The results were compared with the actual model used for the second well test, i.e., 5.5 md permeability and -4.0 skin factor.

Table 5-2: Summary of Horner analysis results for second pressure buildup test

Pseudopressure	Permeability, md	Change	Skin	Change
Single-Phase	4.6	-16%	-3.6	+10%
Steady-State	4.7	-15%	-5.7	-42%
Three-Zone	4.6	-16%	-4.2	+5%

Results indicated that the three pseudopressure methods applied on the second well test had the same behavior as on the first well test. Permeability estimations by the three methods were within 15-16% of the actual model permeability. However, skin factor estimations varied. Unlike the three-zone method which estimated the skin factor accurately, the steady-state method highly underestimated skin for the same reasons discussed for the first well test.

The skin factor estimation by the single-phase method was only slightly overestimated, whereas in the first well test, the single-phase method significantly overestimated the skin factor. The stimulation job before the second well test increased the negative skin around the wellbore causing the pressure drop in the near wellbore region to decrease compared to the first well test. Accordingly, the condensate saturation around the wellbore was lower and the skin due to liquid dropout was minimized.

The Horner analysis results were also predicted accurately by the dimensionless analysis. Figure 5-9 indicates that the three pseudopressure methods should yield similar permeability estimations (similar slopes). Unlike the three-zone pseudopressure which should accurately estimate mechanical skin, the plot indicates that the single-phase pseudopressure and the steady-state pseudopressure should yield high and low skin factor estimations, respectively.

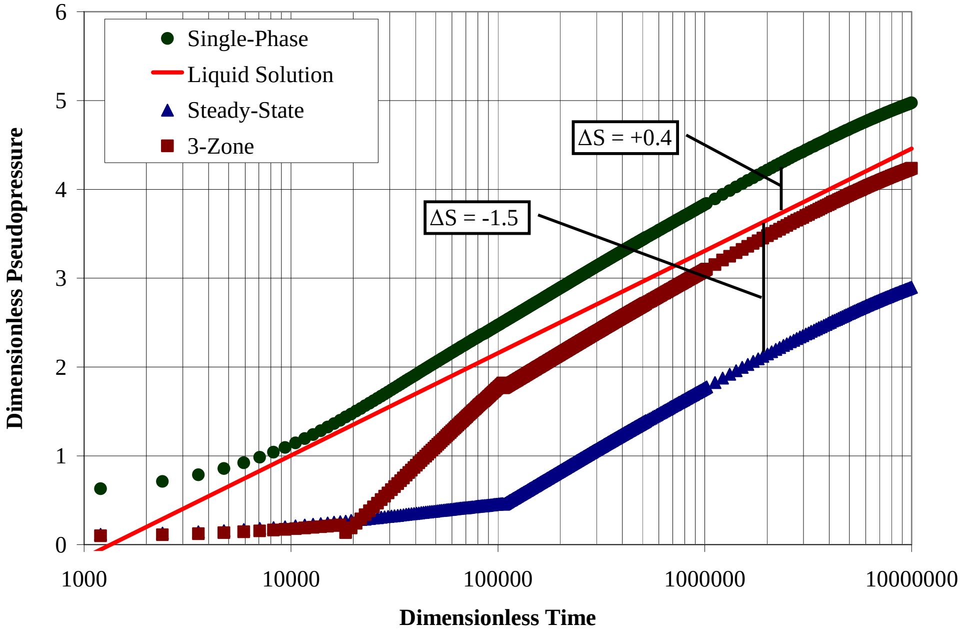

Figure 5-9: Semilog plot of dimensionless pressure as a function of dimensionless time for second pressure buildup test.

5.3. Third Pressure Buildup Test

The third pressure buildup test was conducted after one year of gas and condensate production. The downhole pressure data were regenerated assuming the permeability and mechanical skin of the radial model to be 5.5 md and -4.0, respectively. The compositional simulator predicted 180 ft of condensate bank around the wellbore at the end of the drawdown. The plots that were generated to analyze the pressure buildup test data are presented in Appendix D.

The pressure-saturation relationship estimated for the steady-state model revealed that the saturation profile was predicted accurately by the steady-state model for this test, unlike the first and second well tests. The size of region two where condensate is immobile, to Region 1 where both gas and condensate are mobile, was relatively small and specifically, it was one to seven. Therefore, ignoring Region 2 by the steady-state model did not impact the prediction of the condensate saturation profile significantly. Figure 5-10 compares the condensate distribution around the wellbore predicted by the steady-state model and the three-zone model. The plot indicates that at this stage of well life, the steady-state model and the three-zone model start to behave similarly.

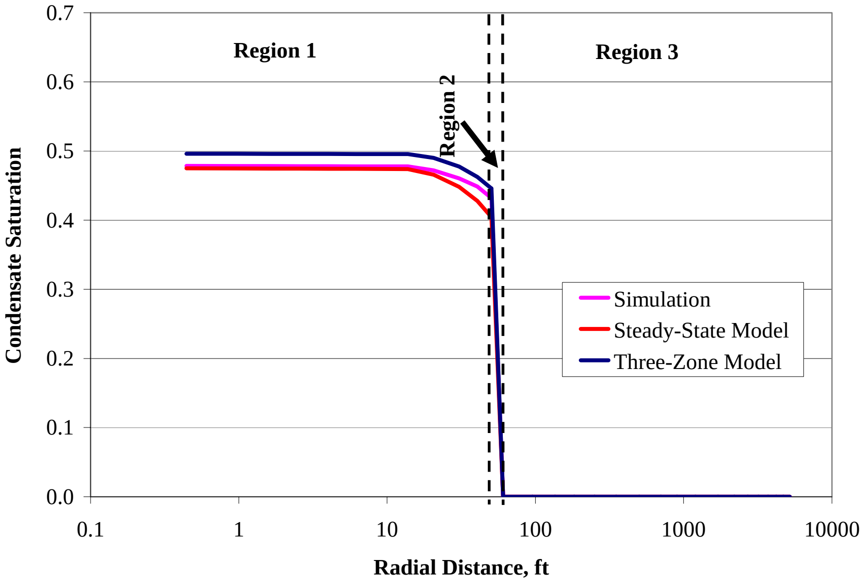

Figure 5-10: Radial distribution of condensate saturation by the steady-state model and the three-zone model for the third well test.

5.3.1. Discussions on third Pressure Buildup Test

The overall results of applying the three pseudopressure methods on the third pressure buildup test are tabulated in Table 5-3. The results were compared with the actual model used for the third well test, i.e., 5.5 md permeability and -4.0 skin factor.

Table 5-3: Summary of Horner analysis results for third pressure buildup test

Pseudopressure	**Permeability, md**	**Change**	**Skin**	**Change**
Single-Phase	5.2	-6%	1	+125%
Steady-State	5.0	-10%	-3.7	-8%
Three-Zone	5.2	-6%	-3.9	-3%

Results indicated that both the steady-state pseudopressure and the three-zone pseudopressure estimated permeability and skin accurately. This result was expected because the pressure-saturation relationships by the two models were comparable.

The single-phase pseudopressure estimated permeability accurately, but skin estimation was excessively high due to the presence of substantial volume of condensate around the wellbore (condensate bank radius = 180 ft). The skin factor estimated by single-phase pseudopressure contained contributions from the mechanical skin as well as skin due to liquid dropout.

The Horner analysis results were also predicted accurately by the dimensionless analysis. Figure 5-11 indicates that the three pseudopressure methods should yield similar permeability estimations (similar slopes). The plot also indicates that both the steady-state pseudopressure and the three-zone pseudopressure should accurately estimate skin. However, skin estimate by the single-phase pseudopressure should be too high.

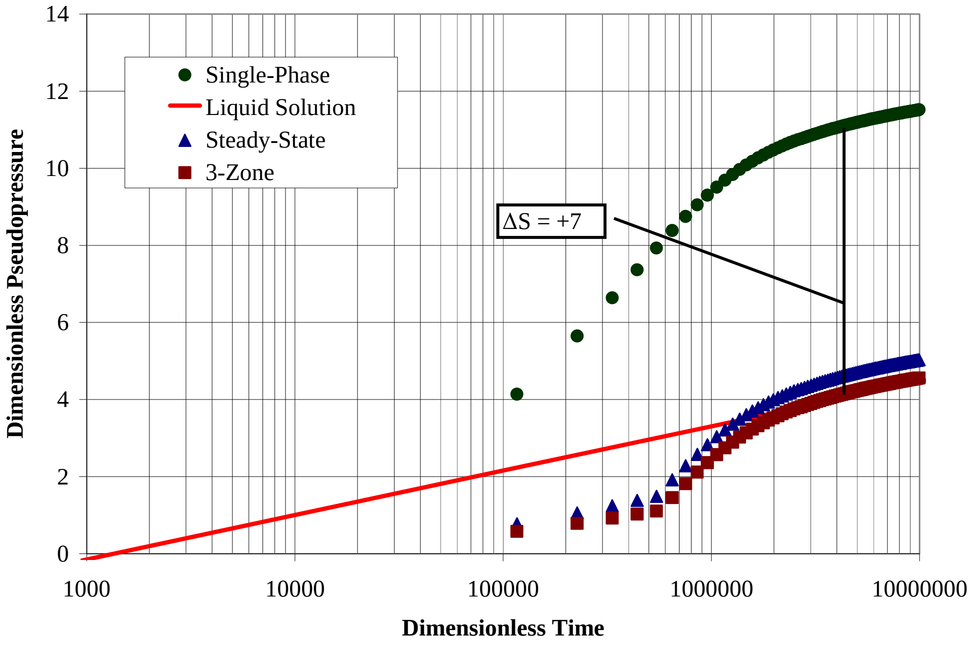

Figure 5-11: Semilog plot of dimensionless pressure as a function of dimensionless time for third pressure buildup test.

5.4. Conclusions

Horner analysis results from the well tests indicate the following:

Single-phase pseudopressure: estimated permeability accurately, but overestimated skin significantly. Skin factor estimates contained contributions from the mechanical skin as well as the skin due to liquid dropout ($s_t = s_m + s_{2p}$). Therefore, this method is not reliable in determining the necessity of pumping an acid stimulation or hydraulic fracturing treatment in a gas-condensate well to remove or bypass any reservoir damage around the wellbore.

Steady-state pseudopressure: estimated permeability accurately, but underestimated the mechanical skin significantly due to the inability of the steady-state method to represent the model pressure-saturation relationship accurately. However, when the size of Region 2 was relatively small compared to Region 1 size, the steady-state model was able to represent the pressure-saturation relationship accurately and thus, mechanical skin factor was estimated accurately.

Three-zone pseudopressure: estimated both permeability and mechanical skin accurately. The three-zone model considered the main flow regions around the wellbore during flow.

This conclusion had also been documented earlier by Jones et al. (1989) and Roussennac (2001).

Chapter 6

6. Further Investigations

This chapter will discuss some of the issues encountered while aiming to fulfill the research objectives. The issues include the gas-oil ratio (GOR) behavior during depletion and the condensate saturation behavior around the wellbore during pressure buildup.

6.1. GOR Behavior During Depletion

From compositional simulations results, the GOR behavior as a function of time during depletion indicated that the GOR below the dew-point pressure increased gradually to a maximum GOR before decreasing and stabilizing at a lower GOR. Figure 6-1 shows the producing GOR behavior during the second well test. The plot indicates that at the dew-point pressure, the GOR started to increase gradually from around 10 Mscf/STB to a maximum GOR of around 12 Mscf/STB. The GOR then decreased and stabilized at 11.3 Mscf/STB.

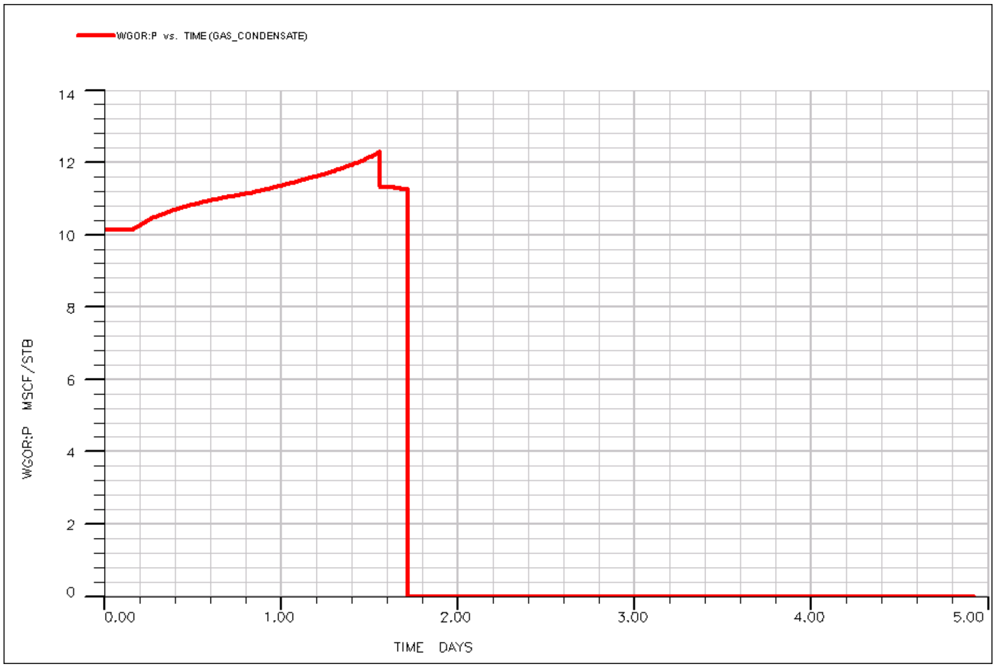

Figure 6-1: Producing GOR behavior during the first well test.

A similar GOR behavior during depletion for a three-component system was reported by Roussennac (2001). However, Roussennac (2001) noted that the sudden reduction of GOR before stabilization was only observed in the nonzero skin case. In the zero-skin case, the GOR increased gradually and then stabilized at the maximum value as shown on Figure 6-2.

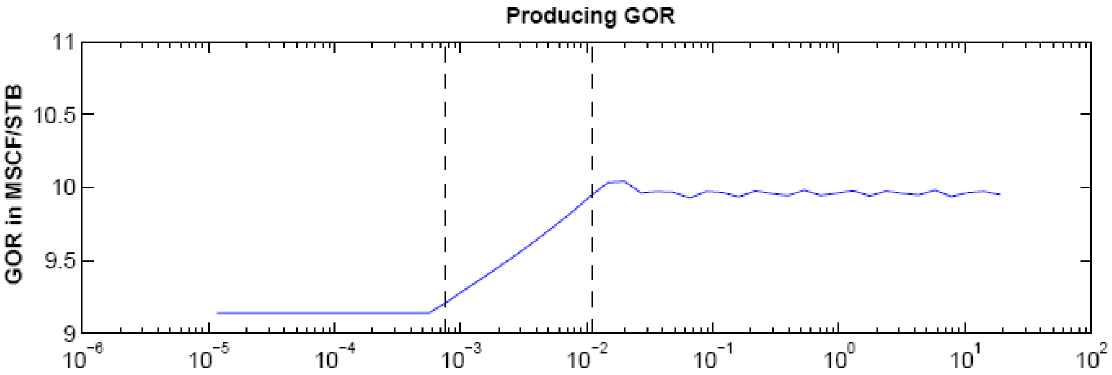

Figure 6-2: Producing GOR behavior for a zero-skin case (from Roussennac 2001).

Figure 6-3 shows gas rate, condensate rate and GOR estimate during the second well test. The plot indicates that the sudden decrease in the GOR is due to a sudden surge in the condensate production rate. The increase in condensate production rate could be attributed to exceeding the critical condensate saturation.

Figure 6-4 shows the radial distribution of condensate saturation at the time step when the GOR was at its maximum. The plot indicates that at the condensate saturation at grid blocks nearest to the wellbore was below the critical saturation. However, at the following time step, the condensate saturation increased to the critical saturation and therefore, more condensate began to flow as shown on Figure 6-5. Hence, this time step corresponds to the end of Region 2 and the start of Region 1.

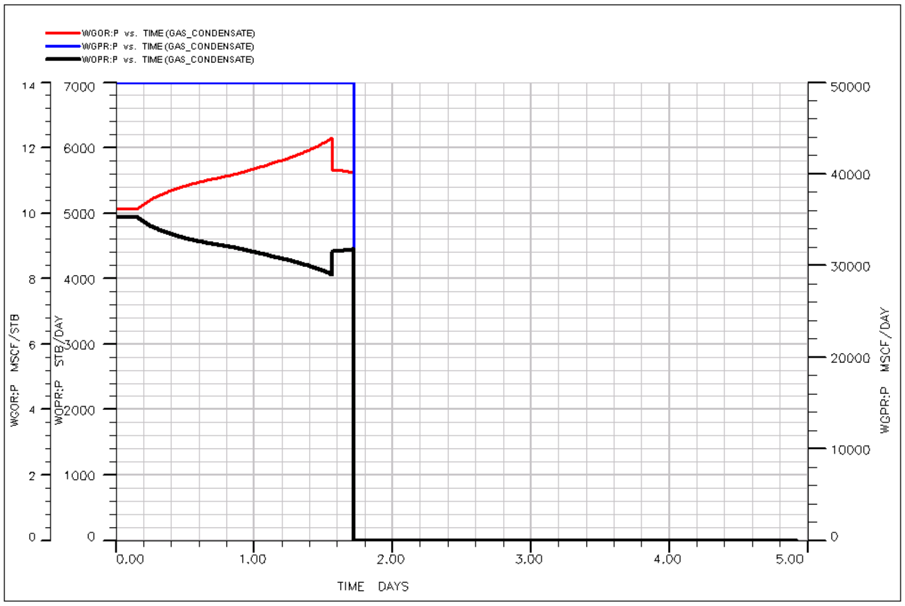

Figure 6-3: Gas rate (blue), condensate rate (black) and GOR (red) as a function of time during first well test.

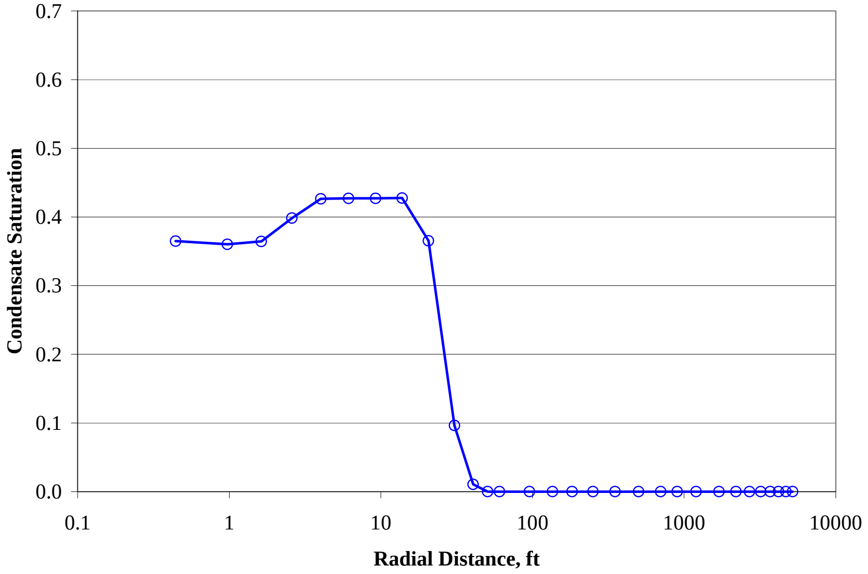

Figure 6-4: Radial distribution of condensate saturation at GOR = 12 Mscf/STB.

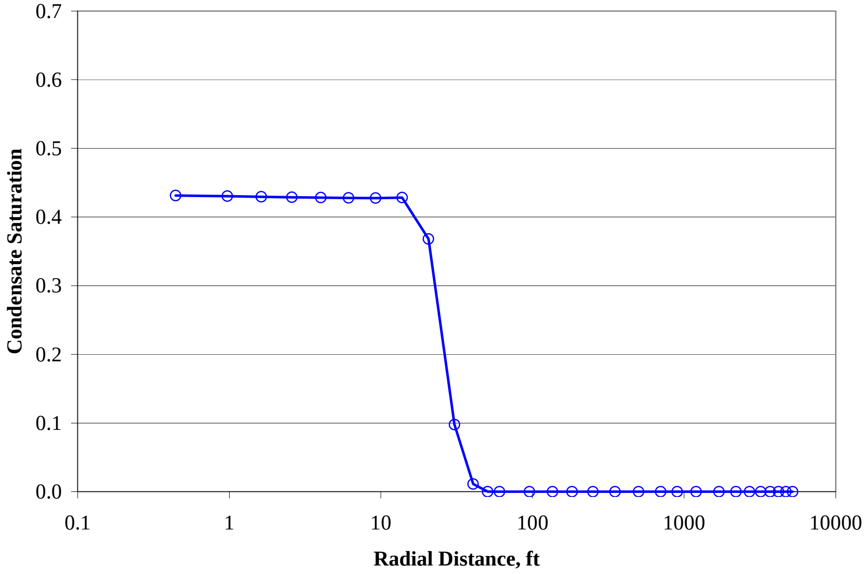

Figure 6-5: Radial distribution of condensate saturation at GOR = 11.3 Mscf/STB.

6.2. Condensate Saturation Behavior During Buildup

Based on the gas-condensate phase behavior discussed in Chapter 2, it is expected that the condensate dropped during pressure depletion would revaporize when the pressure starts to climb above the dew-point pressure during pressure buildup. However, this behavior was not observed during the regeneration of the pressure buildup tests. In fact, the condensate saturation in the near-wellbore region increased slightly when the well was shut in as revealed by Region A of the second well test in Figure 6-6. In other words, gas was dissolving preferentially in the condensate. Therefore, the condensate behavior was analogous to the behavior of black oil system.

On the other hand, Figure 6-6 also revealed that near the outer edge of the two-phase zone (Region B), condensate revaporized. Therefore, in this region, the in-place fluid was still behaving as gas-condensate.

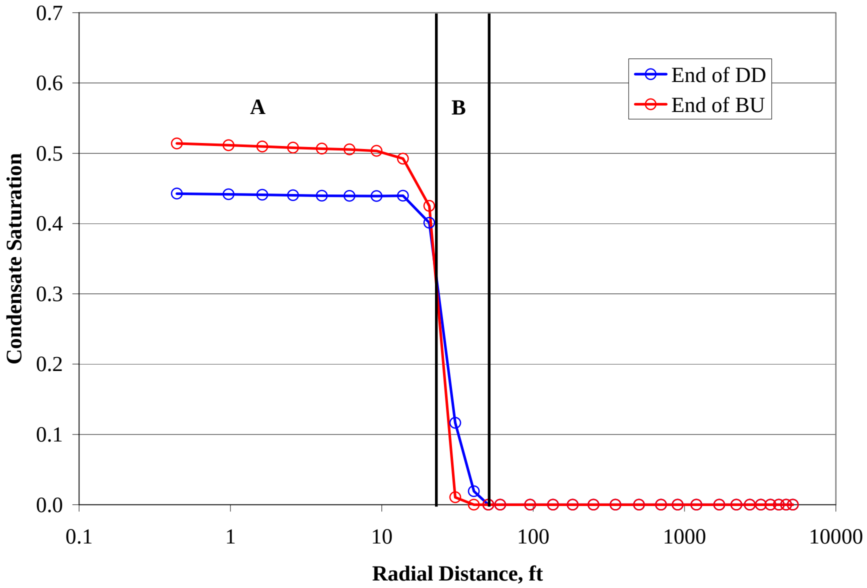

Figure 6-6: Condensate saturation at the end of drawdown vs. buildup for second well test.

Similar behaviors of condensate saturation during pressure buildup for various gas-condensate systems were reported by Vo et al. (1989) and Gringarten et al. (2006). Vo et al. (1989) pointed out the fluid in the near wellbore region had undergone sufficient composition change to transform the in-place fluid from gas-condensate into black oil. However, there were not sufficient composition changes further into the condensate bank to cause this transformation and fluids there still behaved as gas-condensate with revaporization of liquid. Vo et al. (1989) also noted that in the region where the condensate saturation increased during pressure buildup, fluid critical temperature, T_c, was greater than the reservoir temperature, T, and that revaporization occurred where T_c was less than T.

In this work, the accuracy of the current compositional simulator, *Eclipse-300,* was tested in terms of condensate revaporization by comparing *Eclipse-300* with *the General Purpose Research Simulator, GPRS.*

6.2.1. Eclipse-300 vs. GPRS

The gas-condensate system presented in Chapter 2 was used again to simulate a 10-day drawdown, followed by a 5-day pressure buildup on a Cartesian model (Figure 6-7) constructed on both, *Eclipse-300* and *GPRS*. The input simulation parameters are summarized on Table 2-1 and Table 6-1.

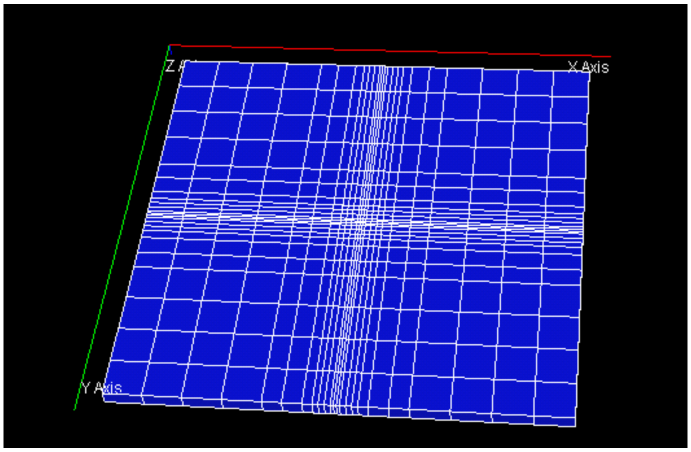

Figure 6-7: The Cartesian model used in *Eclipse-300* and *GPRS.*

Table 6-1: Simulation Parameters for Eclipse-300 and GPRS.

Parameter	**Value**
Initial reservoir pressure, psi	6900
Average porosity	0.17
Formation thickness, ft	75
Reservoir top level, ft	10,500
Roc compressibility, psi^{-1}	5.00E-06
Wellbore radius, ft	0.25
k, md	5.7
k_s, md	50

The *Eclipse-300* code presented in Appendix B was used to simulate this test after modifying the grid block arrangements. The *GPRS* code used in this test is presented in Appendix E. Appendix E also illustrates how the well index, *WI,* required as a *GPRS* input parameter for the block containing the well, was computed.

Figure 6-8 compares the bottom hole pressure estimated by both simulators during the drawdown and buildup. The plot indicates a good agreement between the two simulators. A good agreement was also confirmed for the pressure estimations at the end of the drawdown period in all the grid blocks constructed for the model as illustrated in Figure 6-9.

After establishing pressure agreements between the two simulators, the condensate saturation behavior in the reservoir was examined. Figure 6-10 and Figure 6-11 plot the condensate saturation as a function of distance at the end of drawdown and buildup, respectively. The two figures indicate that for both simulators, the behavior of the in-place fluid in the near wellbore region was similar to black oil. As the pressure increased to above the dew-point pressure during buildup, the condensate saturation increased as well suggesting that gas was preferentially dissolving in condensate. In conclusion, both simulators agree in terms of condensate saturation behavior during buildup.

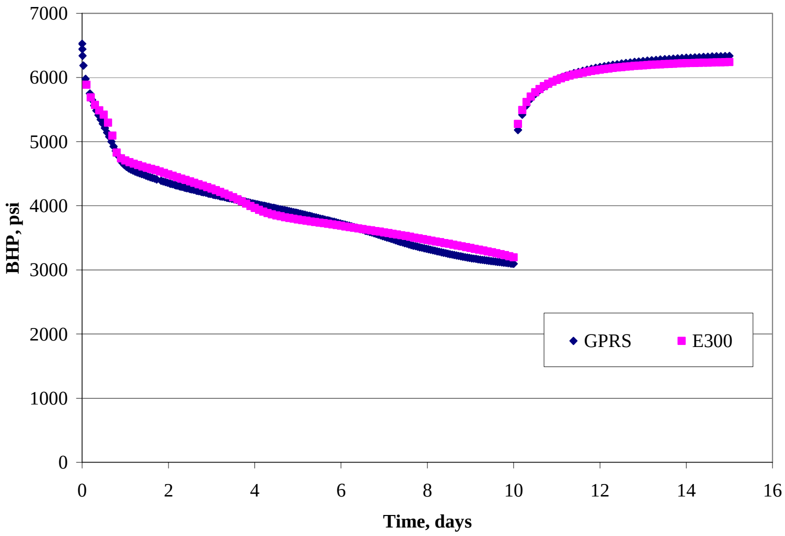

Figure 6-8: Estimated bottom hole pressure (BHP) behavior by *Eclipse-300* and *GPRS.*

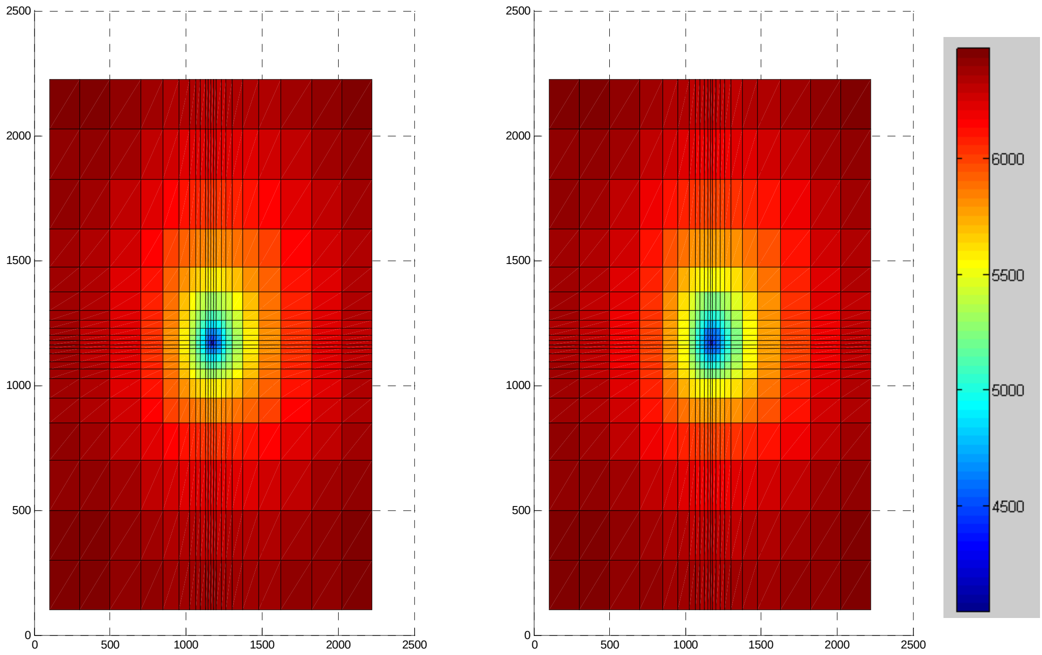

Figure 6-9: Grid block pressures at the end of drawdown estimated by *Eclipse-300* (left) and *GPRS* (right).

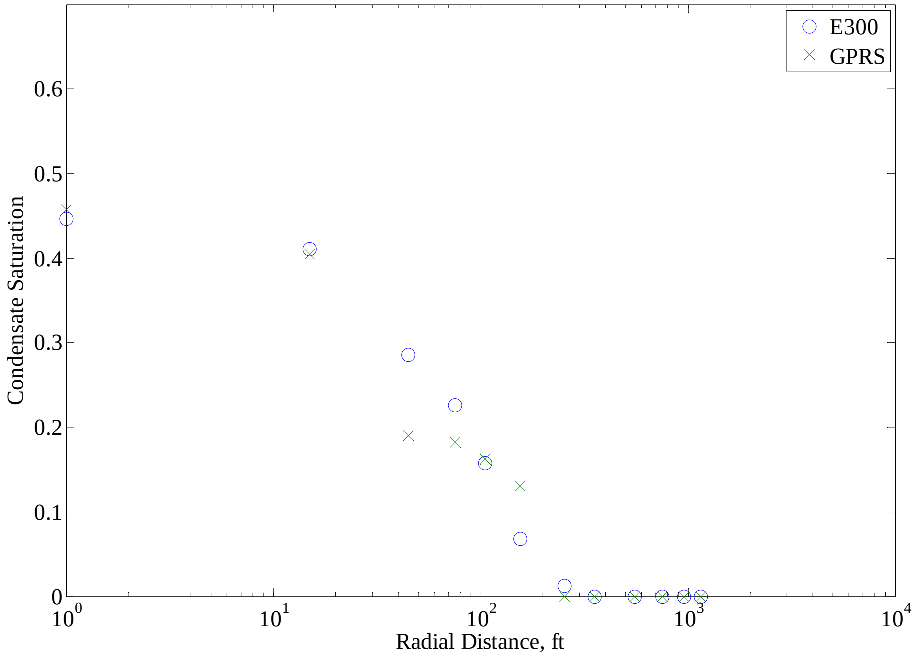

Figure 6-10: Condensate saturation distribution at the end of drawdown estimated by *Eclipse-300* and *GPRS.*

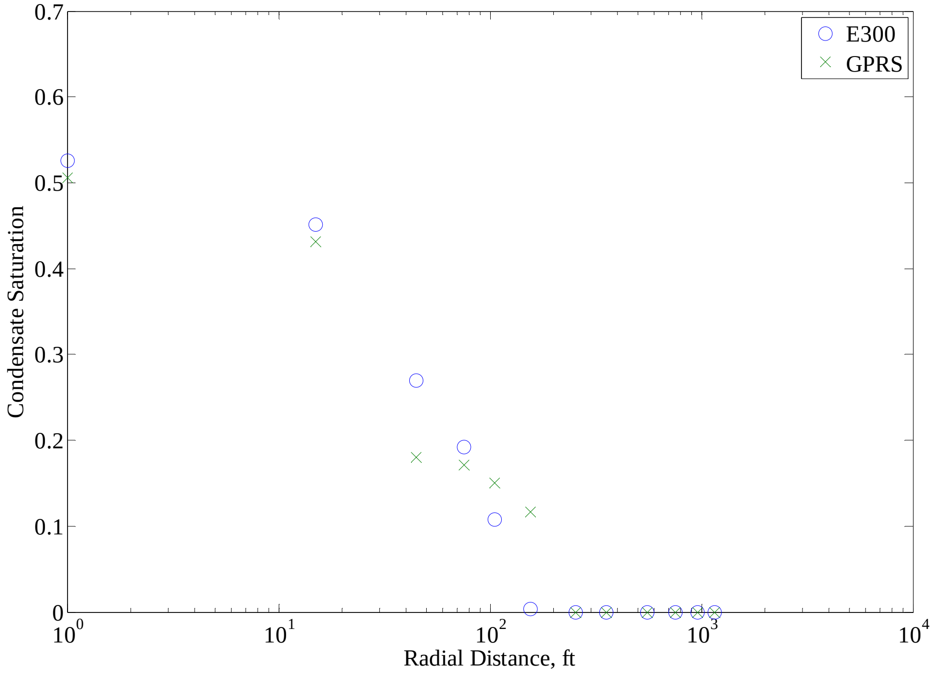

Figure 6-11: Condensate saturation distribution at the end of buildup estimated by *Eclipse-300* and *GPRS.*

Chapter 7

7. Conclusions

This study has confirmed that the three-zone pseudopressure is capable of representing the model pressure-saturation relationship and hence, estimating both permeability and mechanical skin accurately. The three-zone method considers the main flow regions around the wellbore during flow.

On the other hand, unless the steady-state approach is able to predict the model pressure-saturation relationship accurately, this method underestimates mechanical skin and estimates permeability correctly. The steady-state method can predict the model pressure-saturation relationship accurately only if the size of region two (which is ignored by this method) is relatively small compared to region one.

Results for the single-phase pseudopressure have indicated that permeability can be estimated correctly but skin estimates are generally high because skin includes effects from both mechanical skin and skin due to liquid dropout. Therefore, this method is not reliable in determining whether a gas-condensate well requires an acid stimulation or hydraulic fracturing treatment. However, when coupled with the three-zone pseudopressure, the single-phase pseudopressure can be useful in quantifying the skin due to liquid dropout.

References

Agarwal, R. G.: 1979, Real gas pseudotime – a new function for pressure buildup analysis of gas wells, SPE paper 8279.

Al Hussainy, R. and Ramey, H.: 1966, Application of real gas flow theory to well testing and deliverability forecasting, *J. Pet. Tech.* 237, 637–642.

Al Hussainy, R., Ramey, H. and Crawford, P.: 1966, The flow of real gases through porous media, *J. Pet. Tech.* 237, 624–636.

Aziz, K., Durlofsky, L., Tchelepi, H. and Gerritsen, M.: 2006, *Notes for petroleum reservoir simulation,* Stanford University.

Bertram, D. A., McDevitt, B. S. and Al Harthy, N. M.: 1997, Experiences in gas-condensate well test analysis using compositional simulation, SPE paper 37994.

Chopra, A. and Carter, R.: 1985, Proof of the two-phase steady-state theory for flow through porous media, SPE paper 14472.

Coats, K. H. and Smart, G. T.: 1986, Application of a Regression-Based EOS PVT Program to Laboratory Data, *SPE Reservoir Engineering*, May 1986, 277-299.

Evinger, H. H. and Muskat, M.: 1942, Calculation of theoretical productivity factor, *SPE Form. Eval.* 146, 126-139.

Fan, L., Harris, B., Jamaluddin, A., Kamath, J., Mott, R., Pope, G., Shandrygin, A. and Whitson, C.: 2005, Understanding gas-condensate reservoirs, *Oilfield Review*, Schlumberger, Winter 2005/2006, pp. 14-27.

Fevang, O.: 1995, Gas-condensate flow behavior and sampling, *PhD thesis*, Norges Tekniske Hogskole.

Fevang, O and Whitson, C. H.: 1996, Modeling Gas-condensate Well Deliverability, *SPE Reservoir Engineering*, November 1996, 221-230.

Fussel, D. D.: 1973, Single well performance for gas-condensate reservoirs, *J. Pet. Tech.* 255, 860–870.

Gringarten, A. C., Bozorgzadeh, M., Daungkaew, S. and Hashemi, A.: 2006, Well test analysis in lean gas-condensate reservoirs: theory and practice, SPE paper 100993.

Hawkins, M. F.: 1956, A note on the skin effect, *Trans.*, AIME 207, 356-357.

Horne, R. N.: 1995, Modern Well Test Analysis, Petroway, Inc, Palo Alto, CA.

Horner, D. R.: 1951, Pressure buildup in wells, *Proc.*, Third World Pet. Cong., The Hague (1951) II, 503-21.

Jones, J. R. and Raghavan, R.: 1988, Interpretation of flowing well response in gas-condensate wells, SPE paper 14204.

Jones, J. R., Vo, D. T. and Raghavan, R.: 1989, Interpretation of pressure-buildup responses in gas-condensate wells, SPE paper 15535.

Kamath, J.: 2007, Deliverability of gas-condensate reservoirs – field experiences and prediction techniques, *J. Pet. Tech.* V.59 No.4, 94-99.

Katz, D. L. and Firoozabadi, A.: 1978, Predicting phase behavior of condensate/crude oil systems using methane interaction coefficients, *J. Pet. Tech.*, 1649-1655.

Moses, P. L. and Donohoe, C. W.: 1962, Gas-condensate reservoirs, *Petroleum Engineering Handbook*, SPE, pp. 39:1-39-28.

O'Dell, H. G. and Miller, R. N.: 1967, Successfully cycling a low-permeability high yield gas-condensate reservoir, *J. Pet. Tech.* pp. 41–47.

Pedersen, K. S., Fredenslund, Aa. and Thomassen, P.: 1989, Properties of Oils and Natural Gases, Gulf Publishing Company, Houston, TX.

Penuela, G. and Civan, F.: 2000, Predictions of the gas-condensate well productivity, *J. Pet. Science and Engineering* 28, 95-110.

Raghavan, R., Chu, W. and Jones, J. R.: 1995, Practical considerations in the analysis of gas-condensate well tests, SPE Paper 30576.

Reynolds, A. C., Bratvold, R. B. and Ding, W.: 1987, Semilog analysis of gas well drawdown and buildup data, SPE paper 13664.

Roussennac, B.: 2001, Gas-condensate well test analysis, *M.S. thesis*, Stanford University, CA.

Vo, D. T., Jones, J. R. and Raghavan, R.: 1989, Performance predictions for gas-condensate reservoirs, SPE paper 16984.

Wall, C. G.: 1982, Characterization of gas-condensate reservoirs and traditional production methods, *North Sea Gas-condensate Reservoirs and their Development,* Oyez scientific and technical service, pp. 1-12.

Whitson, C. H. and Brule, M. R.: 2000, *Phase Behavior*, SPE monograph V. 20.

Nomenclature

B_{gd}	dry gas Formation Volume Factor (FVF), RB/scf
B_o	oil FVF, RB/STB
c_t	total compressibility, psi^{-1}
h	reservoir thickness, ft
k	absolute permeability, md
ks	skin zone permeability, md
k_{rg}	gas relative permeability
k_{ro}	oil relative permeability
K	hydraulic diffusivity
L	liquid molar fraction
$m(p)$	pseudopressure function
p_D	dimensionless pseudopressure
p_{dew}	original reservoir gas dew-point pressure, psi
p_i	initial reservoir pressure, psi
p^*	pressure at the boundary between Region 1 and Region 2, psi
p_r	reservoir pressure, psi
p_{sc}	pressure at standard conditions, 14.7 psi
p_{wD}	liquid solution
p_{wf}	well flowing pressure, psi
$p_{wf,s}$	well flowing pressure at the moment of shut-in, psi
q_{sc}	gas flow rate at standard conditions, Mscf/day
R_p	producing gas-oil ratio, Mscf/stb
R	gas constant
r_w	well radius, ft
r_s	solution condensate-gas ratio, stb/Mscf
R_s	solution gas-oil ratio, Mscf/stb
s	skin
s_m	mechanical skin
s_t	total skin
s_{2p}	skin due to liquid dropout
S_c	condensate saturation

S_o	oil saturation
S_{oc}	critical oil saturation
S_{oCVD}	oil saturation in lab CVD
S_{wi}	irreducible water saturation
T	reservoir temperature, ^{o}R or ^{o}F
T_{sc}	temperature at standard conditions, 520^{o}R
t	time, days or hours
t_D	dimensionless time
t_p	producing time, days or hours
V	vapor molar fraction
V_{rt}	total relative volume
z_g	gas z factor
z_o	oil z factor

Symbols

μ_g	gas viscosity, cp
μ_o	condensate viscosity, cp
ρ_g	gas molar density, lb-M/ft^3
ρ_o	condensate molar density, lb-M/ft^3
Ω	cubic EOS parameter
Φ	porosity

Abbreviations

BHP	bottom hole pressure, psi
CCE	constant composition expansion
CVD	constant volume depletion
EOS	equation of state
GOR	gas-oil ratio, Mscf/STB
GPRS	general purpose research simulator
HT	Horner time
WI	well index
3-Z	three-zone

Appendix A

A. PVT Experiments

The procedures to conduct the CVD and CCE experiments were illustrated by Pedersen et al. (1989) and Whitson and Brule (2000).

A.1 Constant Volume Depletion CVD

The CVD experiment is performed in order to provide volumetric and compositional data for gas-condensate reservoirs producing by pressure depletion. The experiment is intended to simulate conditions encountered in the reservoir.

Initially, a sample of reservoir gas in a laboratory cell is brought to just below its dew point and the temperate is set to reservoir temperature. The pressure is then reduced by increasing the cell volume causing condensate to form. After that, the cell volume is brought back to the dew point volume by displacing part of the gas into a flash separation system where compositional analyses are performed. The pressure is further reduced and the process is repeated for several pressure steps. A schematic of constant volume depletion experiment is illustrated in Figure A-1.

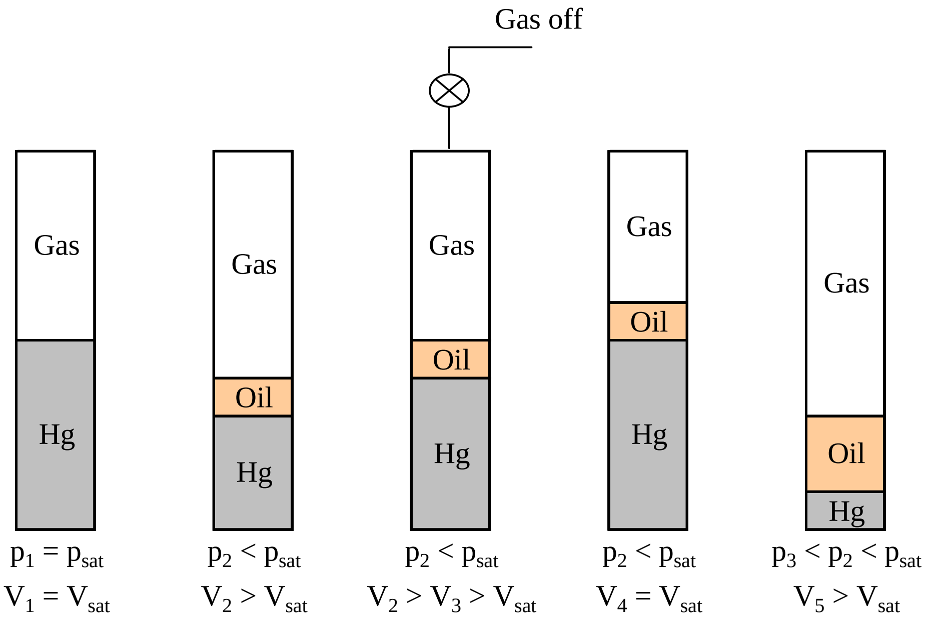
Gas off
Gas
Hg
Gas
Oil
Hg
Gas
Oil
Hg
Gas
Oil
Hg
Gas
Oil
Hg
$p_1 = p_{sat}$
$V_1 = V_{sat}$
$p_2 < p_{sat}$
$V_2 > V_{sat}$
$p_2 < p_{sat}$
$V_2 > V_3 > V_{sat}$
$p_2 < p_{sat}$
$V_4 = V_{sat}$
$p_3 < p_2 < p_{sat}$
$V_5 > V_{sat}$

Figure A-1: Schematic of constant volume depletion experiment.

A.2 Constant Composition Expansion CCE

First, a sample of reservoir gas is placed in a laboratory cell at pressure above the initial reservoir pressure to ensure that the fluid is single-phase and at temperature equal to the reservoir temperature. Then the pressure is reduced in a stepwise manner. At each pressure step, the volume is recorded. Below the dew point, the liquid volume is also recorded. The overall fluid composition remains constant because no gas or liquid is removed from cell at any time throughout the experiment. A schematic of constant composition expansion experiment is illustrated in Figure A-2.

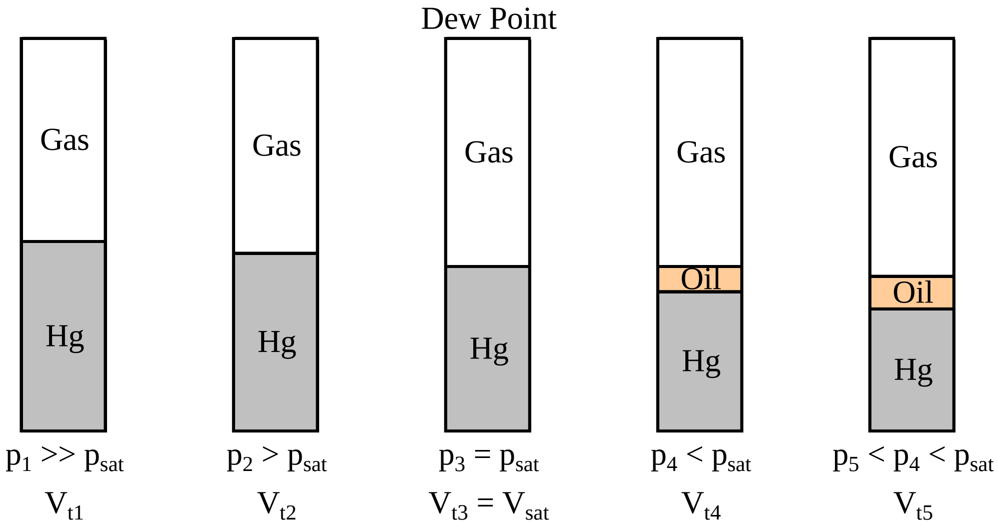
Dew Point
Gas
Hg
Gas
Hg
Gas
Hg
Gas
Oil
Hg
Gas
Oil
Hg
$p_1 >> p_{sat}$
V_{t1}
$p_2 > p_{sat}$
V_{t2}
$p_3 = p_{sat}$
$V_{t3} = V_{sat}$
$p_4 < p_{sat}$
V_{t4}
$p_5 < p_4 < p_{sat}$
V_{t5}

Figure A-2: Schematic of constant composition expansion experiment.

Appendix B

B. Radial Model

B.1 Eclipse-300 Code

```
============================================================
-- Study: Gas-condensate flow simulation
-- SIMULATOR: Eclipse 300
=============================================================
=
RUNSPEC
=============================================================
=
TITLE
Gas-condensate flow simulation

--Flow is radial
RADIAL

--Dimensions of the grid in cylindrical co-ordinate
DIMENS
30 1 1/

--Simulation is for gas-condensate
ISGAS

--Field units are used
FIELD

--Adaptive IMplicit solution option
AIM

--12 components in study
COMPS
12/

--Peng-Robinson equation of state to be used
EOS
PR/
```

```
TABDIMS
1 1 80 1* 1 1* 1* 1*/

WELLDIMS
1 1 1 1/

MULTSAVE
--1/

FMTOUT
==================================================================
=
GRID
==================================================================
=
INIT

INRAD
.25/

--R direction grid block size
DR
0.4429 0.5300 0.6539 0.9655 1.4255 2.1046 3.1072 4.5876 6.7732 10 10 10
10 35 40 47 68 100 150 200 200 300 500 500
500 500 500 500 500 500/

EQUALS
DTHETA
360/
DZ
75/
TOPS
10500/
PORO
0.17/
PERMTHT
5.5    1    30   1    1    1  1/

PERMR
100   1    8   1    1    1  1/

PERMR
5.5   9    30   1    1    1  1/
/
```

```
===============================================================
=
PROPS
===============================================================
=
--Include File with Fluid properties
INCLUDE
'fluid_properties.INC'/
-- Include File with Relative Permeabilities
INCLUDE
'RelPERM.INC'/

RTEMP
275/

ROCK
7000 0.000005/
PVTW
7000 1.0 0.0000026 0.65 0.0/

DENSITY
50.9 63.0 1*/
===============================================================
=
SOLUTION
===============================================================
=
EQUALS
PRESSURE
7000/
SWAT
0/
SGAS
1/
/
--Cell initial total mole composition
ZMF
30*0.1014979161
30*0.02025926627
30*0.02670997792
30*0.6742001597
30*0.06904277311
30*0.0307416727
30*0.005946749801
```

```
30*0.01259904619
30*0.004636448997
30*0.005039618476
30*0.006853881127
30*0.04247248965/

=====================================================================
=
SUMMARY
=====================================================================
=
RUNSUM

RPTONLY

INCLUDE
'OUTPUT.INC'/
=====================================================================
=
SCHEDULE
=====================================================================
=
SEPCOND
SEP FIELD 1 60 14.7 /
/
WELLSPEC
P FIELD 1 1 1* SEP/
/
COMPDAT
P 1 1 1 1 OPEN 1* 1* 0.5 1* 0 1* Z/
/
-- Pressure drawdown
WELLPROD
P GAS 2* 50000 1* 500/
/
-- Simulation for 41.3 hrs
TSTEP
 1.32E-05     1.78E-05     2.40E-05     3.24E-05     4.38E-05     5.91E-05
 7.98E-05     0.00010775   0.00014547   0.0001964    0.00026511   0.0003579
 0.00048317   0.00065228   0.00088058   0.0011888    0.00160485   0.00216655
 0.00292485   0.00394854   0.00533053   0.0071962    0.0097149    168*0.01
/
-- Pressure buildup
WELLPROD
P GAS 2* 0/
/
```

```
-- Simulation for 76.8 hrs
TSTEP
 1.32E-05     1.78E-05     2.40E-05     3.24E-05    4.38E-05     5.91E-05
 7.98E-05     0.00010775   0.00014547   0.0001964   0.00026511   0.0003579
 0.00048317   0.00065228   0.00088058   0.0011888   0.00160485   0.00216655
 0.00292485   0.00394854   0.00533053   0.0071962   0.0097149    310*0.01
/
END
```

Appendix C

C. Plots for Second Pressure Buildup Test Analysis

C.1 Pressure-Saturation Relationship

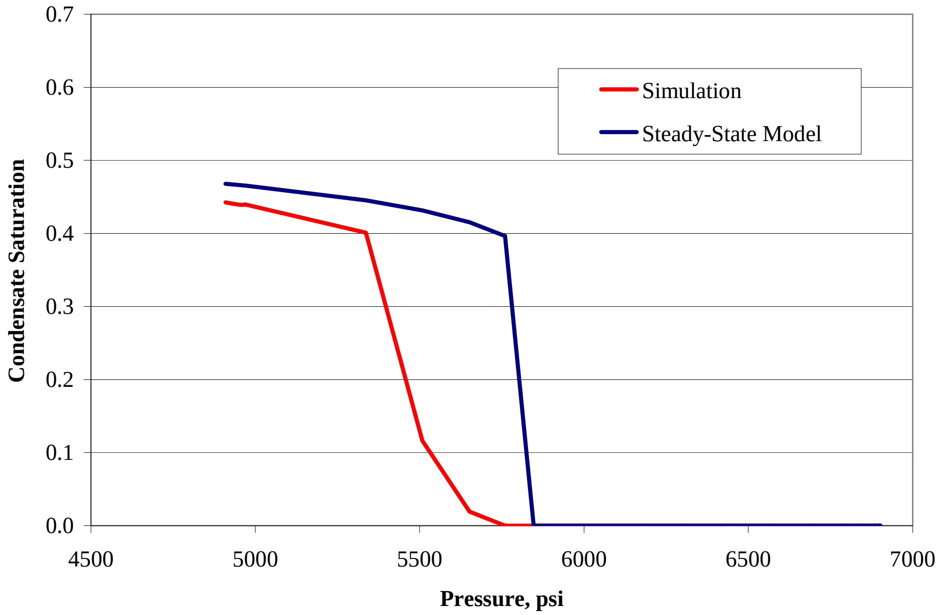

Figure C-1: Pressure-saturation relationship by the steady-state model for the second test.

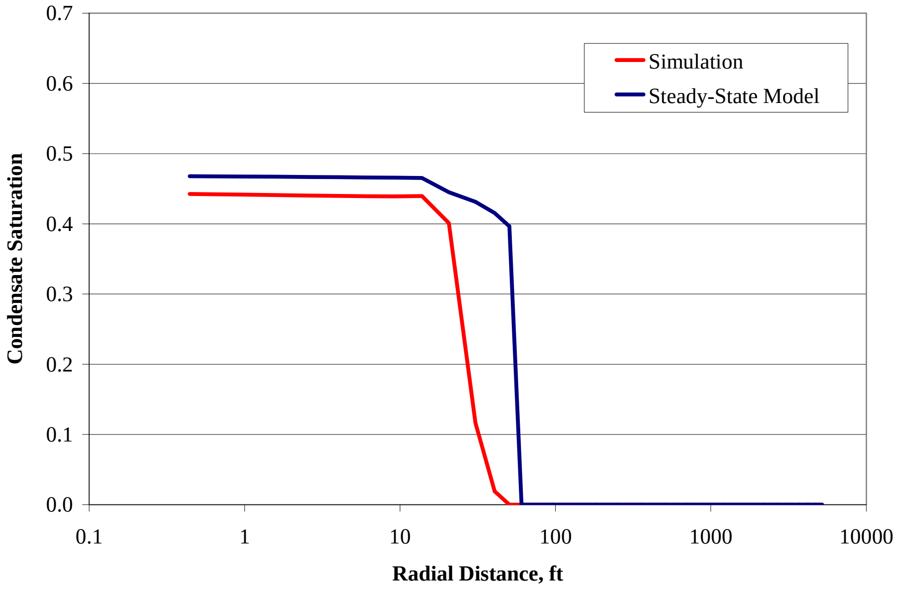

Figure C-2: Radial distribution of cond. saturation by the steady-state model for the second test.

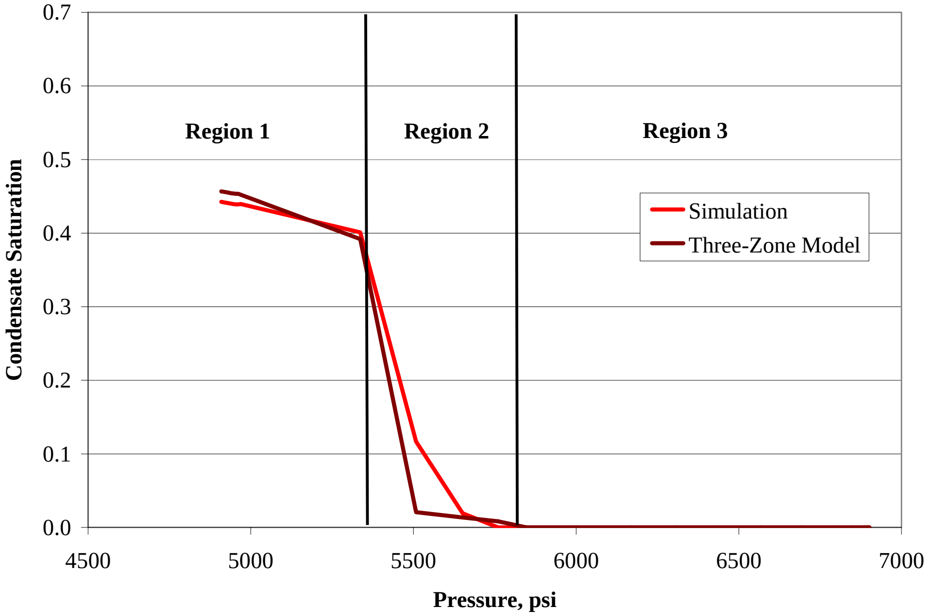

Figure C-3: Pressure-saturation relationship by the three-zone model for the second test.

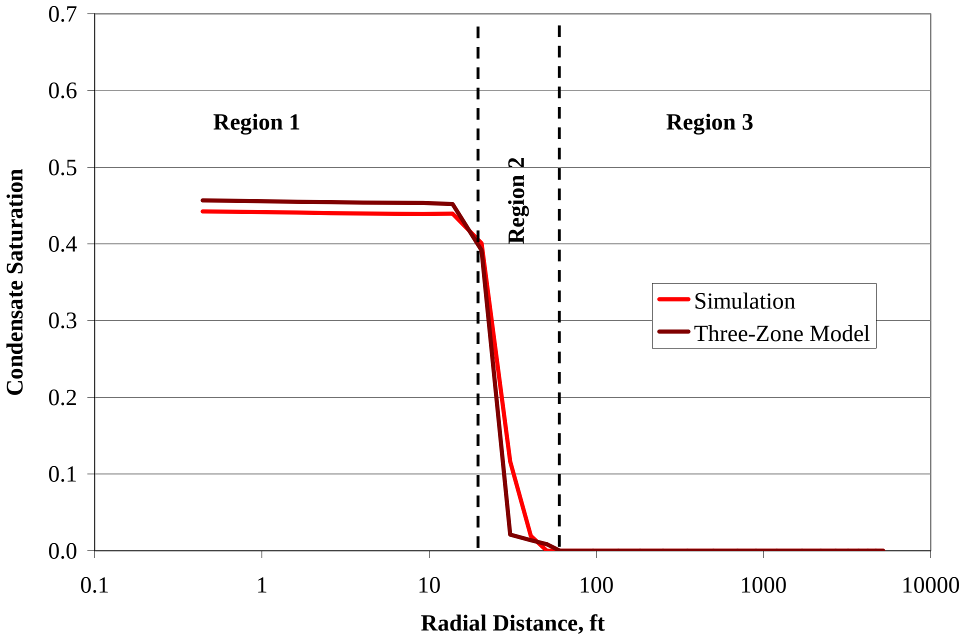

Figure C-4: Radial distribution of cond. saturation by the three-zone model for the second test.

C.2 Horner Plots

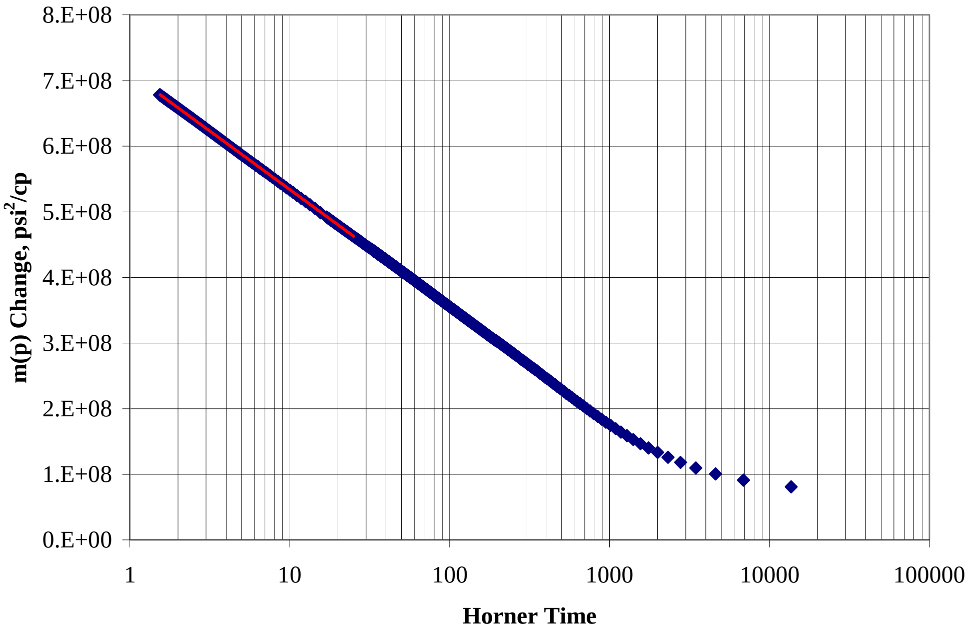

Figure C-5: Horner plot for second pressure buildup test (single-phase pseudopressure).

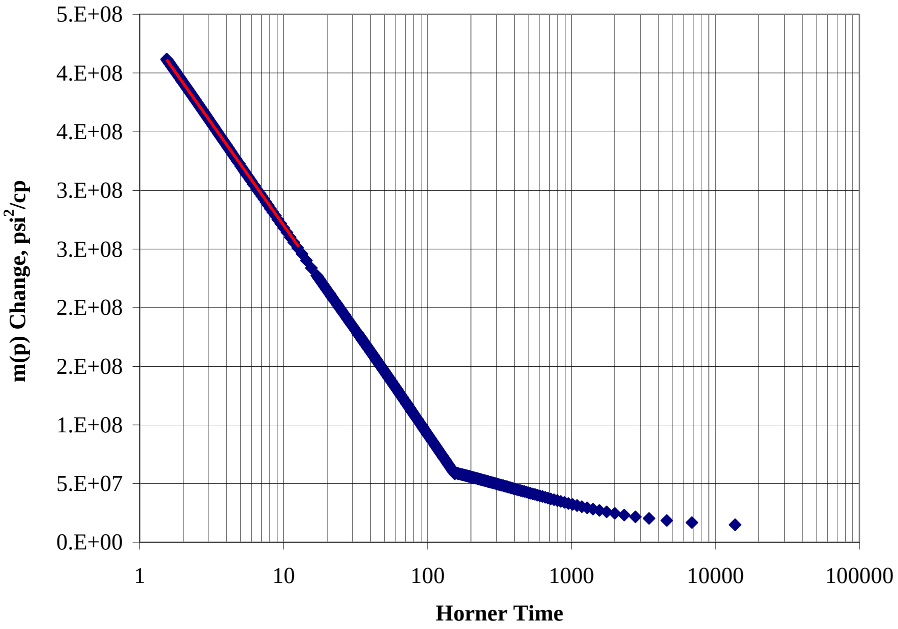

Figure C-6: Horner plot for second pressure buildup test (syteady-state pseudopressure).

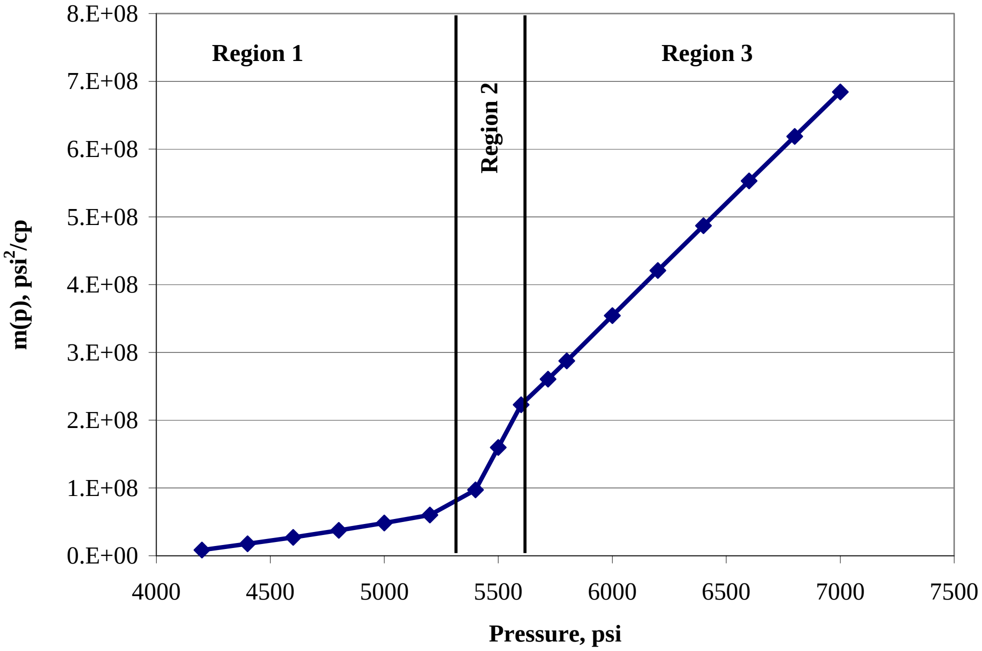

Figure C-7: Two-phase three-zone pseudopressure as a function of pressure for the second test.

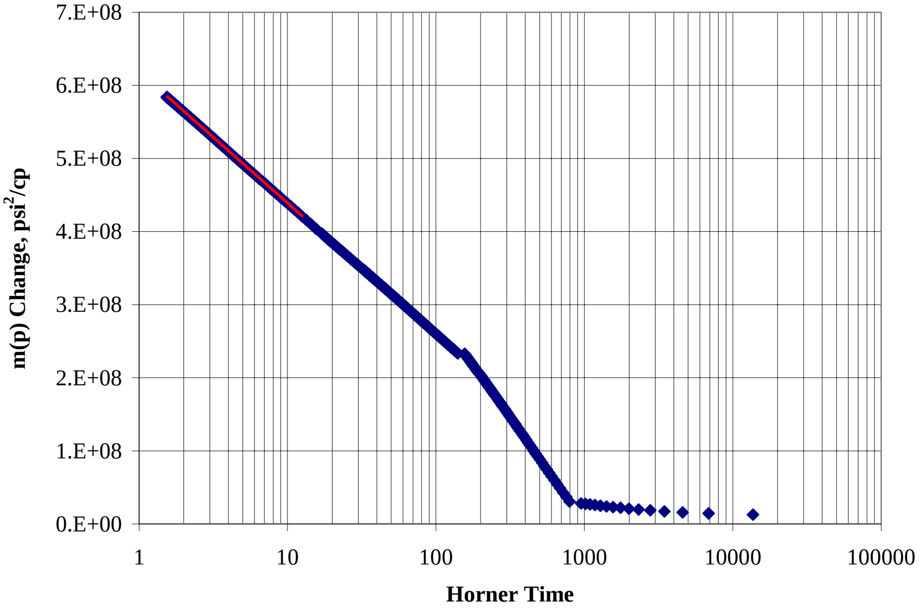

Figure C-8: Horner plot for second pressure buildup test (three-zone pseudopressure).

Appendix D

D. Plots for Third Pressure Buildup Test Analysis

D.1 Pressure Saturation Relationship

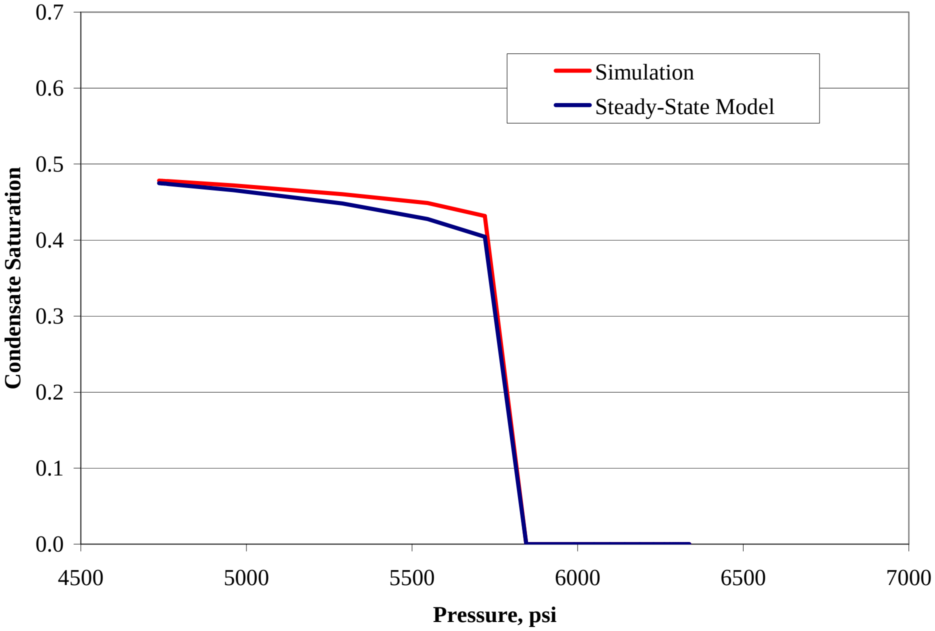

Figure D-1: Pressure-saturation relationship by the steady-state model for the third test.

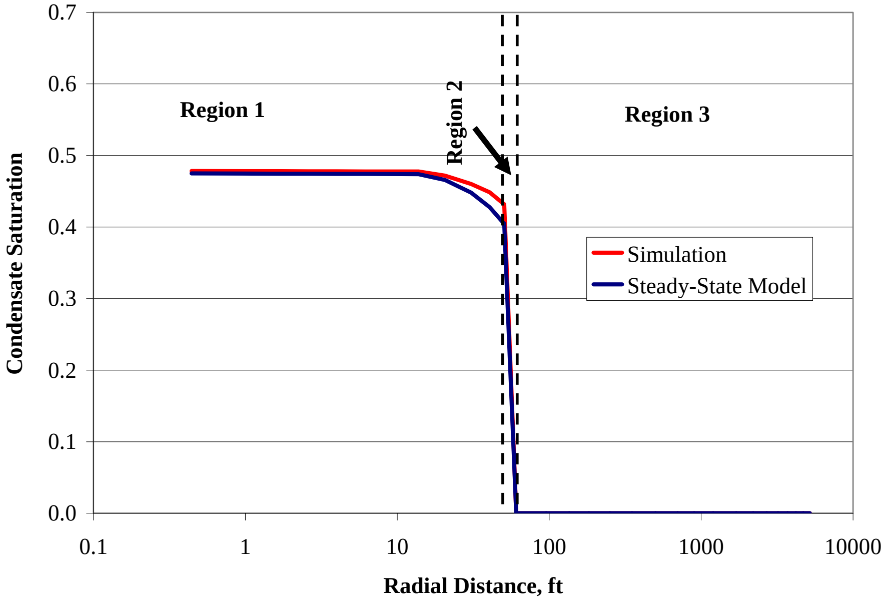

Figure D-2: Radial distribution of cond. saturation by the steady-state model for the third test.

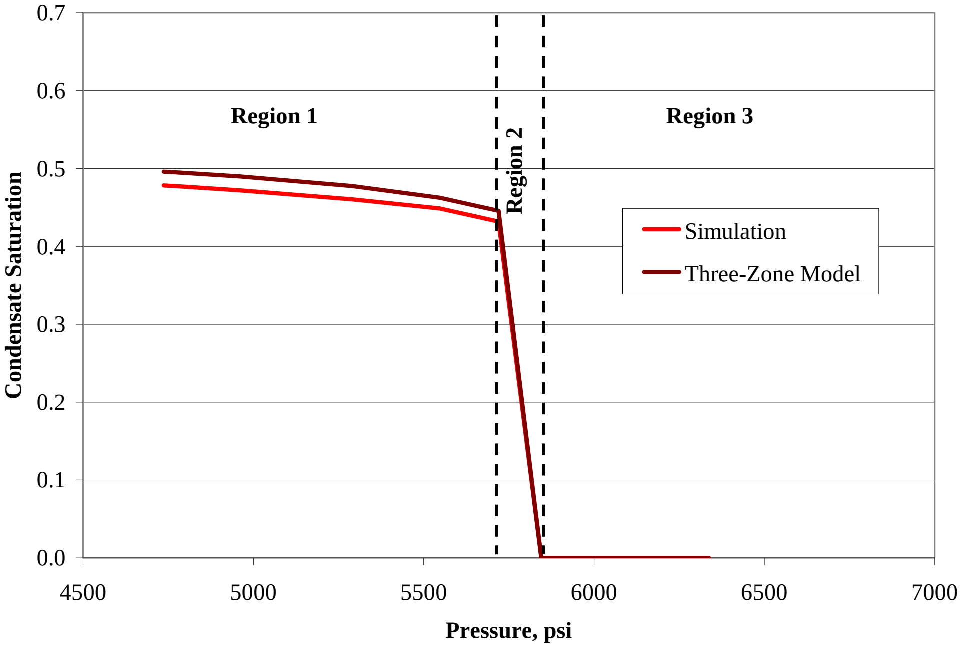

Figure D-3: Pressure-saturation relationship by the three-zone model for the third test.

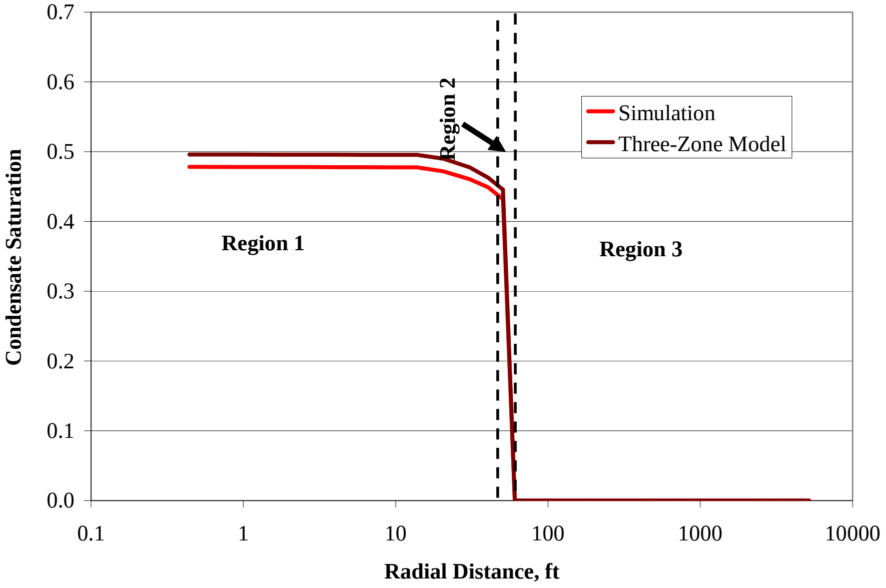

Figure D-4: Radial distribution of cond. saturation by the three-zone model for the third test.

D.2 Horner Plots

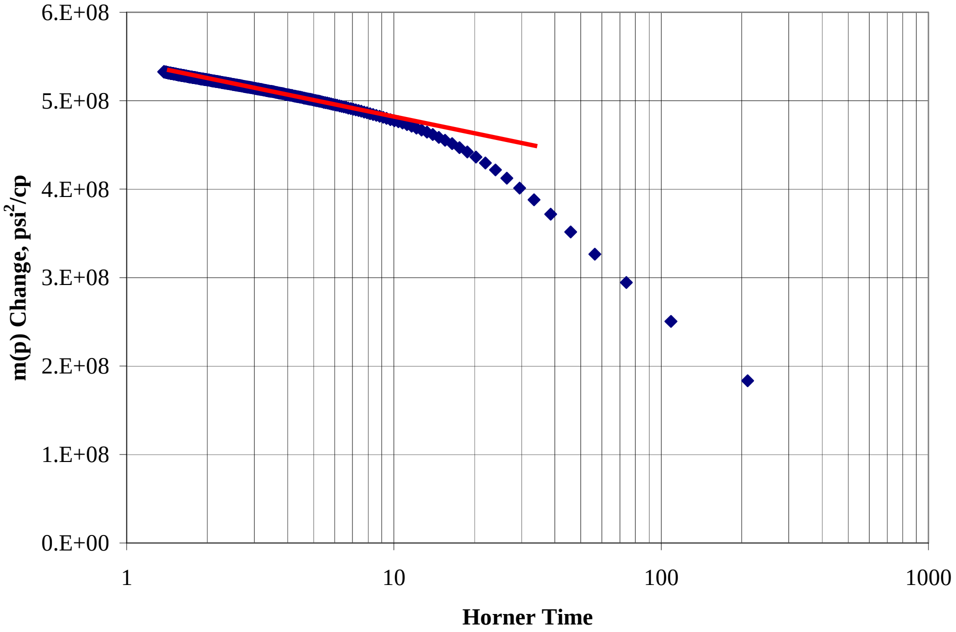

Figure D-5: Horner plot for third pressure buildup test (single-phase pseudopressure).

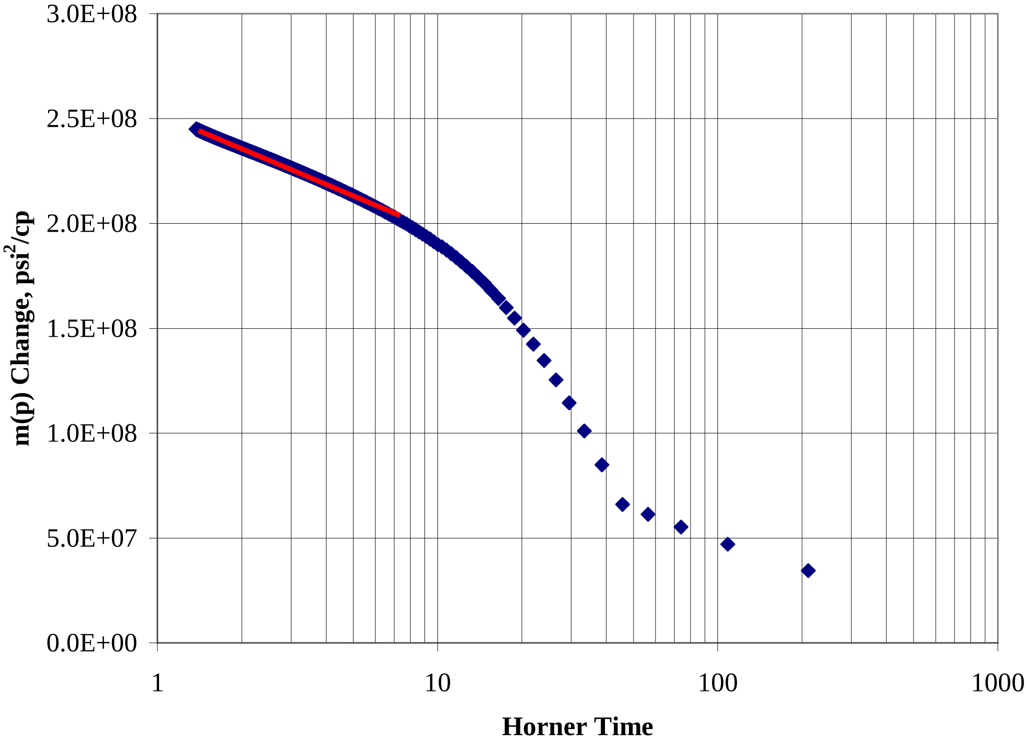

Figure D-6: Horner plot for third pressure buildup test (steady-state pseudopressure).

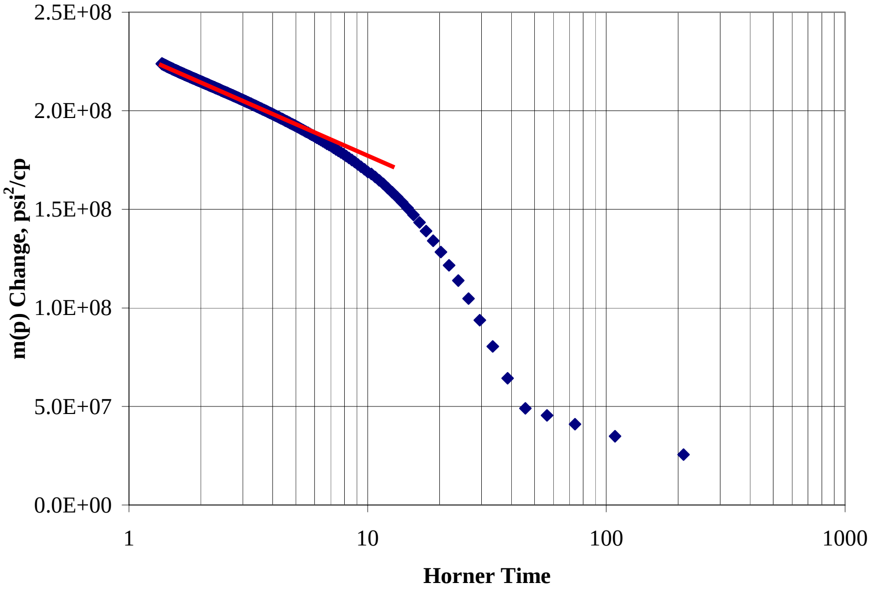

Figure D-7: Horner plot for third pressure buildup test (three-zone pseudopressure).

Appendix E

E. Cartesian Model

E.1 Well Index Calculation

The following two equations were utilized to compute the well index, *WI*, required for *GPRS* compositional simulator. The equations were obtained from Aziz et al. (2006).

The expression for r_o for a well in the center of a square block is given by:

$$r_o = 0.208\Delta x \qquad \textbf{(E-1)}$$

WI is then calculated as follows:

$$WI = \left[\frac{2\pi kh}{\ln(\frac{r_o}{r_w}) + s} \right] \qquad \textbf{(E-2)}$$

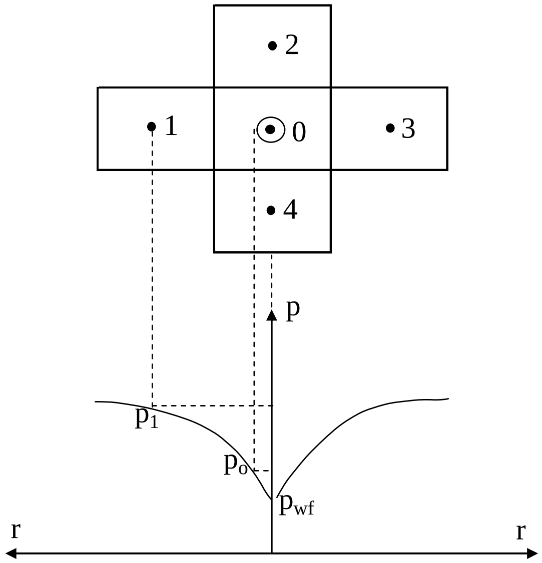

Figure E-1: Determining the pressure of the block containing the well (drawn from Aziz et al., 2006)

E.2 GPRS Code

```
RESERVOIR_NAME   RES1

#MP_CONN

GRID_DATA  ##########################################
GRIDSIZE  23 23 1

DX
4*200 2*100 1*50 3*30 3*15 3*30 1*50 2*100 4*200
4*200 2*100 1*50 3*30 3*15 3*30 1*50 2*100 4*200
4*200 2*100 1*50 3*30 3*15 3*30 1*50 2*100 4*200
4*200 2*100 1*50 3*30 3*15 3*30 1*50 2*100 4*200
4*200 2*100 1*50 3*30 3*15 3*30 1*50 2*100 4*200
4*200 2*100 1*50 3*30 3*15 3*30 1*50 2*100 4*200
4*200 2*100 1*50 3*30 3*15 3*30 1*50 2*100 4*200
4*200 2*100 1*50 3*30 3*15 3*30 1*50 2*100 4*200
4*200 2*100 1*50 3*30 3*15 3*30 1*50 2*100 4*200
4*200 2*100 1*50 3*30 3*15 3*30 1*50 2*100 4*200
4*200 2*100 1*50 3*30 3*15 3*30 1*50 2*100 4*200
4*200 2*100 1*50 3*30 3*15 3*30 1*50 2*100 4*200
4*200 2*100 1*50 3*30 3*15 3*30 1*50 2*100 4*200
4*200 2*100 1*50 3*30 3*15 3*30 1*50 2*100 4*200
4*200 2*100 1*50 3*30 3*15 3*30 1*50 2*100 4*200
4*200 2*100 1*50 3*30 3*15 3*30 1*50 2*100 4*200
```

```
4*200 2*100 1*50 3*30 3*15 3*30 1*50 2*100 4*200
4*200 2*100 1*50 3*30 3*15 3*30 1*50 2*100 4*200
4*200 2*100 1*50 3*30 3*15 3*30 1*50 2*100 4*200
4*200 2*100 1*50 3*30 3*15 3*30 1*50 2*100 4*200
4*200 2*100 1*50 3*30 3*15 3*30 1*50 2*100 4*200
4*200 2*100 1*50 3*30 3*15 3*30 1*50 2*100 4*200
4*200 2*100 1*50 3*30 3*15 3*30 1*50 2*100 4*200
DY
92*200 46*100 23*50 69*30 69*15 69*30 23*50 46*100 92*200
DZ
75

PERMX
216*5.7 5*50 18*5.7 5*50 18*5.7 5*50 18*5.7 5*50 18*5.7 5*50 216*5.7
PERMY
216*5.7 5*50 18*5.7 5*50 18*5.7 5*50 18*5.7 5*50 18*5.7 5*50 216*5.7
PERMZ
1

PORO
0.17
TOPS
10500
TEMP
735
END

FLUID_DATA  ########################################
FLUID_TYPE COMPOSITIONAL
NPHASES      2
NCOMPONENTS 12

# Phase data -------------
#PHASE_NAMES
GAS OIL

# --- component data -------------
#COMP_NAMES
N2 CO2 H2S C1 C2 C3 IC4 NC4 IC5 NC5 C6 C7+

# --- Z(initial total mole fraction) for each component ---
length_of_table 2
1
0.101497916   0.020259266   0.026709978   0.67420016    0.069042773   0.030741673
0.00594675    0.012599046   0.004636449   0.005039618  0.006853881    0.04247249
20000
```

```
0.101497916   0.020259266   0.026709978   0.67420016    0.069042773   0.030741673
0.00594675    0.012599046   0.004636449   0.005039618  0.006853881    0.04247249

# --- Molecular Weight for each component ---
28.013   44.01   34.076   16.043   30.07   44.097   58.123995   58.124005   72.150995
72.151005   84   155

# --- Pc(Psia) for each component ---
492.312649984577     1071.33110996644     1296.17837995939     667.78169597908
708.342379977809     615.75820998071      529.052399983426    550.655372982749
491.5778549846       488.785633984687     436.615188986322      303.57715709049

# --- Tc(R) for each component ---
227.160000017685     548.459999999228     672.480000014636    343.079999988516
549.774000004037     665.640000033438     734.579999959724    765.359999975116
828.719999953583     845.279999992273     913.499999999486    1148.38159862172

#--- Vc (ft3/lb-mole) for each component -----
# --- W for each component ---


# --- Volume Shift Parameter (Dimensionless S) ----


#--- K[ij] for each pair component ----------


#Flash method: SSI or NEWTON
SSI
END

PHASE_COMP_RELATION_DATA ##########################
# --- component phase relation (nPhases by nComps) ---
#comp:
N2    CO2    H2S    C1    C2    C3    IC4    NC4    IC5    NC5    C6    C7+
1      1       1       1     1     1     1       1       1      1      1      1                 #gas
1      1       1       1     1     1     1       1       1      1      1      1                  #oil
END

ROCKFLUID_DATA #####################################
#GASOILPERM 1
GO
NUM_OF_TABLE_ENTRIES 15
#TABLE
SG        KRG      KROg      PCOG
0.1500   0.0000    0.7000       0.0000
```

```
0.2000   0.0004   0.5379       0.0000
0.2500   0.0029   0.4007       0.0000
0.3000   0.0098   0.2870       0.0000
0.3500   0.0233   0.1952       0.0000
0.4000   0.0456   0.1237       0.0000
0.4500   0.0787   0.0708       0.0000
0.5000   0.1250   0.0345       0.0000
0.5500   0.1866   0.0125       0.0000
0.6000   0.2657   0.0022       0.0000
0.6500   0.3644   0.0000       0.0000
0.7000   0.4851   0.0000       0.0000
0.7500   0.6297   0.0000       0.0000
0.8000   0.8007   0.0000       0.0000
0.8500   1.0000   0.0000       0.0000
END


ROCK_DATA #############################################
#          COMP.          REF. PRES
           0.000005        6900
END

EQUILIBRIUM_DATA #############################################
#           Swi          Sor           Sgr
            0.0          0.00          0.0

#           pres        @depth       WOC       GOC
           6900          10500       13000     12000
END

END_RESERVOIR


# ---------- Input of wells data ----------
# //////// WELL No. 1 //////////////////////
# --- well definition -----
#WELSPECS
#     WELL_NAME     GROUP     RES_NAME     TYPE     STATUS
          PROD              GRP1          RES1              P          OPEN
END

# --- well connections-------
#COMPDAT
number_of_connections 1
#  LOC(i,j,k)                    WI
      264                       9521
```

```
END

# --- well control ----------------------
#WCONPROD
#   CTRL        Btime    Etime    Qg        BHP       std_den_g
    TGRATE      0        10       85000     500.0     0.08
    TGRATE      10       15       0         7000      0.08
END

END_WELL
```